UN/JP0003V1
*REV. 01*

# Propagation Effects Handbook for Satellite Systems Design

*Fifth Edition*

# Section 1 Background

**Dr. Louis J. Ippolito**
**STANFORD TELECOM *ACS***
**45145 Research Place**
**Ashburn, Virginia 20147**

***prepared for***
**JPL**
**Jet Propulsion Laboratory**
**4800 Oak Grove Drive**
**Pasadena, CA 91109**

*February 1999*

STANFORD TELECOM®

# PREFACE

This Fifth Edition of the Propagation Effects Handbook for Satellite Systems Design continues the long process of a continuing NASA commitment to provide a comprehensive reference document which provides the latest information on atmospheric propagation effects and how they impact satellite communications system design and performance. The First Edition of the Handbook was published in March 1980, the Second Edition in December 1981, the Third Edition in June 1983, and the Fourth Edition in February 1989. I have been fortunate to have been involved with the Propagation Handbook project since its inception, and this Fifth Edition continues on with the process.

I would like to acknowledge the contributions of the many members of the staff at Stanford Telecom who helped with the development of this handbook. The contributions of Dr. Lynn Ailes, Glenn Feldhake, Dr. Frank Hastings, Chris Pearson, Jennifer Pinder, and John Weinfield are gratefully appreciated. The contributions of previous members of the staff, Jay Gibble, Julie Feil, and Chris Hofer are also acknowledged. The assistance of Ivy Cooper and Marian Montigny in the production of the handbook is also appreciated.

Louis J. Ippolito
Stanford Telecom
Ashburn, Virginia
October 1998

# PREFACE TO REVISION 1

This first revision, REV. 01, of the Fifth Edition of the Propagation Effects Handbook for Satellite Systems Design, incorporates the results of a peer review process on the original Fifth Edition, published in October 1998. Revisions consisted, for the most part, of misspellings, omissions and corrections to the original text and graphics. In addition, clarifications and further discussions were added where indicated in the peer review.

Section 1, Background, had revisions to 16 pages, out of the total of 119 pages. Section 2, Prediction, had revisions to 104 pages out of the total of 226 pages. Four missing exhibits were added to Section 2. The reference lists for both Sections have been completely updated and re-formatted. Corrected pages are indicated by an 'R1' in the file name on the right side of the page footer. Section 3, Applications, was not revised at this time.

I would like to thank the reviewers for their thoroughness and diligence in the review process. A special thanks goes to Dr. Ernest K. Smith for his excellent comprehensive review and comments. I also would like to acknowledge the contributions of Warren Flock, Ken Davies, and Glen Feldake to the review process.

Louis J. Ippolito
Stanford Telecom
Ashburn, Virginia
February 1999

# INTRODUCTION

## I.1 INTRODUCTION TO THE HANDBOOK

The Fifth Edition of the Propagation Effects Handbook for Satellite Systems Design provides, in one complete reference source, the latest information on atmospheric propagation effects and how they impact satellite communications system design and performance. The National Aeronautics and Space Administration, NASA, which has supported a large part of the experimental work in radiowave propagation on space communications links, recognized the need for a reference handbook of this type, and initiated a program in the late 1970's to develop and update a document that will meet this need. This Fifth Edition provides, in a single document, an update to two previous NASA handbooks; the fourth edition of a handbook which focused on propagation effects from 10 to 100 GHz (Ippolito, 1989), and the second edition of a companion handbook which covered propagation effects on satellite systems at frequencies below 10 GHz (Flock, 1987). This Fifth Edition covers the full range of radiowave frequencies that are in use or allocated for space communications and services, from nominally 100 MHz up to 100 GHz.

The basic intention of the Fifth Edition is to combine the scope of the previous handbooks into a single document, with elimination of duplication as much as possible. This Fifth Edition has a completely new outline, different from either of the two previous handbooks. The intent is to provide a more cohesive structure for the reader. The handbook incorporates a unique, new concept with several levels of “entrance” into the handbook.

Several major developments in satellite communications and the study of propagation effects have occurred since publication of the prior NASA handbooks. New propagation measurement campaigns have been completed or are in progress, providing new data for the evaluation of link degradations on satellite links. New propagation models and prediction techniques are available, covering the traditional propagation effects along with several new areas. New satellite applications have been thrust into the forefront of the satellite communications industry, requiring new approaches for the evaluation of propagation effects. The proliferation of new and competing applications in the frequency bands allocated to space communications has increased the importance and priority of understanding spectrum sharing and interference mitigation. Propagation conditions are a critical component of a viable sharing and interference process.

Section I.2 describes the handbook structure. Section I.3 describes how to apply the handbook for the most efficient use of the resource, depending on the readers’ needs and level of interest.

## I.2 HANDBOOK STRUCTURE

The Propagation Effects Handbook for Satellite Systems Design, Fifth Edition, is divided into three sections. Section 1 provides the background, historical development, theory, and basic concepts of the propagation effects of concern to the satellite systems engineer. The prediction techniques developed to address the critical propagation effects are presented in Section 2. Information on how to apply the prediction methods for specific satellite systems applications is provided in Section 3.

**Section 1** begins with an overview of propagation effects on satellite communications. The propagation effects are then introduced and background theory and developments are described. The frequency dependence of radiowave propagation is recognized, and the effects are divided into two groups; ionospheric effects, influencing systems operating at frequencies below about 3 GHz, and tropospheric effects, influencing systems operating at frequencies above about 3 GHz. Radio noise, which can affect satellite systems in all operating bands, is then described. The section concludes with a comprehensive description of propagation databases, including points of contact and electronic addresses.

**Section 2** provides descriptions of prediction models and techniques for the evaluation of propagation degradation on satellite links. Step-by-step procedures are provided where available. The first two subsections present propagation effects for ionospheric effects and for tropospheric effects, respectively. The third subsection presents prediction methods for radio noise. The fourth subsection describes several general modeling procedures, including statistical considerations, frequency scaling and elevation angle scaling. The final subsection presents models for the restoration of links subject to propagation impairments, including site diversity, orbit diversity and adaptive FEC.

**Section 3** provides roadmaps for the application of the prediction models given in Section 2 to specific satellite systems and applications. Suggested approaches to evaluating link propagation effects and their impact on system design and performance are provided.

## I.3 HOW TO USE THE HANDBOOK

The Fifth Edition of the Propagation Effects Handbook for Satellite Systems Design is intended for the systems engineer and link designer who is interested in the latest and most accurate methodology available for the evaluation of radiowave propagation effects on satellite communications. The handbook is structured with several levels of "entrance" into the handbook, as highlighted by the chart below.

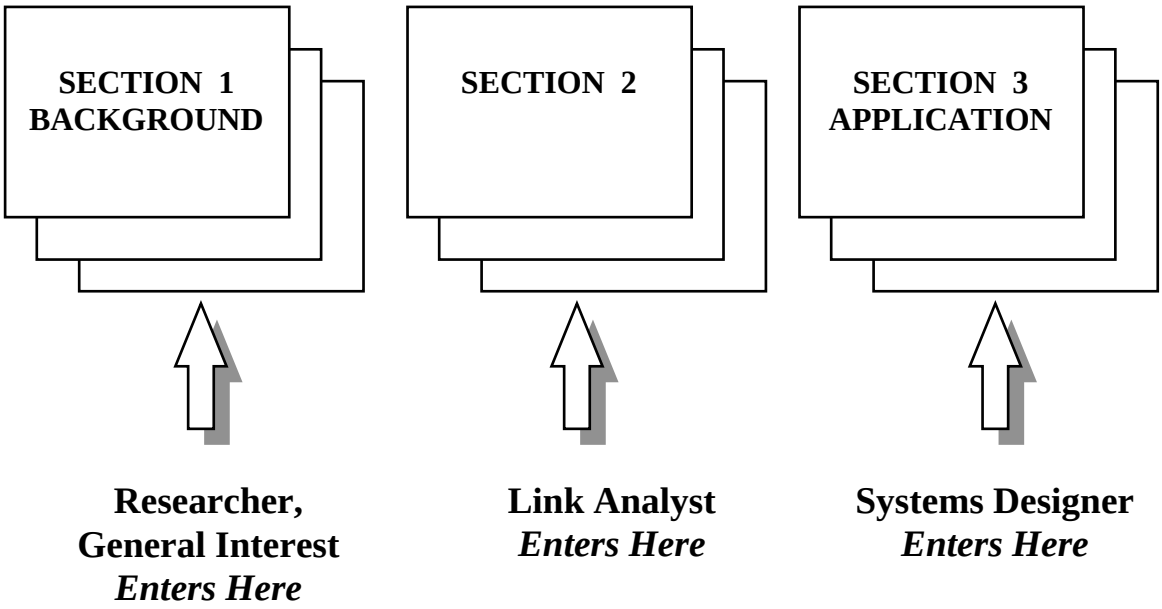


The general researcher or someone new to the subject who may not have a full awareness of the background and history of propagation effects and their impact on satellite communications could enter in Section 1, which provides an overview of propagation effects and the background theory involved in the prediction methodology. Section 1 also provides an extensive listing of resources for additional information and backup data important to the area of propagation effects and satellite communications.

The link analyst or engineer who is familiar with propagation and satellite communications issues and knows which propagation effects are of interest would enter into Section 2 where concise step-by-step procedures for each effect are available. Section 2 also includes general modeling procedures, including statistical considerations, frequency scaling and elevation angle scaling. Section 2, in addition, presents models for the restoration of links subject to propagation impairments, including site diversity, orbit diversity and adaptive FEC.

The system designer who has a good understanding of the system aspects of satellite communications but may not know just which propagation impairments are important to the

particular system or application under consideration would enter through Section 3. Here the reader will find roadmaps for the application of the prediction models given in Section 2 to specific satellite systems and applications. Suggested approaches to evaluating link propagation effects and their impact on system design and performance are also provided in Section 3.

These entrance levels are only suggestions for the reader, to avoid unnecessary reading and to optimize the use of the handbook. Suggestions on ways to improve the document structure, or on specific additional information that would be useful to the reader to include in later editions of the handbook, are always welcome by the author.

# Propagation Effects Handbook for Satellite Systems Design

## Section 1 Background

***Table of Contents***

# SECTION 1
# BACKGROUND

## 1. INTRODUCTION TO SECTION 1

The Propagation Effects Handbook for Satellite Systems Design, Fifth Edition, is divided into three sections. This section, Section 1, provides the background, historical development, theory, and basic concepts of the propagation effects of concern to the satellite systems engineer. The section includes theory and basic concepts, propagation measurements, and available databases. The prediction techniques developed to address the critical propagation effects are presented in Section 2. Information on how to apply the prediction methods for specific satellite systems applications is provided in Section 3.

Section 1 begins with an overview of propagation effects on satellite communications. The propagation effects are then introduced and background theory and developments are described. The frequency dependence of radiowave propagation is recognized, and the effects are divided into two groups; ionospheric effects, influencing systems operating at frequencies below about 3 GHz, and tropospheric effects, influencing systems operating at frequencies above about 3 GHz. Radio noise, which can affect satellite systems in all operating bands, is then described. The section concludes with a comprehensive description of propagation databases, including points of contact and electronic addresses.

The principal topics and associated subsection numbers for Section 1 are listed below.

| Section | Topic |
|---|---|
| 1.0 | Introduction to Section 1 |
| 1.1 | Overview: Propagation Effects on Satellite Communications |
| 1.2 | Ionospheric Effects |
| 1.3 | Tropospheric Effects |
| 1.4 | Radio Noise |
| 1.5 | Propagation Data Bases |
| 1.6 | References – Section 1 |

## 1.1 OVERVIEW: PROPAGATION EFFECTS ON SATELLITE COMMUNICATIONS

The satellite communications industry is expanding rapidly in many areas and new applications are being introduced at an unprecedented pace. Systems are under development for global mobile satellite communications operating in the L and S bands. The traditional fixed satellite service is in the process of a "frequency evolution", moving from the frequency bands that have been in use for decades, C-Band, X-band, SHF, etc., to the allocated bands above 10 GHz. These new bands, designated as $K_u$ band (12-18 GHz), $K_a$ band (20-40 GHz), and Q/V-band (40-50 GHz), offer wider bandwidths, higher data rates, and smaller component sizes, as well as vastly improved anti-jam performance for secure communications applications. The next decade will see the introduction of the first commercial non- geosynchronous orbit (NGSO) constellations providing mobile services, fixed services, and hybrid systems providing a wide array of personal communication and “bandwidth on demand” services.

The expected advantages of these new applications and new frequency bands can be offset very quickly however, by the realities of increased propagation problems as increased mobile communications capabilities are desired, and/or the frequency of operation is increased. Mobile systems operating in the bands below 3 GHz are subject to ionospheric effects, including scintillation and multipath fading. Fixed and mobile systems operating in the bands above 10 GHz can be seriously effected by rain in the path, and careful design and adequate "rain margins" are essential for successful system performance. There are other propagation mechanisms affecting Earth-space communications performance that are also of concern to the systems designer and planner. These include group delay, polarization rotation, gaseous attenuation, cloud and fog attenuation, rain and ice depolarization, and angle-of-arrival variations. And finally, satellite communications systems are subject to radio noise, which must be accounted for in the design and performance of satellite links.

### 1.1.1 Developments Since Last Handbook

Several major developments in satellite communications and the study of propagation effects have occurred since publication of the prior NASA handbooks. New propagation measurement campaigns have been completed or are in progress, providing new data for the evaluation of link degradations on satellite links. New propagation models and prediction techniques are available, covering the traditional propagation effects along with several new areas. New satellite applications have been thrust into the forefront of the satellite communications industry, requiring new approaches for the evaluation of propagation effects. The proliferation of new and competing applications in the frequency bands allocated to space communications has increased the importance and priority of understanding spectrum sharing and interference mitigation. Propagation conditions are a critical component of a viable sharing and interference process. Each of these areas is discussed further below.

**New Propagation Measurements.** New propagation measurements in several frequency bands have been accomplished since the last handbook publication. Exhibit 1.1-1 lists some of the

satellites which had beacons on board specifically intended for the evaluation of propagation effects. Propagation data has also been developed from other sources including terrestrial links, tracking beacons, and from direct measurement of information bearing signals. For example, land mobile propagation data in the 1.5 GHz region was obtained in the Eastern U.S. from MARECS-B2 and in Australia from ETS-V and INMARSAT.

| Satellite | Organization | Launch Date | Frequency (GHz) | Polarization | Measurement Region(s) |
|---|---|---|---|---|---|
| Olympus | ESA | 1989 | 12.5<br>19.7<br>29.7 | LP<br>Dual Switched LP @933 Hz<br>LP | Europe<br>And<br>Eastern U.S. |
| Italsat F1 | Italy | 1991 | 18.685<br>39.592<br>49.49 | Dual LP<br>CP with ± 500 MHz sidebands<br>Dual switched LP @ 933 Hz | Europe |
| ACTS | NASA | 1993 | 20.185<br>27.5 | LP<br>LP | CONUS<br>Alaska<br>Canada |

Exhibit 1.1-1
Recent Satellites Providing Propagation Measurements

**New Propagation Models and Prediction Techniques.** Propagation research since publication of the last handbooks has resulted in the development and publication of propagation prediction models in several new areas. These include:

- Tropospheric Scintillation
- Cloud Attenuation and Scintillation
- Ice Depolarization
- Wet Surface Effects
- Combined Effects

In addition, extensive modeling updates and revisions have been developed for the traditional propagation factors such as

- Rain Attenuation
- Atmospheric Gaseous Attenuation
- Ionospheric Scintillation
- Frequency Scaling
- Worst Month, and
- Site Diversity.

This handbook provides detailed step-by-step procedures for all of the new models and for the updated procedures as provided by the authors. Recommendations for which models to use for specific applications are also provided.

**New Satellite Applications.** . A wide array of new satellite applications has appeared in the decade since publication of the last handbooks. Each application has unique design and performance characteristics requiring new approaches for the evaluation of propagation effects. Also, the extension of satellite communications to non-geosynchronous orbit (NGSO) constellations has added a new level of concern on the proper evaluation of link conditions for proper system operation.

A listing of some of the new applications includes:

- Low-margin VSAT systems in the Ku-band
  - Typical systems have margins of 1 to 3 dB
  - Global deployment
- Direct Broadcast Satellites in the Ku-band
  - Multi-channel digital systems
  - Systems in the U.S., Europe, Japan
- Rapid development of the Ka-band for a range of multi-media applications
  - Filings to U.S. FCC; 14 for GSO, 3 for NGSO
  - Applications to ITU: 21 countries, 380+ satellites for GSO
    8 countries, 1200+ satellites for NGSO
  - GSO/FSS, NGSO/FSS/MSS, NGSO/MSS Feeder Links
- "Big LEO" Mobile Satellite Personal Communications
  - NGSO (LEO, MEO, HEO) constellations, 10 to 66 satellites
  - Service links: 1610-1626.5 MHz uplink
    2483.5-2500 MHz downlink
  - CDMA, TDMA/FDMA access techniques
- "Little LEO" Paging, Messaging Services
  - NGSO (LEO) constellations, 20 to 24 satellites
  - Service links: 137-138, 148-149.9, 400-401 MHz
- Initial systems defined for Q/V-band
  - 37.5 - 40.5 GHz downlink
  - 47.2 - 50.2 GHz uplink
  - 12 organizations (14 systems) filed with U.S. FCC in 9/97
  - Broadband multimedia applications, VSAT and direct to home
  - GSO, NGSO, mixed systems proposed.

Each of these applications has unique propagation characteristics. This handbook provides the tools to evaluate these systems, and the "roadmaps" to adequately identify and analyze the specific propagation factors important to the application.

**Increased Emphasis on Spectrum Sharing and Interference Mitigation**. The explosion in global satellite systems has required the system designer to include spectrum sharing as a critical

part of the system design. The radio spectrum is a fixed and limited resource, and the available bandwidth in most of the bands allocated for satellite applications is not adequate for all of the systems under consideration for deployment. Sharing is required, and often, if band segmentation cannot be employed, mitigation techniques including power control and exclusion zones have to be evaluated. Also, the sharing of GSO and NGSO systems operating in the same allocated bands adds another critical element to the spectrum sharing process.

The inclusion of the appropriate propagation effects in the desired and the interfering links is essential to an acceptable solution. The models and procedures described in this handbook are elements of a comprehensive spectrum sharing process that often includes simulations and analytic procedures of the full range of applications and satellite orbits.

### 1.1.2 Frequency Dependence

The operating frequency of the space link is the critical factor in determining the type and severity of impairments introduced by the Earth's atmosphere. A radiowave will propagate from the Earth's surface to outer space provided its frequency is high enough to penetrate the ***ionosphere***, which is the ionized region extending from about 50 km to roughly 2000 km above the surface. Regions (or layers) in the ionosphere, designated D, E, and F, in order of increasing altitude, act as reflectors or absorbers to radiowaves at frequencies below about 30 MHz, and space communications is not feasible. As the frequency is increased, the reflection properties of the E and F layers are reduced and the signal can penetrate the ionosphere. Radiowaves above about 30 MHz will propagate through the ionosphere, however, the properties of the wave could be modified or degraded to varying degrees depending on frequency, geographic location, and time of day. Ionospheric effects tend to become less significant as the frequency of the wave increases, and above about 3 GHz the ionosphere is essentially transparent to space communications, with some notable exceptions which will be discussed later.

Space communications transmissions will proceed unimpeded as the frequency of transmission is increased up to frequencies where the gaseous constituents of the ***troposphere***, the region from Earth's surface up to 10-20 km in altitude, primarily oxygen and water vapor, will absorb energy from the radiowave. At certain specific ***absorption bands*** where the radiowave and gaseous interaction are particularly intense, space communications are severely limited. It is in the ***atmospheric windows*** between absorption bands that practical earth-space communications have developed, and it is in these windows that we will focus our attention in our study of radiowave propagation effects.

Section 1.2 covers ionospheric propagation, and Section 1.3 will look at the effects of tropospheric conditions on the radiowave transmission. Section 1.4 describes the impact of radio noise on satellite communications links. Section 1.5 presents a comprehensive summary of propagation databases available for the evaluation of communications systems.

## 1.2 IONOSPHERIC EFFECTS

### 1.2.1 Introduction

The ionosphere is a region of ionized gas or plasma that extends from roughly 50km to a not very well defined upper limit of about 500 km to 2000 km about the Earth's surface. The ionosphere is ionized by solar radiation in the ultraviolet and x-ray frequency range and contains free electrons and positive ions so as to be electrically neutral. Only a fraction of the molecules, mainly oxygen and nitrogen, are ionized in the lower ionosphere, and large numbers of neutral molecules are also present. It is the free electrons that affect electromagnetic wave propagation for satellite communications.

Because different portions of the solar spectrum are absorbed at different altitudes, the ionosphere consists of several layers or regions of varying ion density. By increasing altitude, these layers are known as the D, E, and F layers, Exhibit 1.2.1-1. The layers are not sharply defined since the transition from one to the other is generally gradual with no very pronounced minimum in electron density in between. Representative plots of electron density are shown in Exhibit 1.2.1-2. Two good sources of further information about the ionosphere are those by Rishbeth and Garriot (1969) and Ratcliffe (1972).

The production of ions requires direct solar radiation; therefore, the density of charged particles in the ionosphere changes from day to night. More specifically, the D and E regions weaken and eventually disappear during the night but reappear during the day. The F region, on the other hand, is present both day and night. This is because the low density of the atmosphere in this region makes it hard for the positively charged ions and negatively charged electrons to find each other - hence the F layer, although weak in the early morning hours, remains at all times.

The density of electrons in the ionosphere also varies as a function of geomagnetic latitude, diurnal cycle, yearly cycle, and solar cycle (among others). Most U.S. ground station-satellite paths pass through the mid-latitude electron density region, which is the most homogeneous region. Canadian stations may be affected by the auroral region electron densities which are normally more irregular. A discussion of the effects is included in ITU-R Recommendation PI.531-4 (1997).

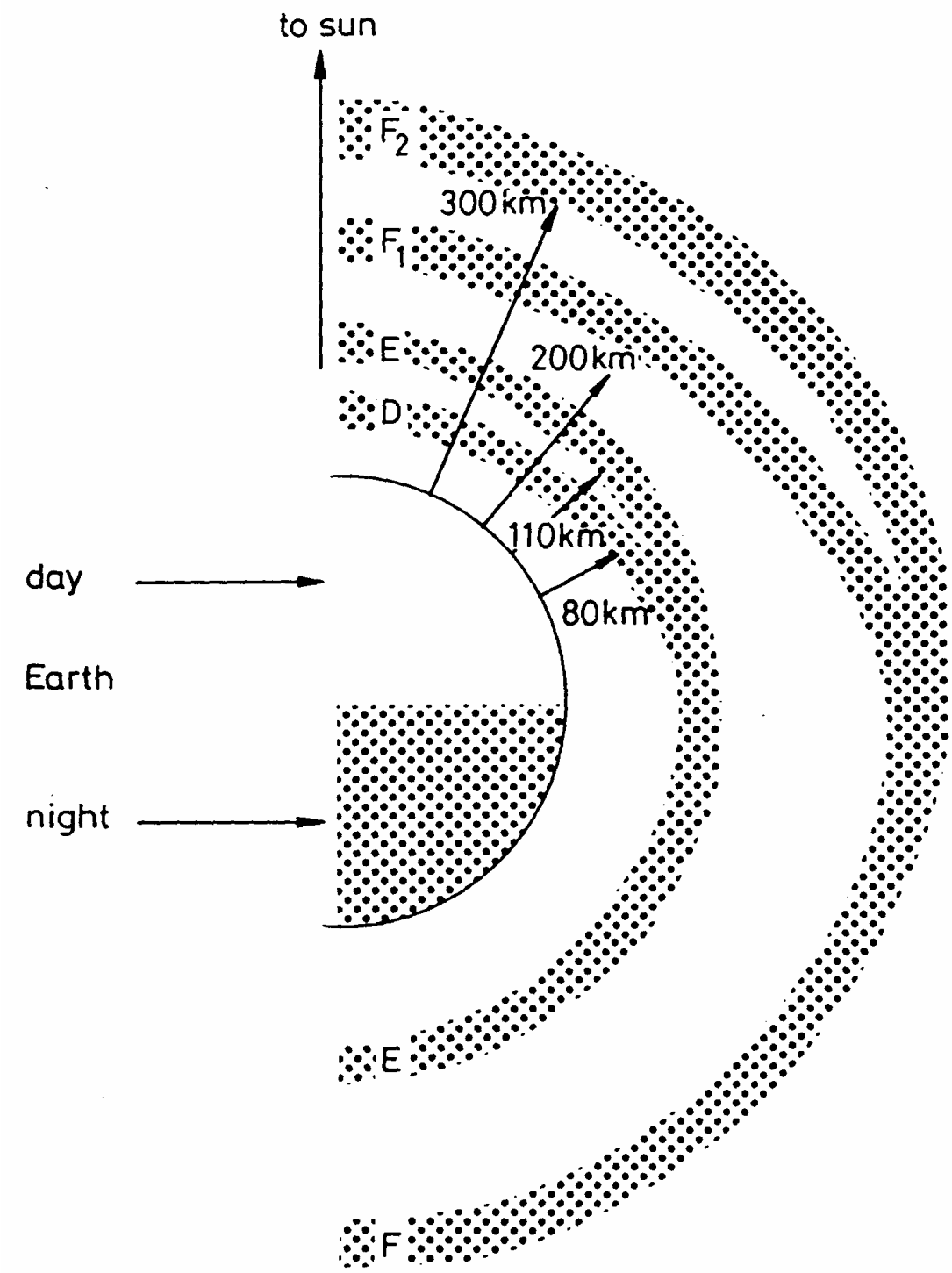


Exhibit 1.2.1-1
Ionospheric regions as a function of height above the Earth's surface.
*[Source: CCIR Rep. 725-1, (1986c)]*

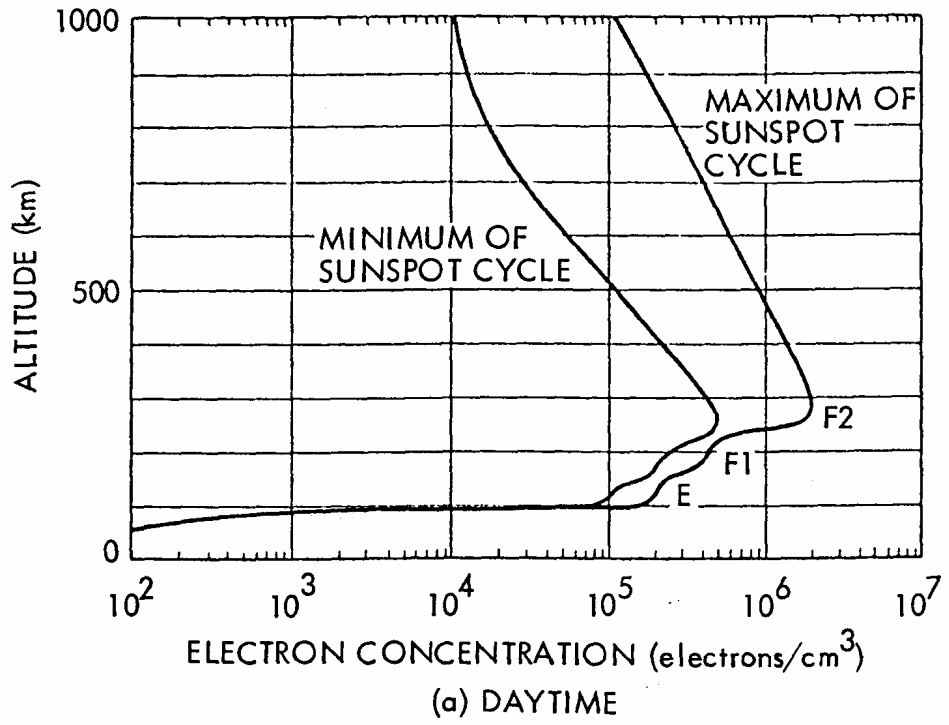


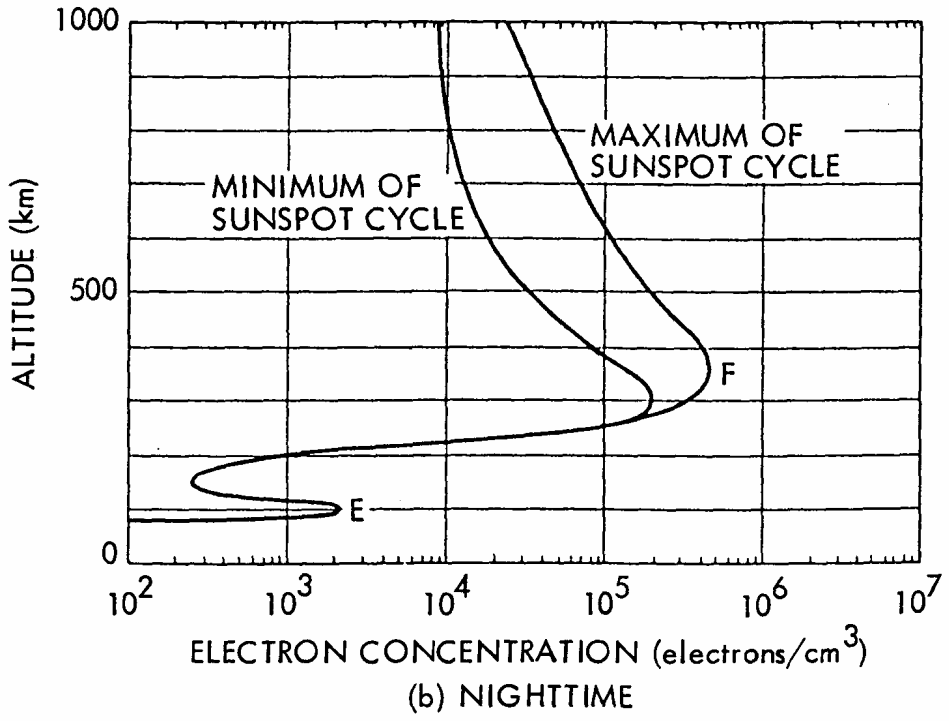


Exhibit 1.2.1-2
Electron density distribution at the extremes of the sunspot cycle (from Hanson, W.B., "Structures of the Ionosphere" in Johnson, F.S. (ed.), Satellite Environment Handbook, Stanford U. Press, 1965).
*[Source: Flock (1987), Fig 1.4]*

#### 1.2.1.1 D Region

The D region, the lowest of the ionospheric layers, extends from approximately 50 to 90 km with the maximum electron density of about $10^9$ /$m^3$ occurring between 75 and 80 km in the daytime. At night electron densities throughout the D region drop to very small values.

As the electron concentration in the D region is very low, it tends to have little effect on high frequency waves. However, attenuation in the ionosphere occurs mainly through collisions of electrons with neutral particles, and as the D region is at a low altitude many neutral atoms and molecules are present and the collision frequency is high. Therefore transmissions in the AM broadcast band are highly attenuated in the day time in the D region, but distant reception becomes possible at night when the D region disappears.

#### 1.2.1.2 E Region

The E region extends from about 90 to 140 km, and the peak electron concentration occurs between about 100 and 110 km. Electron densities in the E region vary with the 11 year sunspot cycle and may be about $10^{11}$ /$m^3$ at the minimum of the solar cycle and about 50 percent greater at the peak of the cycle. Electron concentrations drop by a factor of about 100 at night. Intense electrical currents flow in the equatorial and auroral ionosphere at E region altitudes, these currents being known as equatorial and auroral electrojets. Radio waves are scattered from electron density structure associated with the electrojets at frequencies up to more than 1000 MHz. Backscatter echoes from the auroral electrojets indicate the region of occurrence of aurora and are referred to as radio aurora. The phenomena of sporadic E, thin sporadic, often discontinuous layers of intense ionization, occurs in the E region, at times with electron densities well above $10^{12}$/$m^3$. The E layer is useful for communications, as HF waves may be reflected from the E layer at frequencies that are a function of time of day and period of the sunspot cycle. By causing interference between VHF stations, sporadic E tends to be a nuisance.

#### 1.2.1.3 F Region

The F region has the highest electron densities of the normal ionosphere. In the daytime in normally consist of two parts, the F1 and F2 layers. The F1 layer largely disappears at night but has peak densities of about 1.5 x $10^{11}$ /$m^3$ at noon at the minimum of the solar cycle and 4 x $10^{11}$ /$m^3$ at noon at the peak of the solar cycle. The F2 layer has the highest peak electron densities of the ionosphere and the electron densities there remain higher at night than in the D and E regions. The peak electron density is in the 200 to 400 km height range and may be between about 5 x $10^{11}$ /$m^3$ and 4 x $10^{11}$ /$m^3$ at night, reaching a deep diurnal minimum near dawn. Reflection from the F2 layer is the major factor in HF communications which formerly handled a large fraction of long distance, especially transoceanic, communications.

### 1.2.1.4 Plasmasphere and Magnetosphere

The upper limit of the ionosphere is not precisely defined but for the purposes of space communications may be taken as 2000 km, this being the upper limit for significant Faraday rotation. Above the ionosphere is the plasmasphere or protonosphere, which has an electron content of about 10 percent of the ionospheric content in the daytime and up to 50 percent of ionospheric content at night, as defined along an earth space path.

The Earth's magnetic field is confined inside an elongated cavity in the solar wind, that extends to about 10 earth radii in the direction towards the Sun and has a long tail extending to about 50 earth radii or farther in the opposite direction. The boundary of this cavity is known as the magnetopause, and the region inside the boundary, above the ionosphere, is known as the magnetosphere. The magnetosphere can be defined as the region in which the Earth's field dominates the motion of charged particles, in contrast to the ionosphere where collisions play a major role. The Van Allen radiation belts, discovered on 1958 by use of Explorer1, are in the magnetosphere, The plasmasphere is usually considered to be above the ionosphere ( or above 2000 km). The plasmasphere is bounded on the upper side at about 4 earth radii at the equator by the plasmapause where the plasma density drops by a factor of 10 to 100 or from about $10^8$ $/m^3$ to $10^6$ $/m^3$.

### 1.2.1.5 Irregularities and Disturbed Conditions

Consideration of the ionosphere can be separated into the quiet and disturbed ionosphere. Ionospheric disturbances and irregularities occur at times of magnetic storms and essentially every night to some degree in the auroral and equatorial ionospheres. Both propagation in the quiet ionosphere and the effects of disturbances and irregularities are considered in the following sections.

### 1.2.1.6 Propagation Effects

Signals with frequencies above the ionospheric penetration frequency and up to about 10 GHz are modified by the large- and small-scale variations of electron density in the ionosphere. Ionospheric effects on a propagating signal include scintillation, absorption, variation in the direction of arrival, propagation delay, dispersion, frequency change and polarization rotation (ITU-R, P.531-4, 1997). The following definitions give a brief introduction to these propagation factors (Ippolito, 1986). A more detailed presentation of these effects is presented in later sections.

**Faraday Rotation** is a rotation of the polarization sense of a radio wave, caused by the interaction of a radio wave with electrons in the ionosphere in the presence of the Earth's magnetic field. For satellite systems that employ circular polarization, Faraday rotation is not a concern; however, this condition can seriously affect VHF space communication systems that

use linear polarization. A rotation of the plane of polarization occurs because the two rotating components of the wave progress through the ionosphere with different velocities of propagation. Faraday rotations of 30 revolutions (10,800 degrees) can occur at 100MHz. The effect decreases with increasing frequency by the reciprocal of the frequency squared.

**Group Delay (or Propagation Delay)** is a reduction in the propagation velocity of a radio wave, caused by the presence of free electrons in the propagation path. The group velocity of the radio wave is retarded (slowed down), thereby increasing the travel time over that expected for a free space path. This effect can be extremely critical for radio navigation or satellite ranging links that require an accurate knowledge of range and propagation time for successful performance. Group delay will be about 25 microseconds at 100 MHz for an earth-space path at 30-degree elevation angle, and is approximately proportional to the reciprocal of the frequency squared.

**Angle of Arrival Variations** are changes in the direction of propagation of radio waves caused by refractive index changes in the transmission path. Angle of arrival variations are a refraction process and generally are only observable with large aperture antennas (10 meters or more) and at frequencies well above 10GHz. The angle of arrival change results in an apparent shift in the location of satellite position and can be compensated for by a repointing of the antenna.

**Multipath** occurs when a transmitted radio wave reaches the receiving antenna by two or more propagation paths. Multipath can result from refractive index irregularities in the ionosphere.

**Coherence Bandwidth** is an upper limit on the information bandwidth or channel capacity that can be supported by a radio wave, caused by the dispersive properties of the atmosphere, or by multipath propagation. The coherence bandwidth for typical space communication frequencies is one or more gigahertz.

**Absorption** is a reduction in the amplitude (field strength) of a radio wave caused by an irreversible conversion of energy from the radio wave to matter in the propagation path. Absorption due to the ionosphere is dependent on geographic location and time of day.

**Ionospheric Scintillation** refers to the rapid fluctuation of the amplitude, phase, polarization, and angle-of-arrival caused when radio waves pass through electron density irregularities in the ionosphere. Scintillation effects have been observed on links from 10 MHz to 10 GHz, with the bulk observations of amplitude scintillation in the VHF (30-300 MHz) band (CCIR Rep. 263-9, 1986b and ITU-R Rec. P.531-4, 1997). The scintillation can be very severe and can determine the practical limitation for reliable communications under certain atmospheric conditions. Ionospheric scintillation is most severe for transmission through equatorial, auroral, and polar regions; and during sunrise and sunset periods of the day.

**Fading** is the variation of the amplitude (field strength) of a radio wave caused by changes in the transmission path (or paths) with time. The terms fading and scintillation are often used interchangeably; however, fading usually describes slower time variations, on the order of seconds or minutes, while scintillation refers to more rapid variations, on the order of seconds in duration.

The frequency of a radio wave is a critical factor in determining what impairments will be introduced by the Earth's ionosphere. A radio wave will only propagate from the Earth's surface to outer space provided that its frequency is high enough to penetrate the ionosphere or more specifically if its frequency is much larger than the plasma frequency of the ionosphere. At frequencies below about 30 MHz, the layers of the ionosphere act as reflectors or absorbers, and space communications is not possible. Above 30 MHz, the reflection properties of the E and F layers decrease, and radio waves can propagate through the ionosphere. However, the properties of the wave may be degraded depending on the frequency, geographic location, and time of day. The ionospheric effects on the radio wave decrease with increasing frequency. Above about 10 GHz, the ionosphere is essentially transparent to space communications. Exhibit 1.2.1.6-1 provides a summary of ionospheric effects and their magnitude as a function of frequency. These effects include, Faraday rotation, time delay, refraction, attenuation, variation in direction of arrival, and refraction. All tend to decrease as a function of $1/f^2$. Note that by 10 GHz, all of these effects are for the most part negligible relative to other system error budgets. The one ionospheric effect which might influence wide bandwidth systems operating above 10 GHz is phase dispersion.

Two main characteristics of the ionosphere contribute to the degradation of radio waves: background ionization quantified by the total electron content (TEC) along the propagation path and irregularities along the path. The degradations related to TEC include Faraday rotation, group delay, dispersion, Doppler frequency shift, variation in direction of arrival, and absorption. The main effect attributed to ionization irregularities is scintillation. These factors will be described in more detail in the following sections.

| Effect | Frequency dependence | 100 MHz | 300 MHz | 0.5 GHz | 1 GHz | 3 GHz | 10 GHz |
|---|---|---|---|---|---|---|---|
| Faraday Rotation | $1/f^2$ | 30 rot. | 3.3 rot | 1.2 rot | $108^o$ | $12^o$ | $1.1^o$ |
| Excess time delay | $1/f^2$ | 25 μs | 2.8 μs | 1 μs | 0.25 μs | 0.028 μs | 0.0025 μs |
| Refraction | $1/f^2$ | $\leq 1^o$ | <7 min | <2.4 min | ≤ 0.6 min | <4.2 s | ≤ 0.36 s |
| Variation in direction of arrival | $1/f^2$ | 20 min | 2.2 min | 48 s | 12 s | 1.32 s | 0.12 s |
| Absorption (auroral and polar cap) | $\sim 1/f^2$ | 5 dB | 1.1dB | 0.2 dB | 0.05 dB | $6x\ 10^{-3}$dB | $5x\ 10^{-4}$dB |
| Absorption (mid latitude) | $1/f^2$ | <1dB | 0.1dB | <0.04dB | <0.01dB | $<10^{-3}$dB | $<10^{-4}$dB |
| Dispersion | $1/f^3$ | 0.4 ps/Hz | 0.015 ps/Hz | 0.0032 ps/Hz | 0.0004 ps/Hz | $1.5x10^{-5}$ ps/Hz | $4x10^{-7}$ ps/Hz |

Exhibit 1.2.1.6-1
Estimated maximum ionospheric effects in the United Sates for one-way paths at an elevation angle of about 30 degrees.
*[Source: Flock (1987), Table 2.2]*

### 1.2.2 Effects Due to Background Ionization

This section provides information on the propagation degradation introduced by background ionization of the ionosphere. It begins with a description of the variation of the electron content and the effect of the Earth's magnetic field. The second half of the section describes how these factors affect radio waves.

#### 1.2.2.1 Electron Content of Ionosphere and Plasmasphere

As stated earlier, the integrated or total electron content (TEC) along the ray path from transmitter to receiver is very significant in determining ionospheric effects on communication signals. The total electron content (TEC) along a path is the number of electrons in a column one square meter in cross section (electrons/$m^2$ or el/$m^2$) that coincides in position with the path and is given by

$$\text{TEC} = \int n \, dl \qquad (1.2.2.1\text{-}1)$$

where $n$ is the density of electrons (electrons/$m^3$) and $l$ is the propagation path. The TEC of the ionosphere has a pronounced diurnal variation and also varies with solar activity, especially with geomagnetic storms that may result from solar activity. Faraday rotation, excess time delay and associated range delay, phase advance, and time delay and phase advance dispersion are directly proportional to TEC. Most ionospheric effects, in fact, tend to be proportional to TEC.

Faraday rotation measurements on satellite to Earth paths provide values of the electron content of the ionosphere, and group delay measurements give the total electron content (TEC) along the entire path. By taking the difference of the total and ionospheric values, the electron content of the plasmasphere or protonosphere is obtained. Most electron content data refer to ionospheric values, but data for the plasmasphere as well have been reported by Davies, Hartman, and Leitinger (1977), Klobuchar and Working Group (1978), and Davies (1980).

The ionospheric TEC shows pronounced diurnal variations consistent with the production of ionization by solar radiation in the daytime and the decay of ionization at night. Extreme values of the ionospheric TEC are given by Klobuchar (1978) as $10^{16}/m^2$ and $10^{19}/m^2$; $10^{18}/m^2$ is generally regarded as the maximum zenith value. Zenith values of ionospheric TEC refer to the electron content of a vertical column having a cross section of one square meter and extending to the height of the plasmasphere. Representative curves showing the diurnal variation TEC for an invariant latitude of 54 deg are given in Exhibit 1.2.2.1-1. Invariant latitude equals $\cos^{-1}(1/L)^{½}$ and refers to the magnetic field line that is at a distance L, measured in earth radii, from the center of the Earth at the magnetic equator. The data were obtained at Sagamore Hill, MA using 136 MHz signals from ATS-3.

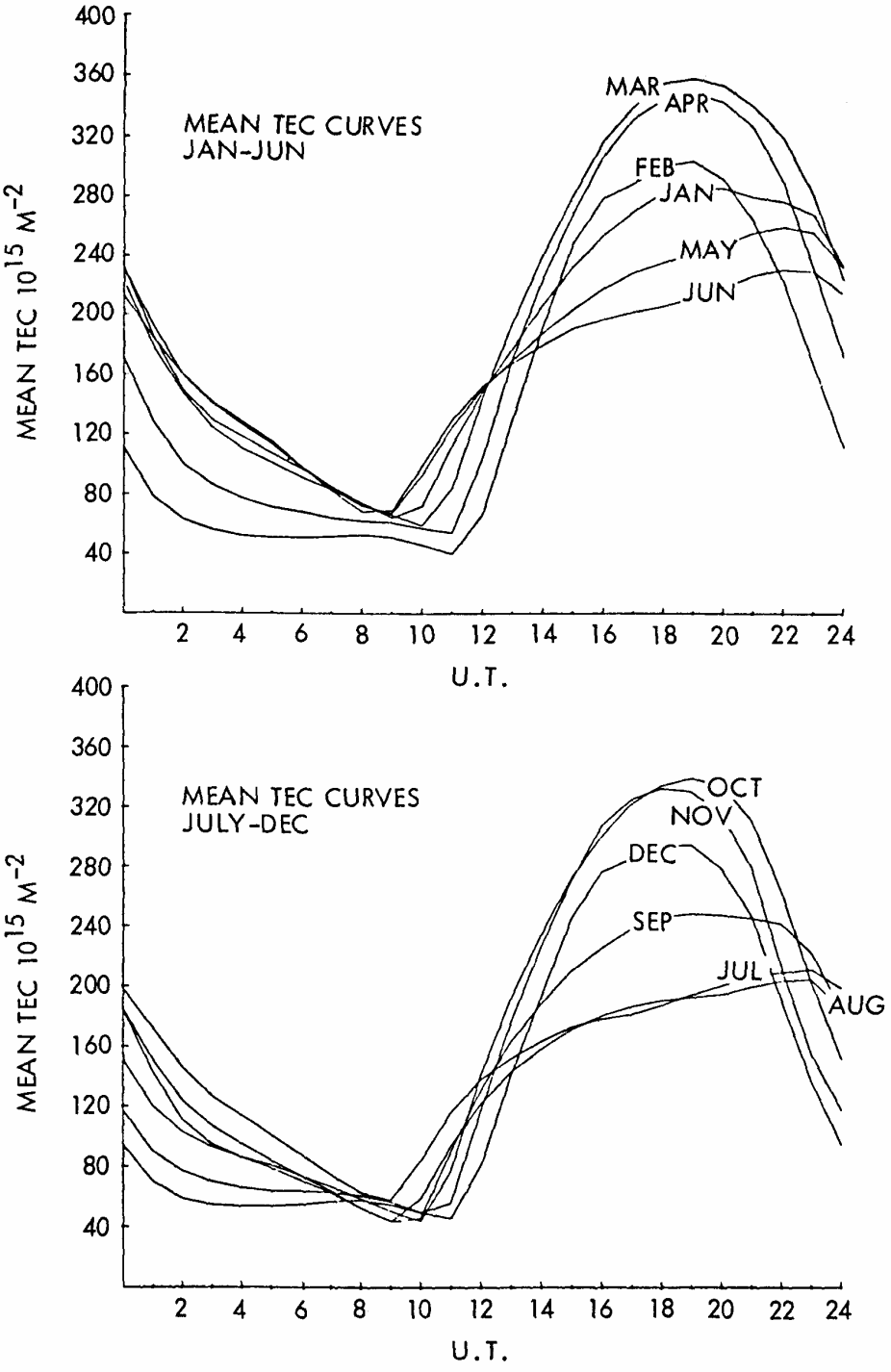


Exhibit 1.2.2.1-1
Diurnal variations in TEC, mean monthly curves for 1967 to 1973 as obtained at Sagamore Hill, MA (after Hawkins and Klobuchar, 1974).
*[Source: Flock (1987), Figure 2.6]*

#### 1.2.2.2 Propagation in Homogeneous Plasmas

The Earth's ionosphere is a partially ionized gas or plasma, which is rendered anisotropic by the presence of the Earth's magnetic field. The concept of characteristic waves is important in considering the propagation of electromagnetic waves in such a medium. Characteristic waves are the waves that propagate without changing their polarization. Changing from right circular to left circular polarization or the direction of linear polarization, for example, constitutes a change in polarization. The following is a brief treatment of propagation in homogeneous plasma. For a more thorough analysis, the reader should refer to Budden(1961, 1985), Davies (1965, 1969, 1989), Kelso (1964), Ratcliffe (1972) and Flock(1979).

##### 1.2.2.2.1 Earth's Magnetic Field

The Earth's field is roughly that of a magnetic dipole, inclined by about 12 degrees with respect to the rotational axis, for which the field decreases as the cube of the radius or distance from the center of the Earth. Figure 4 shows field values given by a dipole model. For a more accurate model, reference can be made to the International Geomagnetic Reference Field (IGRF) model developed by a working group of IAGA ( The International Association of Geomagnetism and Aeronomy) (see Barton, 1996, Langel, et al, 1988). This model is an empirical representation of the Earth's magnetic (main) field based on all available data sources and includes extrapolation ahead, currently to the year 2000. The coefficients of the IGRF models and computer programs for synthesizing field values are available in the United States from the National Space Science Data Center (NSSDC) on diskette or by anonymous FTP and can be run directly on their World Wide Web page.

Hughes STX Corp.
NSSDC Project
7701 Greenbelt Rd., Suite 400
Greenbelt, MD 20770
World Wide Web: http://www.mssdca.gsfc.nasa.gov

Ionospheric effects, such as Faraday rotation, require an accurate value of the magnetic field to predict their effect on radio waves propagating through the ionosphere.

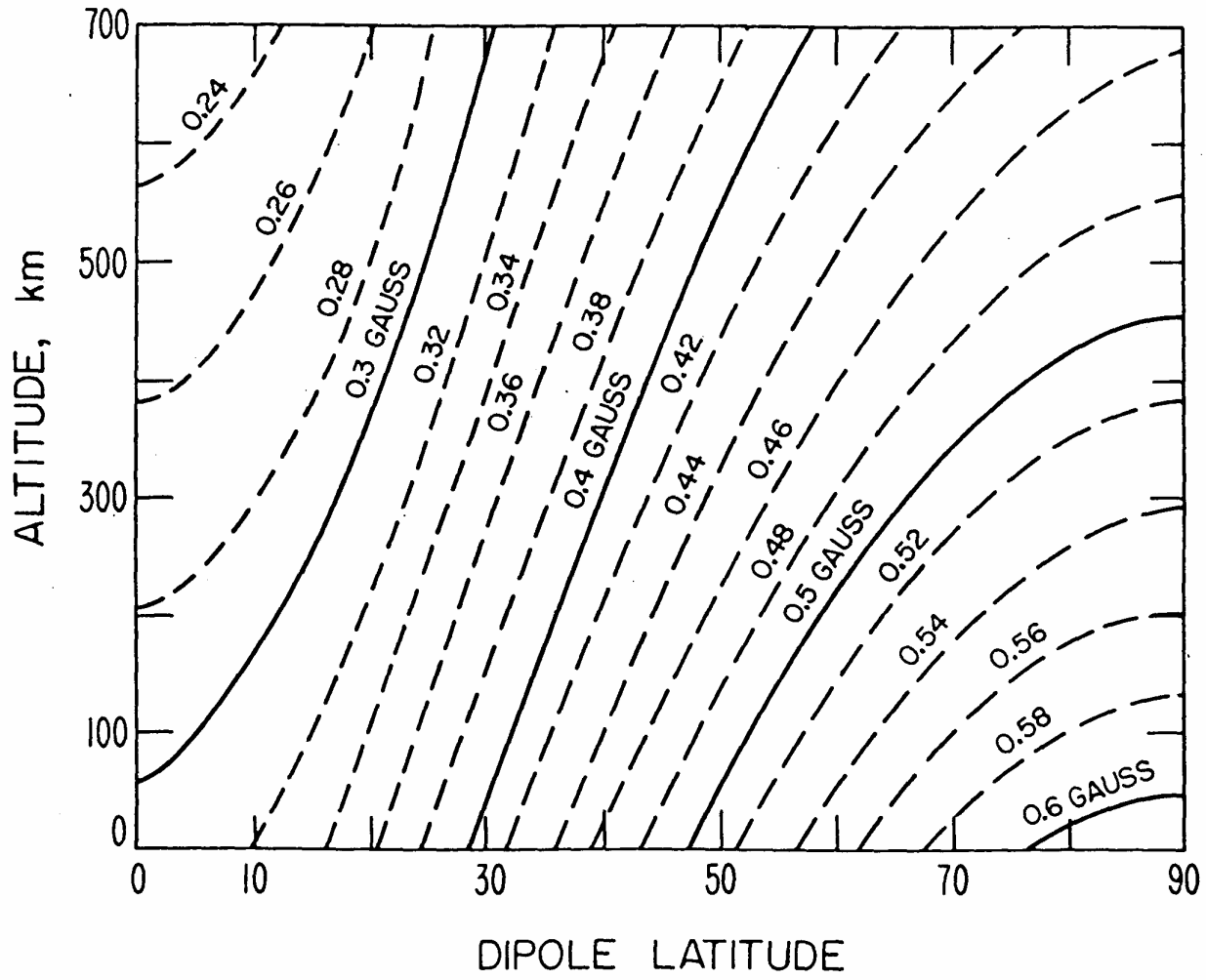


Exhibit 1.2.2.2-1
Total intensity of the Earth's magnetic field as a function of altitude and dipole latitude, assuming an earth-centered dipole of magnetic moment $M = 7.95 \times 10^{25}$ gauss $cm^3$ (after Smith, 1974).
*[Source: Flock (1987), Figure 2.2]*

### 1.2.2.2.2 Characteristic Wave

The nature of the characteristic waves that propagates in an anisotropic plasma such as the Earth's ionosphere can be determined by the application of Maxwell's equations. It develops that there are two characteristic waves and that the parameters of the characteristic waves depend upon the direction of propagation with respect to the Earth's magnetic field: the angle $\theta_B$ of Exhibit 1.2.2.2-2.

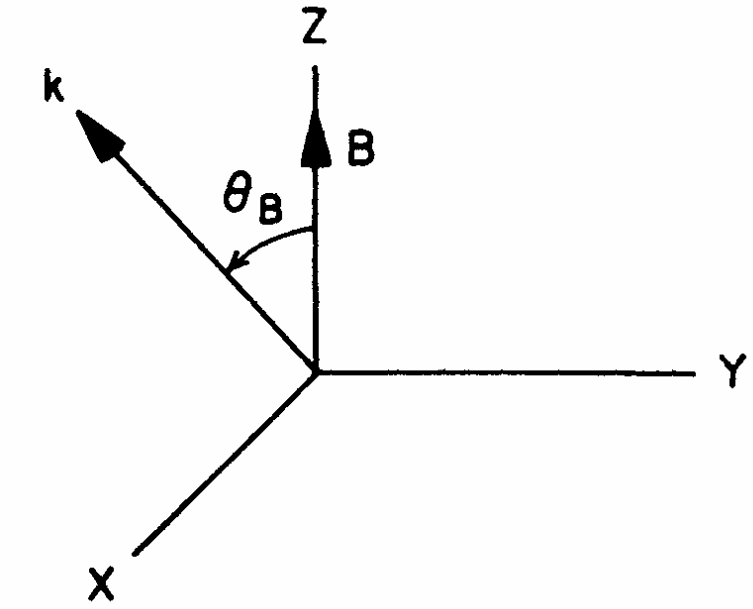


Exhibit 1.2.2.2-2
Coordinate system for considering propagation at an angle $\theta_B$ from the direction of Earth's field
*[Source: Flock (1987), Figure 2.1]*

**Parallel Propagation**

For propagation parallel to the Earth's field B ($\theta_B = 0°$) in the lossless case, the two characteristic waves are left and right circularly polarized and have indices of refraction $n_l$ and $n_r$ given by

$$n_l^2 = K_l = 1 - \frac{\omega_p^2}{\omega\left(\omega + \omega_B\right)} \qquad (1.2.2.2\text{-}1)$$

and

$$n_r^2 = K_r = 1 - \frac{\omega_p^2}{\omega\left(\omega - \omega_B\right)} \qquad (1.2.2.2\text{-}2)$$

$K_l$ and $K_r$ are the relative dielectric constants for the left and right circularly polarized waves. The quantity $\omega$ is the angular frequency of the wave and equals $2\pi f$ where f is frequency in Hz, and $\omega_B$ is the angular gyrofrequency of the electrons in the plasma and is given by

$$\omega_B = \frac{-qB}{m} \qquad (1.2.2.2\text{-}3)$$

where B is the Earth's magnetic field in Wb/m$^2$, q= -e = - 1.6022x10$^{-19}$ C is the charge of the electron, and m is the mass of the electron (9.1096x10$^{-31}$ kg).

The quantity $\omega_p^2$ is the angular plasma frequency squared and can be found by using

$$\omega_p^2 = Nq^2 / \left(m\varepsilon_0\right) \qquad (1.2.2.2\text{-}4)$$

where N is electron density (el/m$^3$), and $\varepsilon_o$ is the electric permittivity of empty space (8.854x10$^{-12}$ F/m). For practical applications it may be convenient to convert from angular frequency to frequency in MHz for propagation at HF and higher frequencies. To this end

$$\left(f_B\right)_{MHz} = 2.7992 \times 10^4 B \cong 2.8 \times 10^4 B \qquad (1.2.2.2\text{-}5)$$

with B in Wb/m$^3$, or $(f_B)_{MHz} \sim 2.8$ B with B in gauss. Also

$$\left(f_p\right)_{MHz} = 8.9788 \times 10^{-6} N^{1/2} \qquad (1.2.2.2\text{-}6)$$

with N the number of electrons per m$^3$. Then

$$n_l = \left[1 - \frac{f_p^2}{f\left(f + f_B\right)}\right]^{1/2} \qquad (1.2.2.2\text{-}7)$$

$$n_r = \left[1 - \frac{f_p^2}{f\left(f - f_B\right)}\right]^{1/2} \qquad (1.2.2.2\text{-}8)$$

**Perpendicular Propagation**

For propagation perpendicular to the magnetic field ( $\theta_B$ = 90 deg) one characteristic wave has its electric field intensity vector directed along the z axis of Exhibit 1.2.2.2-2. The index of refraction $n_O$ and relative dielectric constant $K_O$ in this case are given by

$$n_0^2 = K_0 = 1 - \omega_p^2 / \omega^2 = 1 - f_p^2 / f^2 \qquad (1.2.2.2\text{-}9)$$

which also apply for the case of no magnetic field. The subscript o stands for ordinary; the ordinary wave is unaffected by the magnetic field for perpendicular or transverse propagation. If the electric field intensity is in the y direction in Exhibit 1.2.2.2-2 (or in general perpendicular to B), the situation is somewhat more complicated. In this case, the index of refraction $n_X$ and the relative dielectric constant $K_X$ are given by

$$n_x^2 = K_x = K_l K_r / K_\perp \qquad (1.2.2.2\text{-}10)$$

where

$$K_\perp = 1 - \frac{\omega_p^2}{\omega^2 - \omega_p^2}$$

This wave is referred to as the extraordinary wave. The two characteristic waves for propagation perpendicular or transverse to the magnetic field are linearly polarized in the plane perpendicular to the direction of propagation, but it develops that for the extraordinary wave there is a component of electric field intensity in the direction of propagation (the x direction if the transverse component is in the y direction).

### 1.2.2.2.3 Role of Index of Refraction

The index of refraction n of an electromagnetic wave is by definition the ratio of c~2.9979x10$^8$m/s, the velocity of an electromagnetic wave in empty space, to $v_p$, the velocity of the wave in question in the medium. Thus

$$n = c / v_p \qquad (1.2.2.2\text{-}11)$$

The phase constant ß of an electromagnetic wave gives the phase lag of the wave with distance when used in

$$E = E_0 e^{-j\beta z} \qquad (1.2.2.2\text{-}12)$$

for the case of a wave propagating in the z direction and having an electric field intensity $E_o$ at a reference position where z = 0. The constant ß can be expressed in several ways as;

$$\beta = 2\pi / \lambda = \omega / v_p = \beta_0 n \qquad (1.2.2.2\text{-}13)$$

where λ is wavelength, and $ß_o$ is the phase constant of empty space. It was shown earlier that the two characteristic waves, for propagation either parallel or perpendicular to the magnetic field, have different values of index of refraction. Thus they have different phase velocities, phase constants, and wavelength.

### 1.2.2.2.4 Reflection and Refraction

**Reflection**

Examination of the expressions for relative dielectric constant, equation (1.2.2.2-9), for the ordinary wave for transverse propagation for example, reveals that it is possible for the dielectric constant to be negative and that the index of refraction can thus become imaginary. For $\omega > \omega_p$ in equation (9), $n_o$ is real, but, for $\omega < \omega_p$, $n_o$ is imaginary. An imaginary value of index of refraction determines that ß of equation (1.2.2.2-12) will also be imaginary so that, instead of a propagating wave as indicated in the equation, an evanescent condition will occur so that $E = E_o e^{-\alpha z}$ because the quantity -jß of equation (1.2.2.2-12) has become $-jß(-j|n|) = \alpha$. The different possibilities are summarized in Exhibit 1.2.2.2-3..

| ω | n | E(z) |
|---|---|---|
| $\omega > \omega_p$ | real | $E = E_o e^{-jßz}$ |
| $\omega = \omega_p$ | 0 | $E = E_o$ |
| $\omega < \omega_p$ | imaginary | $E = E_o e^{-\alpha z}$ |

Exhibit 1.2.2.2-3
Characteristics of n and E(z) Corresponding to Different Relative Values of ω and $\omega_p$

The condition $E = E_o e^{-\alpha z}$ of Exhibit 1.2.2.2-3 represents a field that attenuates with z, but the attenuation in this case is not dissipative. Instead it involves reflection and reversal of direction as suggested in Exhibit 1.2.2.2-4(b). In Exhibit 1.2.2.2-4, an increase of electron density with height in the ionosphere is assumed. The frequency ω is much greater than $\omega_p$ in Exhibit

1.2.2.2-4(a), and the ray path is essentially unaffected by the ionosphere, whether the path is vertical or oblique. In Exhibit 1.2.2.2-4(b) the condition $\omega < \omega_p$ is reached in the vertical path shown, and the ray is reflected. Exhibit 1.2.2.2-4(b) suggests the overall result, but the reflection process actually takes place over a range of heights, consistent with $E = E_o\, e^{-\alpha z}$, rather than abruptly at a particular level. Furthermore, if the evanescent region is of limited extent, and E still has a significant value at the far side of the region from the source, then a wave of diminished amplitude will be launched and will propagate beyond the evanescent region.

For the ordinary wave, $\omega_p$ plays the role of a critical frequency with propagation occurring for $\omega > \omega_p$ and not for $\omega < \omega_p$. The situation is similar to propagation in a metallic waveguide having a certain cutoff frequency $f_c$. In a waveguide propagation occurs for $f > f_c$ and an evanescent condition occurs for $f < f_c$. An evanescent section of waveguide can serve as a waveguide below cutoff attenuator. For the left and right circularly polarized waves, Equations (1.2.2.2-1) and (1.2.2.2-2) show that the condition

$$\omega_p^2 = \omega^2 + \omega\,\omega_B \text{ and } \omega_p^2 = \omega^2 - \omega\,\omega_B \qquad (1.2.2.2\text{-}14)$$

separate propagating and nonpropagating regions for the left and right circularly polarized waves, respectively.

The above discussion is idealized in that dissipative attenuation does occur to some degree in the ionosphere so that, for $\omega > \omega_p$, $E(z) = E_o\, e^{-\alpha z}\, e^{-j\beta z}$ where now $\alpha$ represents dissipative attenuation involving the conversion of electromagnetic energy into heat. The topic of absorption or dissipative attenuation is treated in section 1.2.2.5.

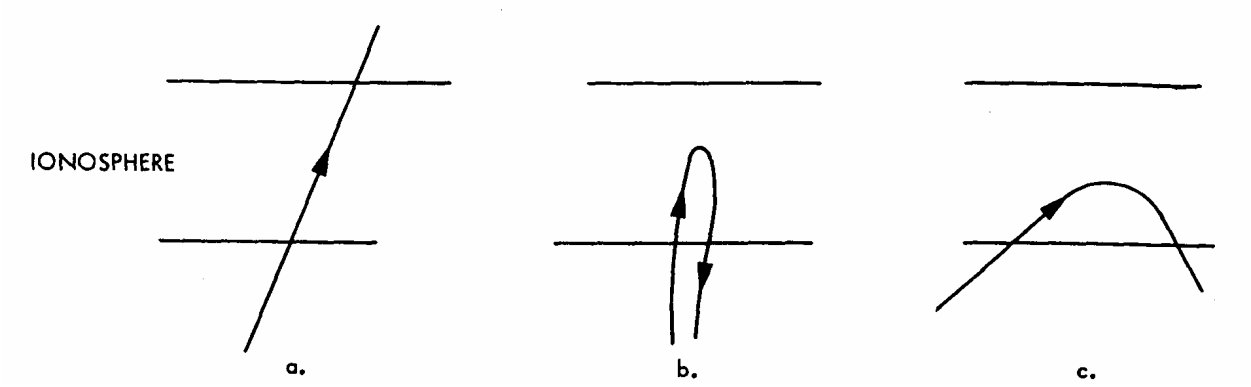


Exhibit 1.2.2.2-4
Ionospheric ray paths.
a. $\omega >> \omega_p$ throughout.
b. The condition $\omega < \omega_p$ is reached along the ray path.
c. Oblique incidence path.
*[Source: Flock (1987), Figure 2.3]*

**Refraction**

In Exhibit 1.2.2.2-4(c), a ray is obliquely incident upon the ionosphere and is shown to experience reflection. In this case $\omega$ is always greater than $\omega_p$, however, and while the overall result is usually viewed as reflection, the process is basically one of refraction. Applying Snell's law with the angle $\chi$ measured from the zenith and neglecting the Earth's curvature, $n \sin\chi = n_o \sin\chi_o$ where $x_o$ is the initial launch angle below the ionosphere, and $n_o$, the index of refraction of the troposphere, is essentially unity. At the highest point in the path of Exhibit 1.2.2.2-4(c), the angle $\chi$ is 90 deg. Therefore, at this point $n = \sin\chi_o$. For the ordinary wave and transverse propagation

$$n^2 = 1 - \left( f_p / f^2 \right) \qquad (1.2.2.2\text{-}15)$$

with $f_p$ the plasma frequency and f the operating frequency. Therefore

$$n^2 = \sin^2 \chi_0 = 1 - \left( f_p / f^2 \right) \qquad (1.2.2.2\text{-}16)$$

from which $\cos\chi_o = f_p/f$ and

$$f = f_p \sec \chi_0 \qquad (1.2.2.2\text{-}17)$$

This expression gives the maximum frequency, f, which will be reflected, or refracted, from or below a height where the plasma frequency is $f_p$ in the case of a wave having a launch angle of $x_o$. If $f_p$ is the peak plasma frequency in the ionosphere then f is the maximum usable frequency, in particular the maximum frequency that will be reflected for a launch angle $\chi_o$.

The above case can be considered to be an extreme example of refraction. At the frequencies of major interest in this handbook, ionospheric refraction will be of rather minor importance but will cause a slight bending of a ray such that the apparent elevation angle of arrival will be higher than the geometric elevation angle. For satellites well above most of the ionization the error in elevation angle $\Delta\theta$ is given by

$$\Delta\theta = \frac{\left(R + r_0 \sin\theta_0\right) r_0 \cos\theta_0}{\left[h_i\left(2r_0 + h_i\right) + \left(r_0 \sin\theta_0\right)^2\right]} \frac{\Delta R}{R} \quad \text{rad} \qquad (1.2.2.2\text{-}18)$$

where $\theta_o$ is the apparent elevation angle, $h_i$ is the height of the centroid of the electron content along the path (normally between 300 and 450 km), and $\Delta R$ is the range error, further defined later in Section 1.2.2.4 (equation 4). For sufficiently low elevation angles or for long ranges corresponding to geostationary satellites for which $R > r_o \sin\theta_o$

$$\Delta\theta = \frac{\cos\theta_0}{2h_i} \Delta R \ \text{rad} \qquad (1.2.2.2\text{-}19)$$

As $\Delta R$, the range error, varies with time, the elevation angle error $\Delta\theta$ also varies with time. Furthermore as $\Delta\theta$ is the difference between the true and apparent elevation angles, the apparent elevation angle or direction of arrival varies with time.

These relations were developed by Millman and Reinsmith (1974). Klobuchar (1978) reports that for a TEC (total electron content) of $10^{19}$ electrons/$m^3$, $\Delta\theta$ will be 0.3 mr. Section 1.2.2.4 shows the range error, and therefore the refraction or elevation angle, to vary inversely with frequency squared.

### 1.2.2.2.5 QL Approximation

Propagation can occur at any angle $\theta_B$ with respect to the magnetic field, and analysis for the general case is more complex than for strictly parallel or perpendicular propagation. The situation is simplified, however, when the QL (quasilongitudinal) approximation is applicable. To state this approximation, we use the common practice of defining $\omega_p^2/\omega^2$ as X and $\omega_B^2/\omega^2$ as Y. Using these quantities, equations (1.2.2.2-1) and (1.2.2.2-2) take the forms

$$n_l^2 = K_l = 1 - X(1 + Y) \qquad (1.2.2.2\text{-}20)$$

and

$$n_r^2 = K_r = 1 - X(1 - Y) \qquad (1.2.2.2\text{-}21)$$

Also defining $Y\cos\theta_B$ as $Y_L$ and $Y\sin\theta_B$ as $Y_T$, the condition for the QL approximation to apply is

$$4(1 - X)^2 Y^2 >> Y_T^2 \qquad (1.2.2.2\text{-}22)$$

When this approximation applies, the characteristic waves for propagation at an angle $\theta_B$ with respect to the magnetic field are circularly polarized, as they are for $\theta_B$ = 0 deg, and their indices of refraction have the forms

$$n_l^2 = K_l = 1 - X(1 + Y_L) \qquad (1.2.2.2\text{-}23)$$

$$n_r^2 = K_r = 1 - X(1 - Y_L) \qquad (1.2.2.2\text{-}24)$$

#### 1.2.2.2.6 Application to Space Communications

The value of X in equation (20) is a major factor in determining if the QL approximation applies, and X is defined as $\omega_p^2/\omega^2$. For space communications $\omega$ tends to be high, X tends to be small, and the QL approximation tends to apply, even for large values of $\theta_B$. Thus the characteristic waves on earth space paths are normally left and right circularly polarized waves. Also examination of equations (1.2.2.2-1) and (1.2.2.2-2) or (1.2.2.2-23) and (1.2.2.2-24) shows that $n_l$ and $n_r$ have values only slightly less than unity for large values of $\omega$ and that these values approach closer to unity and to each other as $\omega$ increases. Thus for $\omega$ sufficiently large, $n_l$ and $n_r$ are essentially unity, reflection does not occur, and the effect of the ionosphere can be neglected. Such is the case for frequencies above 10 GHz, however, one reaches frequencies for which ionospheric effects are important, even though $n_l$ and $n_r$ may still be not far from unity. The next sections consider the propagation effects due to a uniform or homogeneous media and includes information about diurnal variations as well. Ionospheric disturbances and irregularities and the solar cycle also cause variations and are discussed in Section 1.2.3.

### 1.2.2.3 Faraday Rotation and Polarization

Analysis of the propagation of a linearly polarized high frequency wave in the ionosphere shows that it experiences rotation of the plane of polarization such that a wave that is launched with vertical polarization, for example, does not remain vertical. Depending on the frequency, length of path in the ionosphere, and orientation with respect to the Earth's magnetic field, the amount of rotation may vary from a negligible amount to amounts in excess of 360 deg to many complete rotations. The basis for such rotation, known as Faraday rotation, is that a linearly polarized wave consists of left and right circularly polarized components that have different indices of refraction. This can be visualized with the aid of Exhibit 1.2.2.3-1. Note that satellite communication systems that employ circularly polarized waves need not be concerned about Faraday rotation; however linearly polarized waves are subject to Faraday rotation and attention is given hear to this effect.

Consider that $E_l$ and $E_r$ are the electric field intensity vectors of left and right circularly polarized waves. Small auxiliary arrows are used to indicate the direction of rotation for $E_l$ and $E_r$ for a right handed coordinate system with z, the direction of propagation, extending out of the plane of the page. $E_l$ and $E_r$ are the circularly polarized components of a linearly polarized wave having its electric field intensity in the x direction. Exhibit 1.2.2.3-1(a) shows an instant when $E_l$ and $E_r$ both lie on the x axis, and Exhibit 1.2.2.3-1(b) shows conditions an instant later. It can be recognized that as the two vectors rotate their projections on the y axis cancel, and the sum of their projections on the x axis provide co-sinusoidal variation of the amplitude of E, with E always lying along the x axis. Note that as E varies co-sinusoidally, $E_l$ and $E_r$ maintain constant lengths.

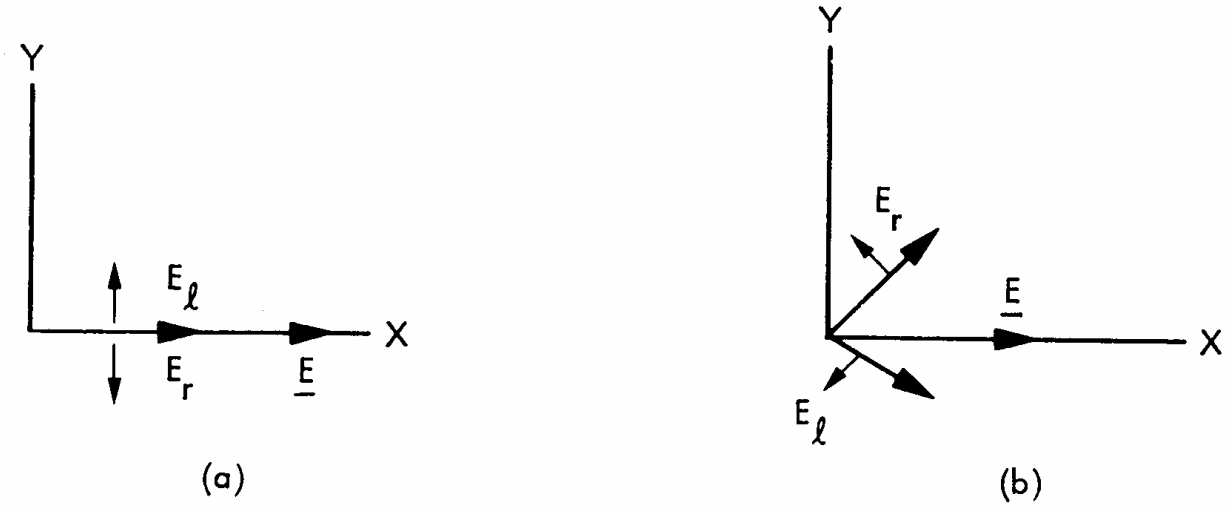


Exhibit 1.2.2.3-1
Illustration suggesting how circularly polarized waves combine to form a linearly polarized wave. *[Source: Flock (1987), Figure. 2.4]*

As the vectors $E_l$ and $E_r$ propagate in the z direction, they continue to rotate with angular velocity ω in their respective directions but the phases of the rotations lag in accordance with the factors $e^{-j\beta_l z}$ and $e^{-j\beta_r z}$. The indices $n_l$ and $n_r$ have different values and therefore $\beta_l$ and $\beta_r$ have different values, in accordance with equation (1.2.2.2-13). Thus after propagating a distance z, the rotations are no longer symmetrical about the x axis, and the field intensity E no longer lies along the x axis but at an angle ϕ from the original x axis where, for the case of a uniform ionosphere,

$$\phi = \left(\beta_l z - \beta_r z\right) / 2 \qquad (1.2.2.3\text{-}1)$$

[More generally $\phi = \int \left(\beta_l - \beta_r\right) / 2 \, dz$, with $\beta_l$ and $\beta_r$ functions of position along the path] The parameter $\beta_l$ is larger than β, but its lag in phase of rotation is in the right circular direction. Thus Exhibit 1.2.2.3-2 shows a possible condition after propagation through some distance z, namely rotation of E through an angle ϕ in the right circular direction.

Consider now propagation at an angle $\theta_B$ with respect to the magnetic field when the QL approximation applies. For sufficiently high frequencies the calculation of rotation can be simplified by noting that

$$\begin{aligned} \frac{\beta_0\left(n_l - n_r\right)}{2} &= \frac{\beta_0}{2}\left[\left\{1 - \frac{X}{1+Y_L}\right\}^{1/2} - \left\{1 - \frac{X}{1-Y_L}\right\}^{1/2}\right] \\ &\cong \frac{\beta_0}{2}\left[1 - \frac{X}{2\left(1+Y_L\right)} - 1 + \frac{X}{2\left(1-Y_L\right)}\right] = \frac{\beta_0}{2} XY_L \end{aligned} \qquad (1.2.2.3\text{-}2)$$

The electron density and magnetic field along the path will in general not be uniform but total rotation can be determined by first defining the differential rotation $d\phi$ in an increment of path length *dl* and then integrating along the length of path. Thus

$$d\phi = \left(\beta_0 / 2\right) XY_L \, dl \text{ rad} \qquad (1.2.2.3\text{-}3)$$

and, using the definitions of X and $Y_L$, the total rotation ϕ in radians along a path is given by

$$\phi = \frac{e^3}{2c\varepsilon_0 m^2 \omega^2} \int NB \cos\theta_B \, dl \text{ rad} \qquad (1.2.2.3\text{-}4)$$

where $e=1.6002\times10^{-19}$ C, $m=9.1096\times10^{-31}$ kg, $c\sim3\times10^{8}$ m/s, $\varepsilon_o=8.854\times10^{-12}$ F/m, and $\omega=2\pi f$.

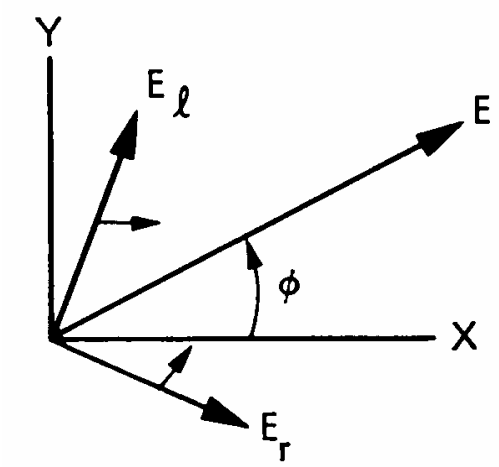


Exhibit 1.2.2.3-2
Faraday rotation through an angle ϕ from the conditions of Exhibit 1.2.2.3-1.
*[Source: Flock (1987), Figure 2.5]*

Also

$$\phi = \left(2.36 \times 10^4 \ / \ f^2\right) \int NB \cos\theta_B \, dl \ \text{rad} \qquad (1.2.2.3\text{-}5)$$

with f in Hz, N standing for electrons/$m^3$, and B the Earth's field in Wb/$m^3$. It should be kept in mind that equations (1.2.2.3-2)-(1.2.2.3-5) are approximations that are valid only at sufficiently high frequencies, perhaps above about 100 MHz.

The total rotation can be seen to vary inversely with $f^2$ and to be proportional to the integral of electron density, weighted by the value of B $\cos\theta_B$ along the path. The integration can be carried out over the slant path by introducing a factor sec$\chi$, where $\chi$ is the zenith angle or angle of the path measured from the vertical, and integrating over the vertical direction *dl = dh*. B varies inversely with the cube of the radius from the Earth's center and has very low values above about 2000 km, and Faraday rotation is insensitive to ionization above that level. Therefore Faraday rotation measurements of signals from geostationary satellites provide a measure of ionospheric total electron content but not of total electron content along the entire path to a satellite. The region above the ionosphere, above about 2000 km, may have an electron content that is about 10 percent of the ionospheric content in the daytime and 50 percent at night (Davies, Hartmann, and Leitinger, 1977).

For some situations, it is sufficiently accurate to replace B $\cos\theta_B$ in equation (1.2.2.3-5) by an average value, namely $B_L$, and to take it outside the integral. The expression for the Faraday rotation angle then becomes

$$\phi = \left(2.36 \times 10^4 \ / \ f^2\right) B_L \int N \, dl = \left(2.36 \times 10^4 \ / \ f^2\right) B_L \ \ \text{TEC} \qquad (1.2.2.3\text{-}6)$$

with $B_L = \left(\int N B \cos\theta_B \, dl\right) / \int N \, dl$. The quantity TEC stands for total ionospheric electron content along the path in this case. Equation (1.2.2.3-6) can be inverted to find TEC by use of

$$\text{TEC} = \phi f^2 \ / \left(2.36 \times 10^4 B_L\right) \qquad (1.2.2.3\text{-}7)$$

On a fixed path, when the above procedure is applicable, the amount of Faraday rotation depends on TEC, which exhibits a pronounced diurnal variation as well as a variation with the season, solar flare activity, and period of the solar cycle. When the form of the variation of electron density with altitude changes the value, of $B_L$ may change also.

Typical values of Faraday rotation as a function of ionospheric TEC and frequency for a northern mid latitude earth station viewing a geostationary satellite near the station meridian are shown in Exhibit 1.2.2.3-3. A practical consequence of Faraday rotation is that, in the frequency range where Faraday rotation is significant, one cannot transmit using one linear polarization and receive using an antenna with the same linear polarization without a high probability of a significant polarization loss. Among the techniques for avoiding or dealing with the problem are using a sufficiently high frequency that Faraday rotation is negligible, using a receiving antenna that can accept both orthogonal linear polarizations so that no polarization loss occurs, and using circular rather than linear polarization. As a right or left circularly polarized wave is a characteristic wave, it does not change polarization as it propagates and thus presents no problem, as long as both antennas of the link are designed for the same circular polarization. Another possibility, if Faraday rotation is not too great or highly variable, is to vary the orientation of a linear transmitting or receiving antenna to compensate for the Faraday rotation expected along the path, as a function of time of day, season, and period of the sunspot cycle.

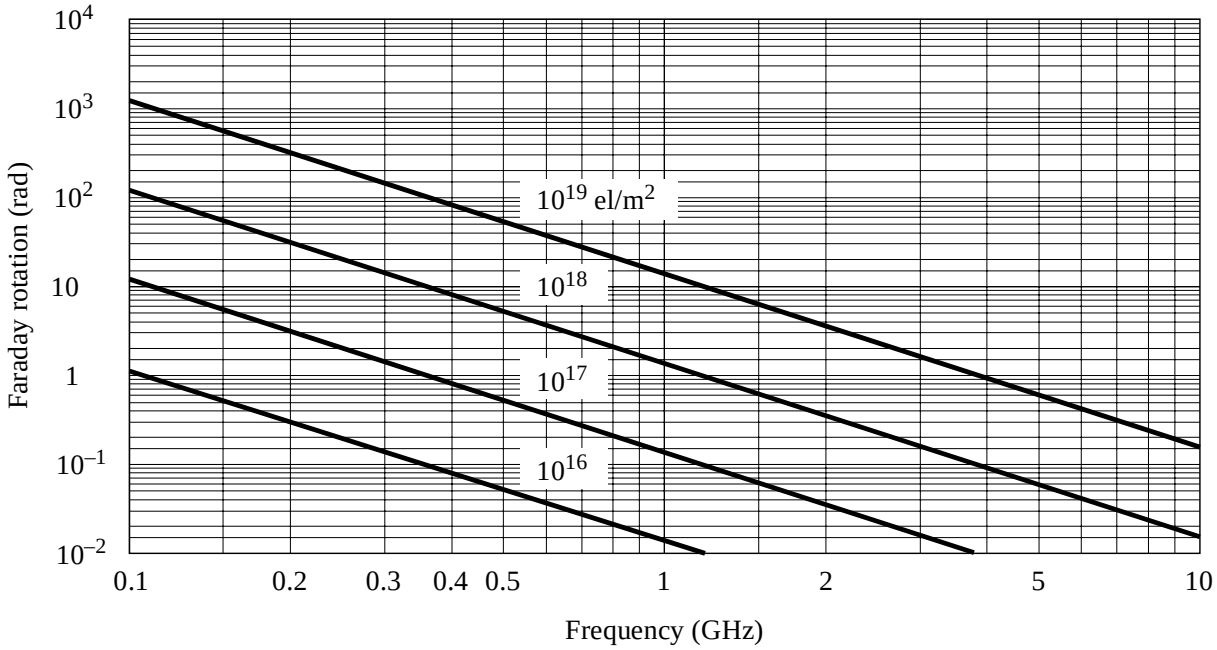


Exhibit 1.2.2.3-3
Faraday rotation as a function of ionospheric TEC and frequency
*[Source: ITU-R Rec. P.531-4 (1997)]*

### 1.2.2.4 Group Delay, Phase Advance, Doppler Frequency, and Bandwidth Coherence

#### 1.2.2.4.1 Group Delay

To consider excess ionospheric group delay, or excess range delay, at high frequencies, note that the integral $\int$ n dl, evaluated along a path with n representing index of refraction, gives the true distance along the path length, which is different from the true distance if n does not equal unity. Thus $\Delta$R, the difference between P and the true length R, is given by

$$\Delta R = \int (n-1)\,dl \qquad (1.2.2.4\text{-}1)$$

Neglecting refraction and considering that f > 100 MHz so that $n^2 \cong 1 - X$ ,

$$n^2 = 1 - f_p^2 / f^2 = 1 - 80.6N / f^2 \qquad (1.2.2.4\text{-}2)$$

where N is electron density (el/m$^3$ ) and f is frequency in Hz. Taking X as being small compared to unity as is the case for sufficiently high frequencies (f > 100 MHz),

$$n \cong 1 - X/2 = 1 - 40.3N / f^2 \qquad (1.2.2.4\text{-}3)$$

For group delay, however, one is concerned with the group velocity rather than phase velocity. As $v_g\, v_p = c^2$ for ionospheric propagation when $v_p > c$, where $v_g$ is group velocity, and $v_p$ is phase velocity, one should use the group refractive index, $n_g = 1 + X/2$. The result is that

$$\Delta R = \frac{40.3}{f^2} \int \mathrm{Ndl}\ \ m \qquad (1.2.2.4\text{-}4)$$

where $\Delta$R is a positive range error (excess range delay) and is the difference between the true range and that which would be inferred by assuming a velocity of c. (The true range is less than the inferred range). The excess range delay $\Delta$R corresponds to an error in time or excess time delay of

$$\Delta t = \frac{40.3}{cf^2} \int N\,dl = \frac{1.34 \times 10^{-7}}{f^2} \int N\,dl \ \ \mathrm{s} \qquad (1.2.2.4\text{-}5)$$

where $\int$ Ndl is the TEC (total electron content) along the path. If the TEC is known or can be estimated closely, $\Delta$t can be determined from equation (1.2.2.4-5).

Use of a second lower frequency allows determining $\Delta t$ and TEC without any advance information. Let $\Delta t_1 = 40.3\ \text{TEC} / c\ f_1^2$ where $f_1$ is the frequency of major interest and let $\Delta t_2 = 40.3\ \text{TEC} / c\ f_2^2$. Then

$$\delta t = \Delta t_2 - \Delta t_1 = \frac{40.3\ \text{TEC}}{c}\left[\frac{1}{f_2^2} - \frac{1}{f_1^2}\right] \tag{1.2.2.4-6}$$

It is now possible to solve for $\Delta t_1$ which is given by

$$\Delta t_1 = \frac{f_2^2}{f_1^2 - f_2^2}\,\delta t \tag{1.2.2.4-7}$$

The quantity $\delta_t$ can be readily measured by suitably modulating both carrier frequencies, but $\Delta t$ cannot be measured directly for lack of a suitable reference. Plots showing ionospheric time delay as a function of TEC and frequency are shown in Exhibit 1.2.2.4-1. A worldwide model giving ionospheric time delay at a frequency of 1.6 GHz is shown in Exhibit 1.2.2.4-2.

Equation (1.2.2.4-6) can be rearranged to give the value of TEC, i.e.

$$\text{TEC} = \frac{\delta t\, c}{40.3}\,\frac{f_1^2 f_2^2}{f_1^2 - f_2^2} \tag{1.2.2.4-8}$$

A procedure has been described for determining $\Delta t$ at the expense of utilizing a second frequency. Such a correction is important in the case of satellite positioning system such as the GPS (global positioning system). Using GPS it may be possible to determine position to an accuracy of a few meters, whereas if no allowance is made a TEC of $10^{18}/\text{m}^3$ can cause an error of 134 ns or 40 m at a frequency of 1 GHz (Klobuchar, 1978).

Another case where high accuracy is desired is that of the DSN (Deep Space Network) of the Jet Propulsion Laboratory, where it may be desired to determine ranges to spacecraft with an accuracy of 3 m or better. Coded signals are transmitted to spacecraft at S or X band and retransmitted back to the station at X band. Also range measurements are used for determining the declination angle of a spacecraft near zero declination by VLBI techniques. This procedure involves determining the difference in distance to the spacecraft from Goldstone, California and Canberra, Australia. Correction for excess time delay is essential for this purpose.

Equation (1.2.2.4-8), when applied to an earth space path, gives the TEC along the entire path, in contrast to Faraday rotation measurements that give the electron content of the ionosphere only.

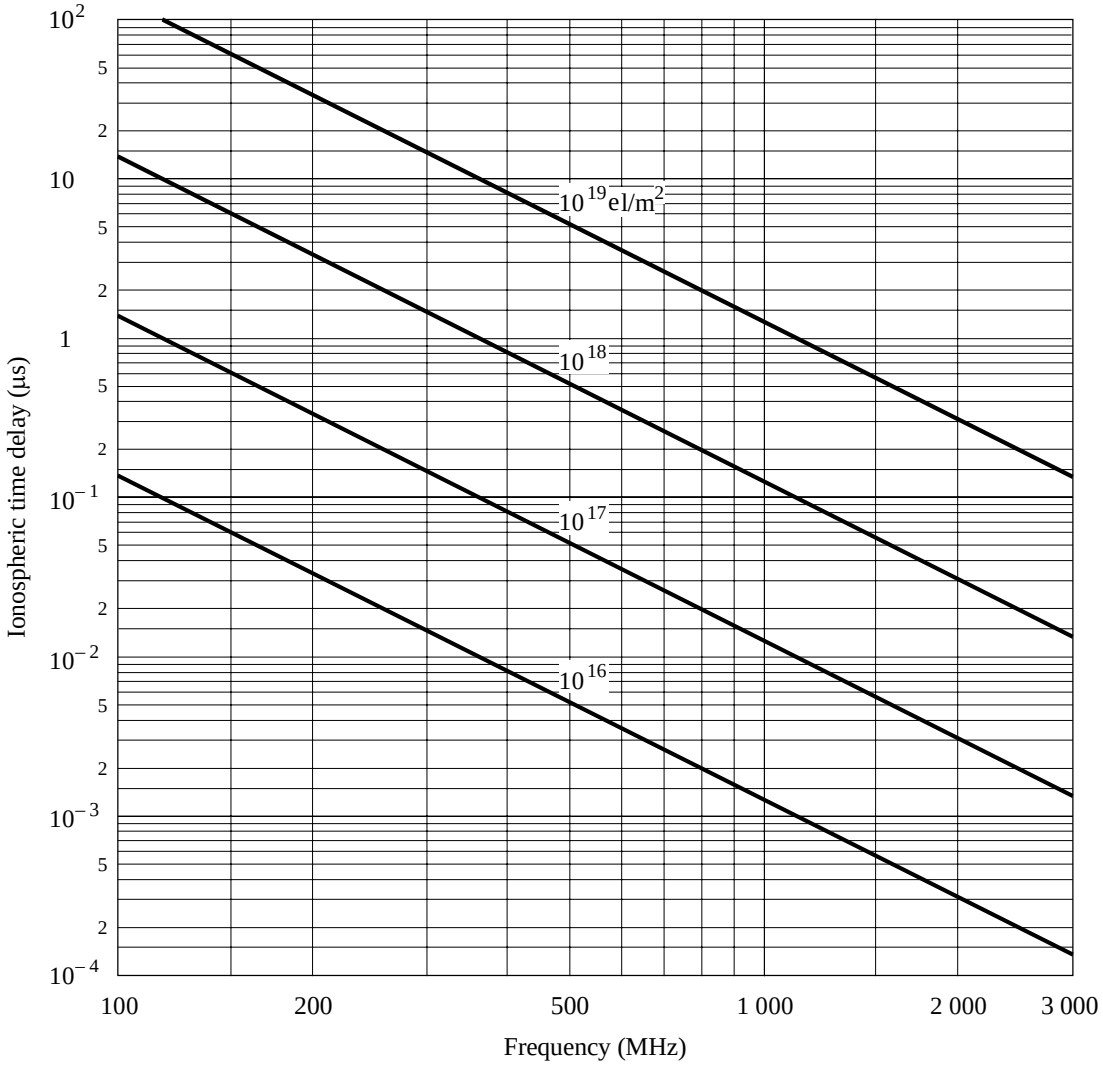


Exhibit 1.2.2.4-1
Ionospheric time delay as a function of ionospheric TEC and frequency (after Klobuchar, 1978).
*[Source: ITU-R Rec. P.531-4 (1997)]*

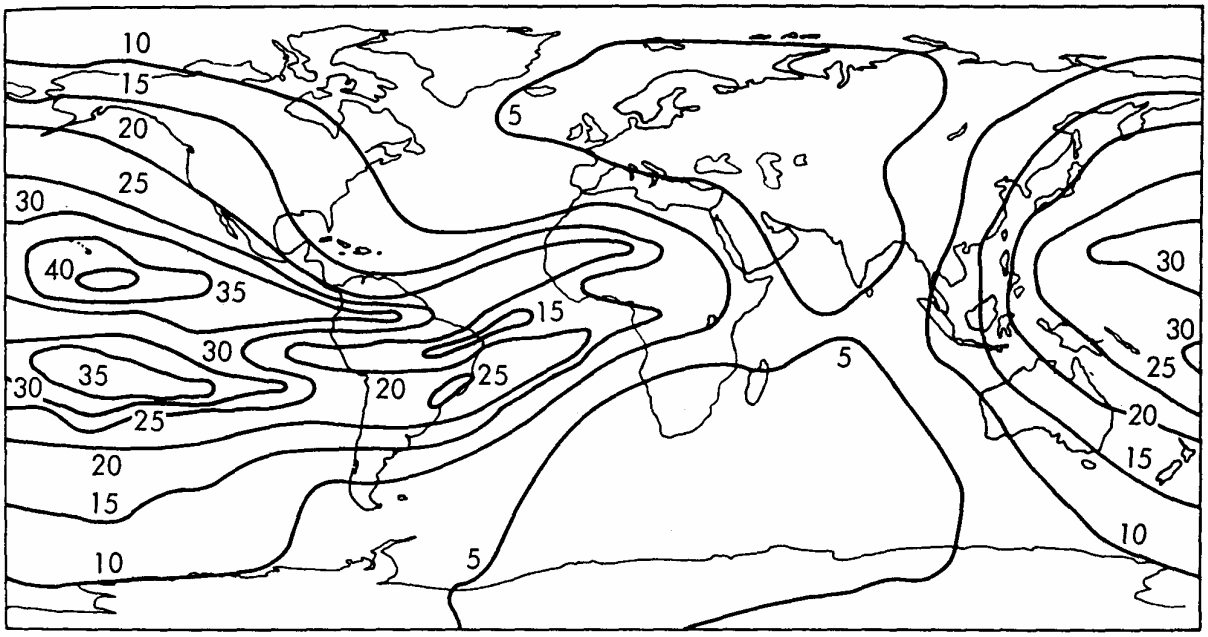


Exhibit 1.2.2.4-2
Ionospheric time delay in nanoseconds at a frequency of 1.6 GHz, based on the Bent model of ionospheric TEC (after Klobuchar, 1978).
*[Source: Flock (1987), Figure 2.8]*

### 1.2.2.4.2 Phase Advance

The presence of the ionosphere advances the phase $\phi$ of a received signal with respect to the value for unionized air. (Do not confuse phase with Faraday rotation. The same symbol $\phi$ is used here for these two different phenomena). The phase advance $\Delta\phi$ can be found by multiplying the excess range delay $\Delta R$ by the phase constant ß $=2\pi/\lambda=2\pi f/c$, with the result that

$$\Delta\phi = \frac{40.3(2\pi f)}{f^2 c}\,\mathrm{TEC} = \frac{8.44\times10^{-7}}{f}\,\mathrm{TEC}\ \ \mathrm{rad} \qquad (1.2.2.4\text{-}9)$$

Dividing by $2\pi$ gives the value of $\Delta\phi$ in cycles.

$$\Delta\phi = \frac{1.34\times10^{-7}}{f}\,\mathrm{TEC}\ \ \mathrm{cycles} \qquad (1.2.2.4\text{-}10)$$

### 1.2.2.4.3 Doppler Frequency

The Doppler frequency shift of the radio wave propagating in the ionosphere is a relatively small-order effect when compared to the other factors presented in this text. It is related to TEC by the following formulation.

Frequency and phase are related by

$$f = \frac{1}{2\pi}\frac{d\phi}{dt} \tag{1.2.2.4-11}$$

with f in Hz and $\phi$ in radians. The Doppler shift in frequency, $f_D$, corresponding to the phase change of equation (1.2.2.4-10) is given by

$$f_D = \frac{1.34\times10^{-7}}{f}\frac{\Delta(\mathrm{TEC})}{T_C} \tag{1.2.2.4-12}$$

where the TEC changes by $\Delta$(TEC) in the time interval or count time $T_C$, and $f_D$ is the average value during $T_C$.

### 1.2.2.4.4 Differenced Range versus Integrated Doppler

A technique known as differenced range versus integrated Doppler (DRVID) has been used at the Jet Propulsion Laboratory for obtaining information about changes in columnar electron content (TEC) (Callahan, 1975). The basis for the technique is the difference in group and phase velocities, the group velocity being less than c and the phase velocity being greater than c. In terms of index of refraction,

$$n_g = 1 + 40.3N\ /\ f^2 \text{ and } n = 1 - 40.3N\ /\ f^2$$

where $n_g$ is the group index and n is the phase index (which is normally what one refers to when speaking of index of refraction). Total columnar electron content TEC and electron density N are related by TEC=$\int$ Ndl , where the integral is taken along the path length.

The Deep Space Network of the Jet Propulsion Laboratory has utilized a system for measuring range delay by the use of two way transmissions of coded pulse trains. For the time interval between $t_o$ and t, this system provides a value $\Delta R_g$ which is a combination of a true change in range, R(t)-R($t_o$), and the excess range delay 40.3 $\Delta$(TEC)/$f^2$. That is

$$\Delta R_g(t, t_0) = R(t) - R(t_0) + \frac{40.3\Delta\mathrm{TEC}}{f^2} \tag{1.2.2.4-13}$$

A similar expression applies for $\Delta R_\phi(t,t_o)$, which is obtained from a phase or Doppler frequency measurement.

$$\Delta R_\phi(t,t_0) = R(t) - R(t_0) - \frac{40.3\Delta\text{TEC}}{f^2} \qquad (1.2.2.4\text{-}14)$$

The difference $\Delta R_g$-$\Delta R_\phi$ is designated as DRVID and is given by

$$\text{DRVID}(t,t_0) = \Delta R_g - \Delta R_\phi = \frac{80.6\Delta(\text{TEC})}{f^2} \qquad (1.2.2.4\text{-}15)$$

The change in TEC, Δ(TEC), can be determined from equation (1.2.2.4-15), and if a series of consecutive measurements of this kind are made, a record of the variation of TEC can be constructed. Note that the absolute value of TEC can not be determined by this method but that the effects of motion of the spacecraft and of the troposphere are canceled out as $n_g$ and n are the same in the troposphere.

The quantity $\Delta R_\phi$ can be obtained from the expression, in terms of finite increments of phase and time, for Doppler frequency $f_D$, namely

$$f_D = \frac{1}{2\pi}\frac{\Delta\phi}{T_C} \qquad (1.2.2.4\text{-}16)$$

and from the expression relation $\Delta\phi$ and $\Delta R_\phi$, which is

$$\Delta\phi = \frac{2\pi}{\lambda_0}\Delta R_\phi \qquad (1.2.2.4\text{-}17)$$

By substituting equation (1.2.2.4-17) into equation (1.2.2.4-16), $\Delta\phi$ can be eliminated, with the result that

$$f_D = \frac{1}{\lambda_0}\frac{\Delta R_\phi}{T_c} \text{ or } \Delta R_\phi = f_D\lambda_0 T_c \qquad (1.2.2.4\text{-}18)$$

### 1.2.2.4.5 Bandwidth Coherence and Dispersion

When a radio wave propagates through the ionosphere with a significant bandwidth, the propagation delay, which is a function of frequency, introduces dispersion.

The rate of change of time delay with frequency, or the time delay dispersion, is found by taking the derivative of equation (1.2.2.4-5) yielding

$$\frac{dt}{df} = \frac{-80.6}{cf^3} \int Ndl = \frac{-2.68 \times 10^{-7}}{f^3} \text{TEC} \qquad (1.2.2.4\text{-}19)$$

The rate of change of phase angle with frequency, or the phase dispersion, is found by taking the derivative of equation (1.2.2.4-9) giving

$$\frac{d\phi}{df} = \frac{-8.44 \times 10^{-7}}{f^2} \text{TEC} \qquad (1.2.2.4\text{-}20)$$

Therefore the differential delay across the bandwidth is proportional to TEC along the path and is proportional to the inverse of the frequency cubed. The effect of dispersion is to introduce distortion into broadband signals. Exhibit 1.2.2.4-3 shows the dependence of differential delay on the frequency and pulse width for TEC = $5 \times 10^{17}$ el/m$^2$. The delay decreases with increasing frequency and decreasing pulse width.

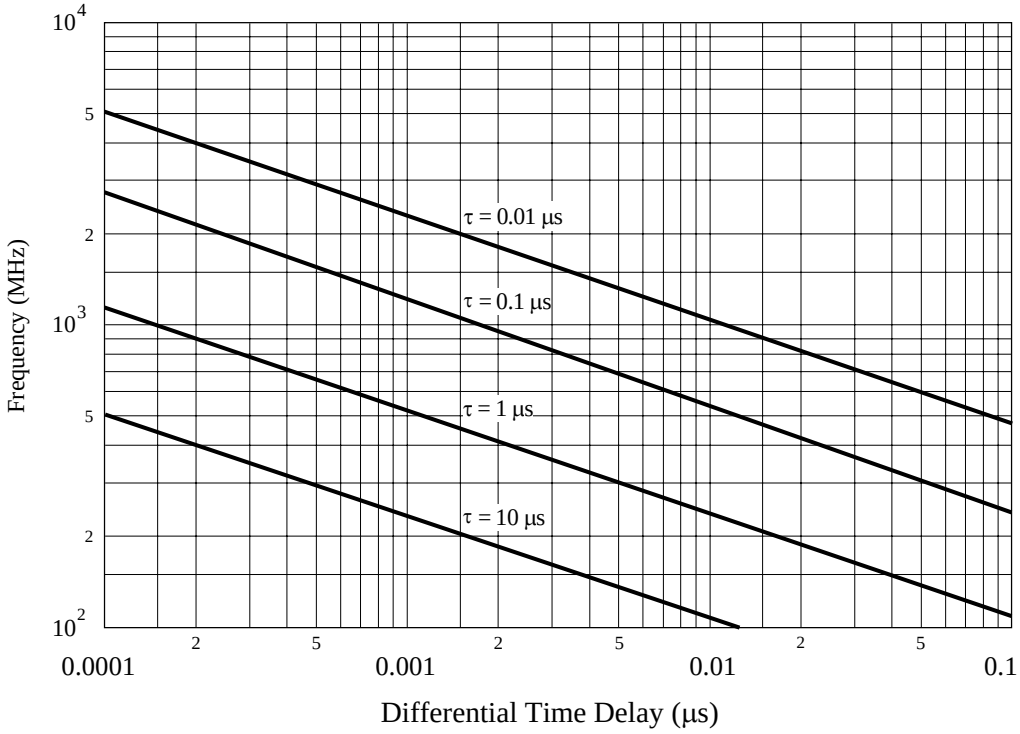


TEC = 5 x $10^{17}$ el/$m^2$

Exhibit 1.2.2.4-3
Differential Time Delay for Lower and Upper Frequencies of the Spectrum for Pulse Width τ, Transmitted Through the Ionosphere with TEC = 5 × $10^{17}$ el/$m^2$
*[Source: ITU-R, Rec. PI.531-4 (1997), Figure 4]*

### 1.2.2.5 Absorption

Waves propagating in the ionosphere experience dissipative attenuation which becomes increasingly important with decreasing frequency. A principal mechanism of attenuation is collisions of free electrons with neutral atoms and molecules. An electromagnetic wave propagating in a plasma imparts an ordered component of velocity to the electrons but the electrons lose some of the associated energy in the collision process. Hence the electromagnetic wave is attenuated. The attenuation coefficient $\alpha$, determining the rate of decrease of electric field intensity with distance in accordance with $e^{-\alpha z}$ for the left circularly polarized wave, is given, using conventional magneto-ionic theory, by

$$\alpha_l = \frac{Nq^2\upsilon}{2m\varepsilon_0 n_r c\left[\left(\omega+\omega_B\right)^2+\upsilon^2\right]} \quad \text{Nepers / m} \qquad (1.2.2.5\text{-}1)$$

where $\upsilon$ is the collision frequency. For the right circularly polarized wave, the corresponding expression is

$$\alpha_r = \frac{Nq^2\upsilon}{2m\varepsilon_0 n_r c\left[\left(\omega-\omega_B\right)^2+\upsilon^2\right]} \quad \text{Nepers / m} \qquad (1.2.2.5\text{-}2)$$

All quantities are in SI units.

N is in electrons/$m^3$;
q, the electron charge, equals $1.66022 \times 10^{-19}$ C;
m = $9.1096 \times 10^{-31}$ kg;
$\varepsilon_o = 8.854 \times 10^{-12}$ F/m;
$n_r$ is the real part of the index of refraction;
c = $2.9979 \times 10^{+8}$ m/s;
$\omega = 2\pi f$ with f in Hz; and
$\upsilon$ is collision frequency in Hz.

When attenuation is taken into account, the index of refraction becomes complex and is a function of collision frequency as well as electron density. The value of the real part $n_r$ can be calculated precisely, based on assumed values of N and $\upsilon$, gut if losses are slight $n_r$ has essentially the same value as for the lossless case, for which $n = n_r$ and is entirely real. Note that $\omega$ appears in the denominator and that for $\omega >> \omega_B$, where $\omega_B$ is angular gyrofrequency, and $\omega >> \upsilon$, attenuation varies inversely with $\omega^2$. The frequencies used for space communication are generally sufficiently high that attenuation does vary inversely with frequency squared, and $n_r$ does have the same value as in the lossless case. Also, $n_r$ approaches unity as frequency increases.

For frequencies above about 30 MHz or for transverse propagation of the ordinary wave, the attenuation constant varies inversely with frequency squared and takes the simpler form

$$\alpha = \frac{Nq^2\upsilon}{2m\varepsilon_0 n_r c\omega^2} \quad \text{Nepers / m} \qquad (1.2.2.5\text{-}3)$$

To obtain attenuation in dB/m, the value of $\alpha$ in Nepers/m can be multiplied by 8.686.

For oblique paths, total attenuation is proportional to $\sec\chi / f^2$, where $\chi$ is the zenith angle, for frequencies above 30 MHz (ITU-R Rec. P.531-4, 1997). Attenuation tends to be low at the frequencies used for space communications, the highest attenuation occurring under conditions of auroral and polar cap absorption, which are described in sections 1.2.3.1.2 and 1.2.3.1.5.

### 1.2.3 Effects Due to Ionization Irregularities

This section provides information on the propagation degradation introduced by ionization irregularities of the ionosphere. It begins with a description of the variation of the ionosphere both with time and geographically. The second half of the section describes the effects these factors have on propagating radio waves.

#### 1.2.3.1 Ionospheric Disturbances and Irregularities

##### 1.2.3.1.1 Equatorial Ionosphere

Because of atmospheric solar and lunar tidal forces and heating by the Sun, horizontal movements or winds occur in the ionosphere. As a result, electric fields are developed by the dynamo effect, described by $\mathbf{E}=\mathbf{V}\times\mathbf{B}$, where **E** is electric field intensity, **V** is the velocity of the charged particles of the ionosphere, and **B** is the Earth's magnetic field. (This is a vector relation and **E** is perpendicular to both **V** and **B**). The electric fields in turn drive a current system in the ionosphere that involves two systems of current loops in the daytime hemisphere, one in the Northern Hemisphere and one in the Southern Hemisphere. The currents flow counterclockwise in the Northern Hemisphere and clockwise in the Southern Hemisphere so that the currents of both systems flow from west to east near the geomagnetic equator. It develops that the conductivity becomes high over a restricted range of altitude in this equatorial region. In addition the equatorial ionosphere is favorably situated to intercept solar radiation, which is the main agent causing ionization in the ionosphere. As a result of the factors mentioned, a strong, concentrated current, known as the equatorial electrojet, flows at heights from 90 to 130 km in the E region of the equatorial ionosphere. Electron density irregularities and variations associated with the electrojet cause scattering of electromagnetic waves which are incident upon and propagate through this region. Strong radar backscatter echoes are received from the equatorial electrojet. The Jicamarca Radar Observatory near Lima, Peru, operating at a frequency near 50 MHz, has provided a large amount of information concerning the equatorial ionosphere. It can record both discrete echoes from E and D irregularities and weak incoherent scatter echoes from the entire ionosphere (Evans, 1969, Farley, 1963, Balsley, 1969).

The occurrence of plasma bubbles (McClure et al., 1977) has been as object of investigation since Woodman and La Hoz (1976) reported the appearance of rising plume like structures, using the Jicamaraca radar. The bubbles typically have a width of 100 km and electron densities 1 to 2 orders of magnitude less than the surroundings (Heron, 1980). Such bubbles are considered further in Section 1.2.3.2.

### 1.2.3.1.2 Auroral Ionosphere

Energetic particle precipitation into the auroral ionosphere causes the visible aurora, excess ionization that attenuates and scatters radio waves, and concentrated electrical currents known as auroral electrojets. The currents in turn cause characteristic variations in the geomagnetic field. These phenomena occur in the form of an oval, see Exhibit 1.2.3.1-1, which surrounds but is eccentric with respect to the Earth's magnetic dip pole, with the oval center displaced by about 3 degrees toward the dark hemisphere (Akasofu, 1968). The oval is fixed approximately with respect to the Sun, and the Earth rotates beneath the oval. The term auroral zone is applied to the area that is swept out by the midnight portion of the auroral oval, where auroral activity occurs essentially every night to some degree. The concept of the auroral oval has been reviewed recently by Feldstein (1986).

The excess ionization occurs prominently in the E region and can be regarded as a variety of sporadic E. Intense radar backscatter or radar auroral echoes can be received at HF, VHF, and UHF frequencies. The irregularities in ionization are field aligned, having a considerable extent along the Earth's magnetic field lines and a small extent perpendicular to the lines. The line of sight to the echoing region must be close to perpendicular to the magnetic field to receive VHF-UHF echoes which must therefore be at ranges of 500-900 km in Alaska. An auroral radar facility at Anchorage, Alaska has transmitted data to the NOAA-USAF Space Environment Services Center in Boulder, Colorado. HF waves experience sufficient refraction in the auroral ionosphere to achieve perpendicularity without being launched originally in the perpendicular direction. An ionospheric trough, namely a region of reduced ionization, separates the auroral and mid latitude ionosphere. This trough appears to be linked by magnetic field lines to the plasmapause of the magnetosphere.

The riometer (relative ionospheric opacity meter) has been a valuable tool for studying the auroral and polar ionosphere. It operates typically at a frequency of 30 MHz and, by recording the amplitude of cosmic noise, monitors auroral and polar cap activity and the associated attenuation experienced by radio waves propagating through the auroral ionosphere. An incoherent scatter radar facility at Chatanika, Alaska near Fairbanks, has been in operation since about 1972 and has provided extremely valuable information about the auroral ionosphere (Leadavrand et al., 1972); Baron, 1974; Hunsucker, 1974 ). Auroral absorption is considered further in Sec. 1.2.3.1.2.

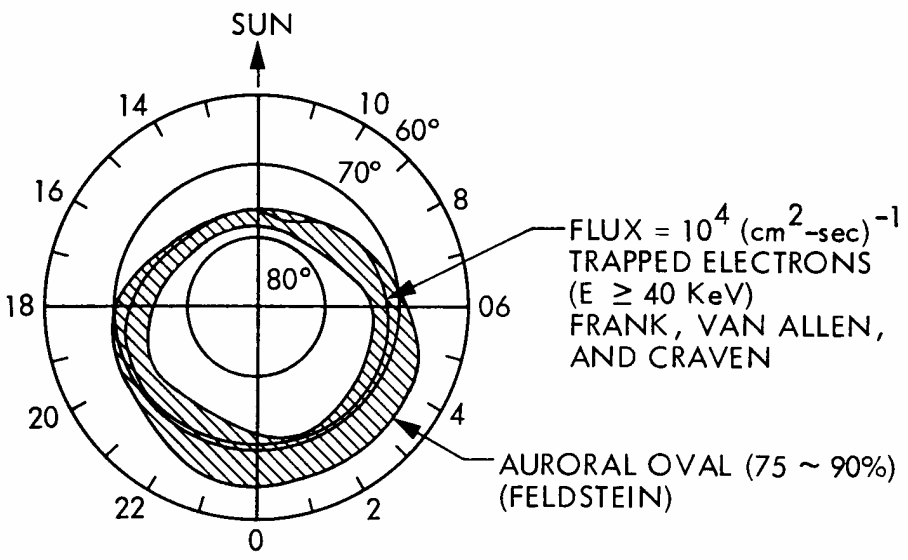


Exhibit 1.2.3.1-1
The auroral oval (Akasofu, 1968).
*[Source: Flock (1987), Figure 2.10]*

**Auroral Absorption**

Enhanced absorption can occur at high latitudes due to auroral events. These events occur at random intervals and their durations are on the order of hours (ITU-R Rec. P.531-4, 1997). They are functions of the location of the terminals and the elevation angle. Exhibit 1.2.3.1-2 shows values of auroral absorption at a frequency of 127 MHz as published in ITU-R Rec. P.531-4. In a typical night of auroral activity at Fairbanks, Alaska, long quiet auroral arcs appear to the north before midnight. These progress southward and may reach close to the zenith by 23-h local time. One or two westward traveling folds or surges in the otherwise quiet arcs may have been observed by this time. Between 23 h and 02 h the auroral forms become widespread and active in the sky, this phase being known as the auroral breakup. After the breakup, patchy, luminous forms appear in the sky. Quiet arcs may then appear as the opening phase of a second cycle of activity. Auroral absorption is usually greatest in the breakup and post breakup periods.

| Percentage of Time | Elevation Angle $20^o$ | $5^o$ |
|---|---|---|
| 0.1 | 1.5 | 2.9 |
| 1 | 0.9 | 1.7 |
| 2 | 0.7 | 1.4 |
| 5 | 0.6 | 1.1 |
| 50 | 0.2 | 0.4 |

Exhibit 1.2.3.1-2
Auroral Absorption at 127 MHz, dB
*[Source: ITU-R, Rec. P.531-4 (1997)]*

### 1.2.3.1.3 SID'S and Ionospheric Storms

The equatorial and auroral ionospheres are characterized by irregularities and disturbed conditions on a more or less continuous basis, but varying as to degree and subject to diurnal variation. The mid-latitude ionosphere exhibits less activity and disturbance generally but is subject to the effects of solar flares and sporadic E. Auroral activity is also enhanced by flare activity.

The effects of solar flares can be divided into the categories of simultaneous and delayed. The simultaneous effects result from the radiation X-ray from the flares. X-rays propagate with the velocity c, the velocity of light. The simultaneous effects are known as sudden ionospheric disturbances (SID's), a term which covers a variety of phenomena including SWF (shortwave fadeout), SCNA (sudden cosmic noise absorption), SPA (sudden phase anomaly) and SFD (sudden frequency deviation). These effects tend to be important at HF frequencies. Phase $\phi$ and frequency f are related by

$$f = \frac{1}{2\pi}\frac{d\phi}{dt} \qquad (1.2.3.1\text{-}1)$$

and if a change in phase occurs, a corresponding change in the frequency of the recorded signal also occurs. The change in frequency is similar to that encountered in reflection from a moving object and the term Doppler frequency is applied in both cases. Solar X-ray affects primarily the D region of the ionosphere.

Delayed effects from solar flares are caused by particles that are emitted from the Sun and may take 20 to 40 or more hours to reach the Earth. The particles cause magnetic and ionospheric storms (Rishbeth and Garriott, 1969), which can result in blackout at HF frequencies and also cause variations in phase and Doppler frequency. Ionosphere storms strongly affect the F region of the ionosphere. Magnetic storms are manifested by large irregular variations in the magnitude and direction of the Earth's magnetic field, as recorded on magnetometers, and are accompanied by ionospheric storms.

It is mot always possible to make a clear distinction between quiet ionospheric conditions and the disturbed conditions of magnetic storms. Some magnetic activity and associated ionospheric effects, especially the TID's and spread F discussed in the following subsection, tend to occur to some degree nearly every night even in temperate latitudes.

### 1.2.3.1.4 Traveling Ionospheric disturbances and Spread F

Traveling ionospheric disturbances (TID's) propagate as acoustic gravity waves in the Earth's ionosphere (Hines, 1974). These waves involve variation in pressure and corresponding variations in electron density. Measurements of the Faraday rotation of signals from satellites indicate a cyclical variation in total electron content as TID's propagate though an earth space path. TID's frequently appear to originate in the auroral zone and to propagate toward the equator. The condition of spread F is commonly associated with TID's (Booker, 1979). Spread F manifests itself and was originally identified on ionosonde records, which are made by vertically pointing radar systems whose frequency is varied periodically from about 0.5 to 25 MHz. Under quiet ionospheric conditions, the traces on an ionosonde record have the form shown in Exhibit 1.2.3.1-3. In an ionogram, the virtual height of reflection is plotted as a function of frequency. The symbols $f_o$ and $f_x$ in Exhibit 1.2.3.1-3 stand for penetration frequencies of the ionospheric layers E, $F_1$, and $F_2$) for the " ordinary" and "extraordinary" waves. The highest penetration frequency shown, $f_xF_2$, is about 7 MHz. Waves at higher frequencies pass through the ionosphere without reflection. A main point for present purposes is that the traces are relatively clean and distinct, although those of Exhibit 1.2.3.1-3 have been redrawn to provide greater clarity.

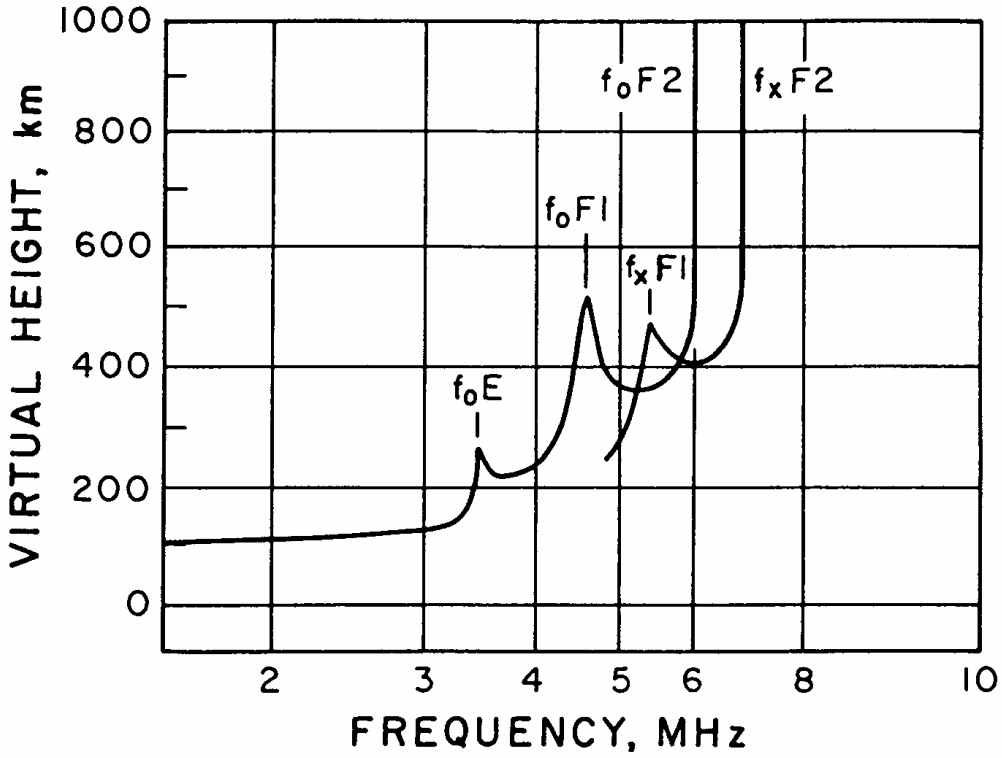


Exhibit 1.2.3.1-3
Ionospheric traces under quite ionospheric conditions, Washington, D.C.
June 3, 1962 (after Davies, 1969)
*[Source: Flock (1987), Figure 2.11]*

When spread F occurs, the trace for the F region is broken up into a multiplicity of separate traces. Spread F has been divided into two main types, which are range spreading and frequency spreading. Range spreading involves two or more traces having different virtual heights well below the penetration frequency as in Exhibit 1.2.3.1-4 (a). The high frequency portions of the traces are branched or blurred in frequency spreading as in Exhibit 1.2.3.1-4 (b). Spread F occurs for the largest percentage of time in equatorial and auroral latitudes, but as mentioned previously tends to occur nearly every night in temperate latitudes to some degree as well. It is positively correlated with magnetic activity at high latitudes and negatively correlated at low latitudes (Rishbeth and Garriott, 1969).

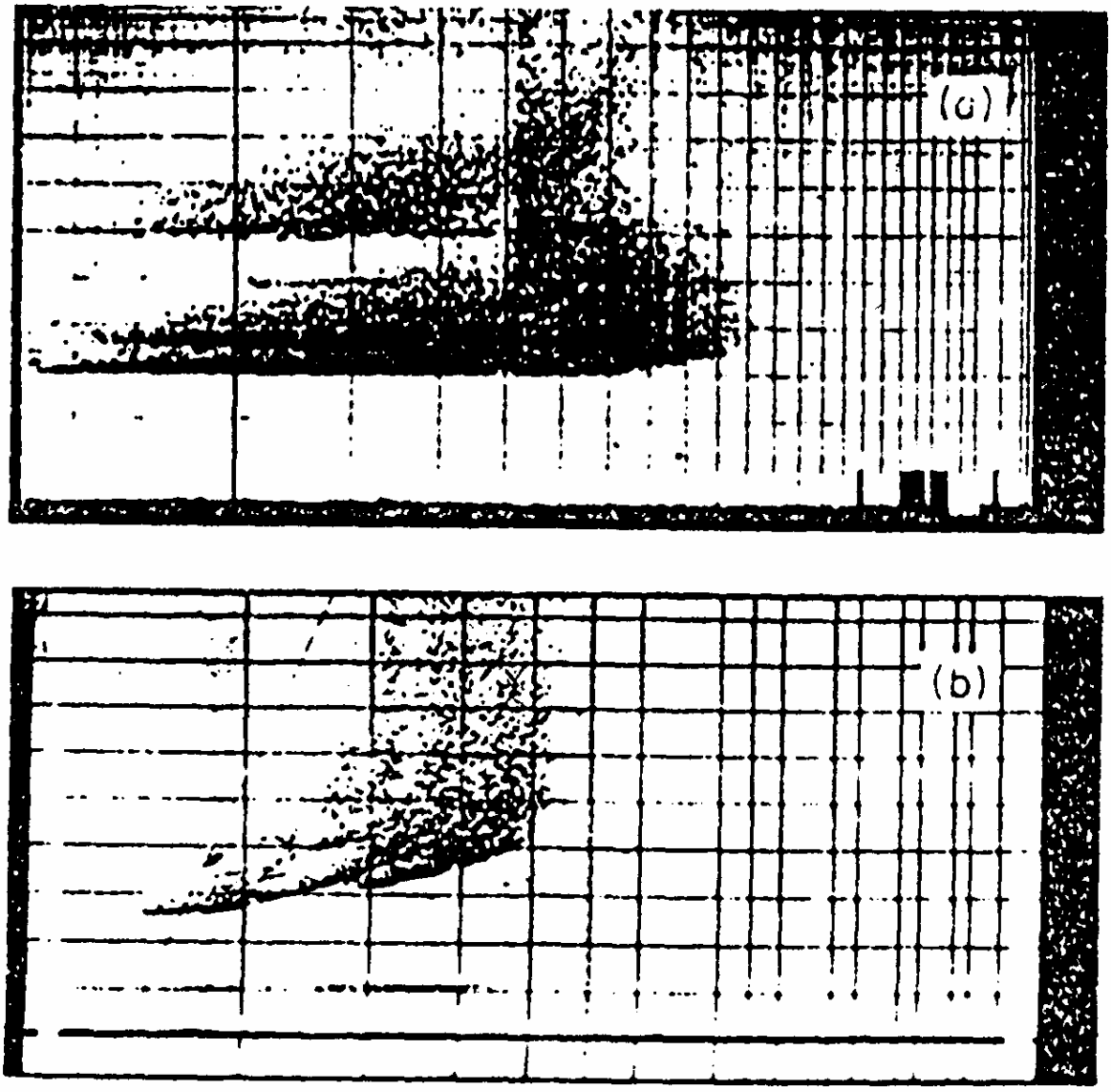


Exhibit 1.2.3.1-4
Ionograms showing spread-F. (a.) Range spreading. (b.) Frequency spreading. Virtual height versus frequency. (Davies, 1965)
*[Source: Flock (1987), Figure 2.12]*

### 1.2.3.1.5 Polar-cap Absorption

Very energetic protons or solar cosmic rays, which may reach the Earth in only 15 minutes to several hours after a flare, are associated with some intense solar flares. These particles are guided by the Earth's magnetic field to the polar regions, above about 64 deg in geomagnetic latitude, where they cause polar cap absorption. Such polar cap absorption events occur most frequently near the peak of the sunspot cycle and tend to last for several days. When the polar regions have periods of both daylight and darkness, the absorption decreases significantly at night with respect to daytime values. The auroral oval partially overlaps the equatorward edge of the region where polar cap absorption occurs, and both polar cap and auroral absorption can occur in the auroral zone.

Exhibit 1.2.3.1-5 shows illustrative hypothetical plots of absorption during a polar cap absorption event at 30 MHz, as could be derived from riometer events. The top curve applies in the summer when sunlight occurs for 24 hours a day. The other two curves for equal periods of day and night show a pronounced diurnal variation in absorption. The decrease in absorption at night is due to the decreased density of free electrons that occurs when solar radiation is absent.

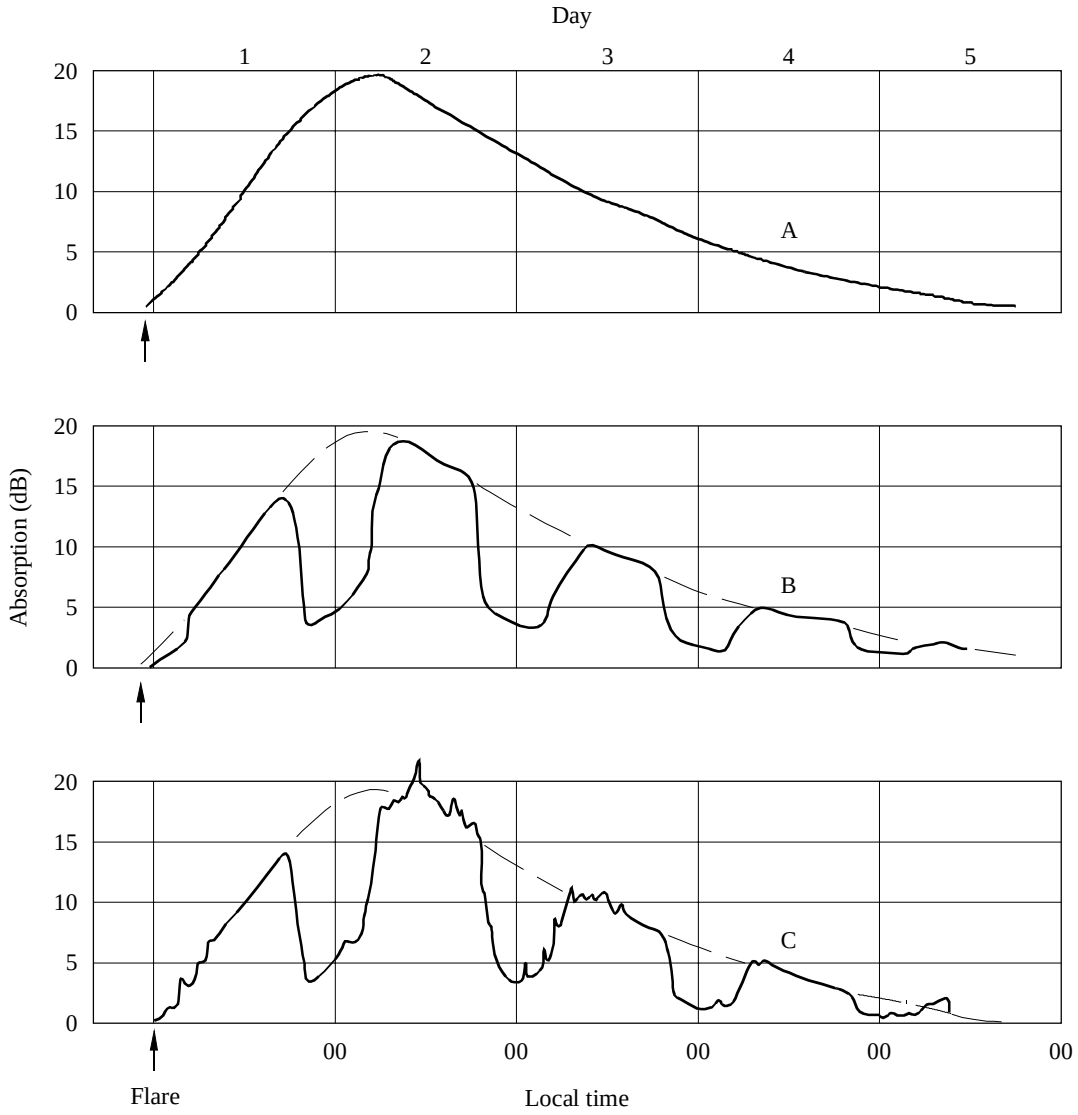


Exhibit 1.2.3.1-5
Hypothetical model showing polar cap absorption following a major solar flare as expected to be observed on riometers at approximately 30 MHz.

A. High latitudes - 24 h of daylight.
B. High latitudes - equal period day and night.
C. High latitudes - auroral zone.

*[Source: ITU-R Rec. P.531-4, Figure 11]*

### 1.2.3.2 Ionospheric Scintillation

#### 1.2.3.2.1 Introduction

Irregular variations or scintillations of the amplitude of radiowaves from radio stars were first recorded by Hay, Parsons, and Phillips (1946) who reported variations in the amplitude of signals from Cygnus and Cassiopeia at 36 MHz. At first, it was thought that the emissions from the stars might be varying with time, but records obtained simultaneously from stations separated by 200 km showed no similarity whereas when the receiver separation was only about 1 km the records were closely similar (Smith, 1950; Lottle and Lovell, 1950). These results showed that the scintillations were not caused by the stars but were of localized origin, and it was concluded that their source was in the ionosphere. The scintillations were attributed by Hewish (1952) to a diffraction pattern formed at the ground by a steadily drifting pattern of irregularities in the ionosphere at a height of about 400 km. According to Aarons, Whitney, and Allen (1971), the irregularities are mostly in the F layer at heights predominantly from 225 to 400 km.

With the advent of satellites, scintillations of signals from such spacecraft were also observed (Yeh and Swebson, 1964). The signals from radio stars are incoherent and broadband and allow the recording of amplitude and angle of arrival scintillations but not phase scintillations. Coherent, monochromatic signals from spacecraft have the advantage of allowing the recording of phase scintillations (Crane, 1977; Woo, 1977; Smith and Edeksib, 1980). The early observations of scintillations were at comparatively low frequencies and, on the basis of the assumed form of decrease of scintillation intensity with frequency, it was expected that frequencies as high as those of the 4 to 6 GHz bands planned for the INTELSAT system would be free from scintillation effects. It developed, however, that scintillation occurs at 4 to 6 GHz at equatorial latitudes (Craft and Westerlund ,1972; Taur,1973).

Scintillation may involve weak scattering or strong scattering. The strongest scattering is observed in the equatorial and auroral regions, especially the equatorial areas. The resulting scintillation is correspondingly intense and extends to higher frequencies than elsewhere. Scintillation tends to be weak at temperate latitudes. Maximum scintillation occurs at night in all three regions. The pattern of occurrence is suggested in Exhibit 1.2.3.2-1. It is generally agreed that the weak mid latitude scintillation is due to diffractive scattering, and it has sometimes been assumed that such is the case for all scintillation. Certain analyses of strong scattering, including that responsible for scintillation at microwave (SHF) frequencies, however, have led to conclusions that such scintillation must be caused by a higher portion of the atmosphere, in particular the plasmasphere (Booker, 1975) or by a different mechanism, namely refractive scattering rather than diffractive scattering (Crain. Booker, and Ferguson, 1979). The refractive scattering is said to be caused by ionization structure in the form of "holes" or "bubbles" that are perpendicular to the line of sight. Refractive scattering is considered to involve irregularities of scale larger than the Fresnel scale, and diffractive scattering is assumed to involve irregularities having sizes near the Fresnel scale.

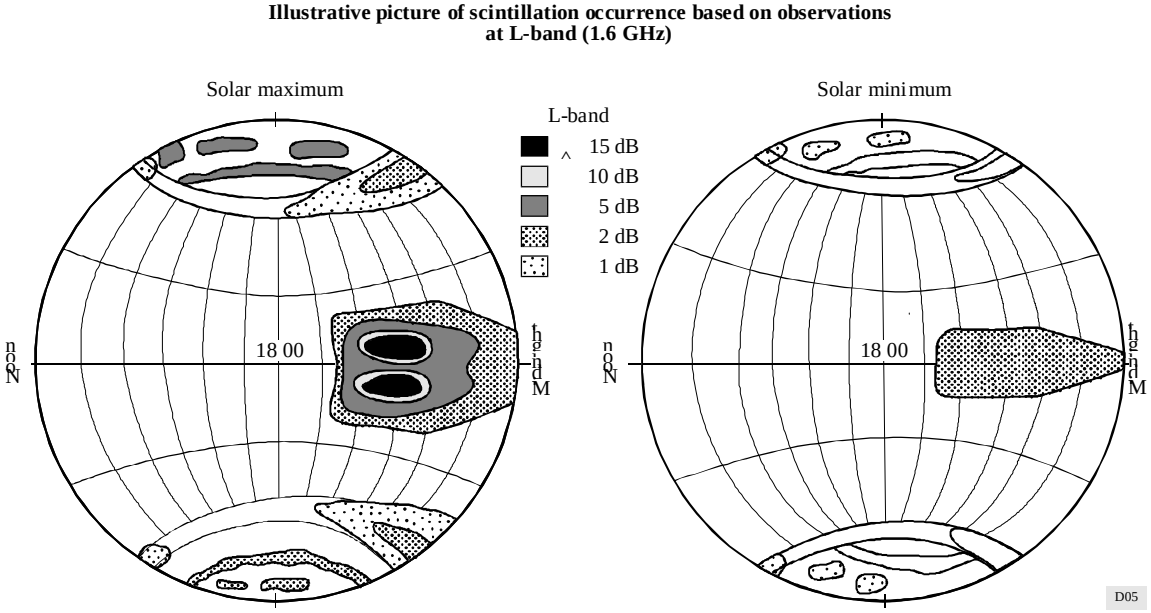


Exhibit 1.2.3.2-1
Pattern of ionospheric scintillation based on observations a L-Band (1.6GHz)
*[Source: ITU-R Rec. P.531-4 (1997)]*

Several measures or indices of scintillation have been used. Attention was given to the subject of indices by Briggs and Parkin (1963) who introduced indices designated by S, $S_1$, $S^2$, and $S_4$. The index $S_4$, representing the standard deviation of received power divided by the mean value is said to be the most useful of the several indices (Klobuchar and Working Group, 1978). It is given by

$$S_4 = \frac{1}{\overline{E^2}}\left[\overline{\left(E^2 - \overline{E^2}\right)^2}\right]^{1/2} \qquad (1.2.3.2\text{-}1)$$

where E is field intensity. A similar index, m, is defined as the ratio of rms fluctuation to mean value of power.

The index SI has been proposed as a convenient approximate measure of scintillation (Whitney, Aarons, and Malik, 1969). It is defined by

$$SI = \frac{P_{max} - P_{min}}{P_{max} + P_{min}} \qquad (1.2.3.2\text{-}2)$$

where the P's represent power. In order to avoid over-emphasizing extreme conditions, it is recommended that the third peak down from the maximum that the third minimum up from the absolute minimum be used to define $P_{max}$ and $P_{min}$.

The parameter $\tau_c$, the fade coherence time, is pertinent to digital communications. If $\tau_c$ is long compared to the time interval corresponding to one bit, the average bit error can be computed in terms of $S_4$. It has been stated that knowledge of $S_4$, $\tau_c$, and a rough measure of coherence bandwidth are what is needed for considering the effect of scintillation on transionospheric communication systems (Klobuchar and Working Group, 1978).

#### 1.2.3.2.2 Theoretical Background

Discussions of ionospheric scintillation may refer to Fresnel scale sizes and distances. To introduce these concepts, consider a path of length d between transmitting and receiving locations. At distance $d_T$ from the transmitter and $d_R$ from the receiver, the first Fresnel zone radius $F_1$ is given by

$$F_1 = \left( \frac{\lambda d_T d_R}{d} \right)^{1/2} \qquad (1.2.3.2\text{-}3)$$

All the elements of radiation passing through the first Fresnel zone have components of electric field intensity that add constructively. If the distance to the transmitter $d_T$ becomes very large compared to $d_R$, $d_T$ approaches d and the first Fresnel zone radius is given by

$$F_1 = (\lambda d)^{1/2} \qquad (1.2.3.2\text{-}4)$$

The first Fresnel zone is circular in cross section and has an area of $\pi F_1^2$. Converting to different symbols, corresponding to irregularities that occur with a radius or scale size L about equal to $F_1$ at a height h = z above a point of observation equation (1.2.3.2-4) becomes

$$L = (\lambda z)^{1/2} \qquad (1.2.3.2\text{-}5)$$

Upon rearrangement, one obtains

$$z = L^2 / \lambda \qquad (1.2.3.2\text{-}6)$$

In equations (1.2.3.2-5) and (1.2.3.2-6), L takes the place of $F_1$ and z takes the place of $d_R$. In some cases, one may wish to know the Fresnel distance z corresponding to a certain value of L. In other applications, one may wish to know the Fresnel scale size L corresponding to a certain distance z. If $d_T$ is not sufficiently large to justify using equation (1.2.3.2-5), one can revert to equation (1.2.3.2-3).

Some analyses of ionospheric scintillation are based on consideration of scattering in an ionospheric layer or screen containing identical roughly isotropic or ellipsoidal irregularities of scale size L, as in Exhibit 1.2.3.2-2. Let the irregularities of the layer be characterized by ΔN, the deviation in electron density from that of surroundings. The corresponding deviation Δn in index of refraction n can be determined by use of equation (1.2.2.4-4) to be given by

$$\Delta n = -40.3\Delta N \,/\, f^2 \qquad (1.2.3.2\text{-}7)$$

Therefore

$$\overline{(\Delta n)^2} = 1.624 \times 10^3 \overline{(\Delta N)^2} \,/\, f^4 \qquad (1.2.3.2\text{-}8)$$

where the overbars indicate mean values. The phase change Δϕ in traversing a single irregularity of size L is

$$\Delta\phi = (2\pi / L)(L\Delta n) \qquad (1.2.3.2\text{-}9)$$

where $2\pi/\lambda$ is the phase constant. Equation (1.2.3.2-3) can be written in an alternative form as

$$\frac{\overline{(\Delta n)^2}}{n} = \frac{1}{4\pi^2} r_e^2 \lambda^4 \overline{(\Delta N)^2} \qquad (1.2.3.2\text{-}10)$$

where $r_e$ is the classical electron radius ($82 \times 10^{-15}$m). Using this form and considering a layer of thickness D rather than a layer of negligible thickness, the total mean square phase fluctuation $\overline{(\Delta\phi)^2}$ in a layer of thickness D at a zenith angle χ is given by

$$\overline{(\Delta\phi)^2} = 4 r_e^2 \lambda^2 \overline{(\Delta N)^2} LD \sec\chi \qquad (1.2.3.2\text{-}11)$$

Note that n of equation (1.2.3.2-10) is essentially unity and that Δn can be either a positive or negative quantity. The classical electron radius, $r_e$, is given in terms of other quantities by $r_e = \mu_o e^2/4\pi m$, (CRC,1972) where $\mu_o = 4\pi \times 10^{-7}$ H/m is the magnetic permittivity of empty space and e and m are the charge and mass of the electron, respectively. It is not essential that the quantity classical electron radius be introduced into equations (1.2.3.2-10) and (1.2.3.2-11). Instead one can employ equation (1.2.3.2-7) and $f = c/\lambda$ giving directly the result that

$$|\Delta n|^2 = (4.484 \times 10^{-16})^2 \lambda^4 |\Delta N|^2$$

[A check of the numerical coefficient of $|\Delta N|^2$ shows that it equals $r_e^2/4\pi$]

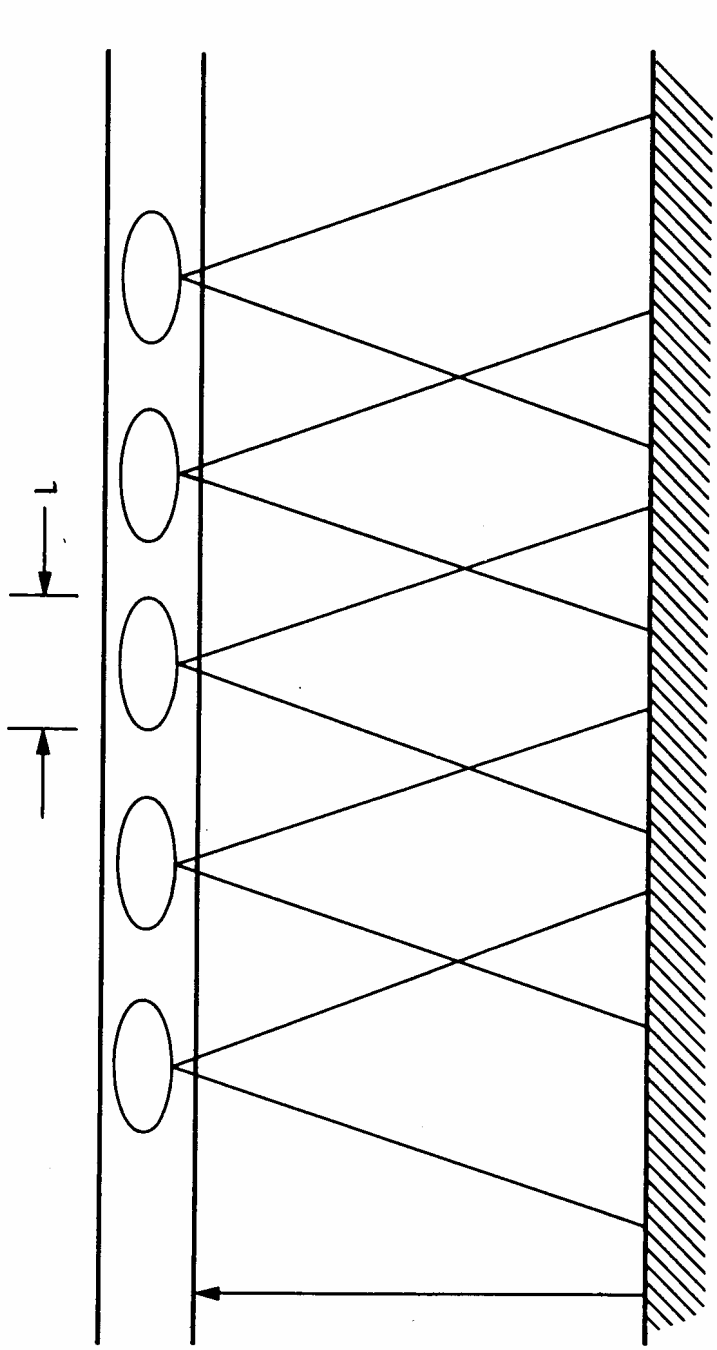


Exhibit 1.2.3.2-2
Layer of irregularities of scale size L
*[Source: Flock (1987), Figure 2.14]*

Only phase variations occur immediately below the layer of Exhibit 1.2.3.2-2, but amplitude variations develop farther below the layer. The distance h that is required for amplitude fluctuations to develop is in the order of the Fresnel distance $z = L^2/\lambda$ of equation (1.2.3.2-1). In particular, if $h > \pi L^2/\lambda$ amplitude fluctuations are said to develop (Booker, 1975). The phasor diagram of Exhibit 1.2.3.2-3 can help to visualize the association of phase and amplitude fluctuations. The parameter A represents the undisturbed component of field intensity and $\overline{(\Delta A)^2} = \overline{(\Delta\phi)^2} A^2$ so that

$$\overline{(\Delta A / A)^2} = \overline{(\Delta\phi)^2} \tag{1.2.3.2-12}$$

in the fully developed case. In the diagram ΔA represents a quantity that adds with random phase to A to produce amplitude variations.

Using results obtained by Bowhill (1961) but expressing relations in his own notation, Booker (1975) obtained the following expressions for phase and amplitude scintillations for weak scattering. The relations are in terms of $Z = \pi L^2/\lambda$.

$$\overline{(\Delta\phi)^2} = 4r_e^2\lambda^2\overline{(\Delta N)^2} LD\sec\chi \frac{1 + 0.5(h\sec\chi / X)^2}{1 + (h\sec\chi / Z)^2} \tag{1.2.3.1-13}$$

$$\overline{(\Delta A / A)^2} = 4r_e^2\lambda^2\overline{(\Delta N)^2} LD\sec\chi \frac{0.5(h\sec\chi / X)^2}{1 + (h\sec\chi / Z)^2} \tag{1.2.3.1-14}$$

when $h\sec\chi >> Z$

$$\overline{(\Delta\phi)^2} = \overline{(\Delta A / A)^2} = 2r_e^2\lambda^2\overline{(\Delta N)^2} LD\sec\chi \tag{1.2.3.1-15}$$

when $h\sec\chi << Z$

$$\overline{(\Delta\phi)^2} = 4r_e^2\lambda^2\overline{(\Delta N)^2} LD\sec\chi \tag{1.2.3.1-16}$$

$$\overline{(\Delta A / A)^2} = \frac{2}{\pi^2} r_e^2\lambda^4\overline{(\Delta N)^2} \frac{h^2}{L^3} D\sec^3\chi \tag{1.2.3.1-17}$$

These relations are said to explain weak mid latitude scintillation for parameters in the order of L = 800 m (scale size of Exhibit 1.2.3.2-2), D = 200 km (thickness of ionosphere), and h=300 km (height to center of ionosphere). In the analysis outlined above, a layer of substantial thickness is considered, but in other treatments the layer is replaced by an equivalent two-dimensional screen. Thus scintillation may be discussed in terms of a diffracting screen model (Cronyn, 1970). For present purposes, we will not distinguish between scattering by a layer or a screen.

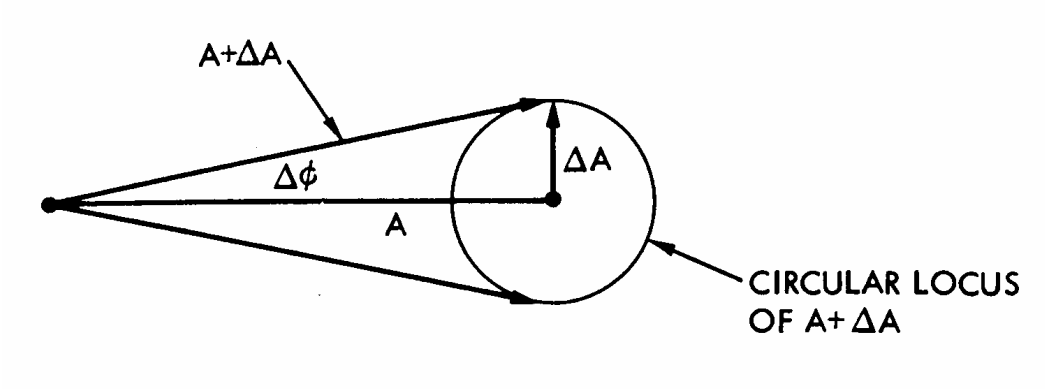


Exhibit 1.2.3.2-3
Phasor representation of amplitude and phase variations
*[Source: Flock (1987), Figure 2.15]*

For the theory of weak scattering to apply, it has been assumed that the phase variation introduced by the ionosphere is restricted to about 1 radian. For this condition, the amplitude variations observed at the ground are considered to correspond to the pattern of irregularities in the ionosphere, for irregularities below a certain size. If the phase variation is greater than 1 radian, the correspondence breaks down (Lawrence, Little, and Chivers, 1974). The amplitude scintillation index tends to increase with distance below the ionospheric layer but remains less than unity for weak scattering. The amplitude scintillation index for strong scattering can reach a value of unity and saturate or limit at that value, whereas phase scintillation does not reach a saturation point but continues to increase if the intensity of scattering continues to increase. An analysis by Rino and Fremouw (1977) indicated that phase variations are commonly in excess of 1 radian even when amplitude scintillation is weak.

The total field intensity at the ground is the sum of an unperturbed component and the perturbations in field intensity due to irregularities as in Exhibit 1.2.3.2-3. The generation of perturbations can be understood in terms of electrical currents that flow in the irregularities due to the incident field intensity. Because of these currents, having a density different than that of the surrounding ionosphere, the irregularities act like antennas having roughly conical radiation patterns as suggested in Exhibit 1.2.3.2-2. The beamwidth of the conical beams is about $\lambda/L$, the larger the irregularity the narrower the beamwidth and vice versa. At an observing point at a distance d below the layer where $d << z = L^2$, with z the Fresnel distance corresponding to the scale length L, only one beam is intercepted and only phase variations are recorded. For larger distances, the cones of radiation overlap and conditions for interference and consequent amplitude scintillations occur.

Assuming weak scattering and a pattern of ionospheric irregularities drifting horizontally, the above discussion indicates qualitatively how amplitude scintillations develop. A further

question, however, is under what conditions will the amplitude scintillations correspond to and allow determination of the sizes of the irregularities. An additional requirement, if this condition is to be met, is that, as mentioned above, the irregularities must not be too large. In particular, the irregularities must not fill more than the first Fresnel zone. Radiation from the even Fresnel zones interferes with that from the odd zones and this condition introduces effects that preclude the identification of irregularities having scale sizes larger than $(\lambda z)^{1/2}$ [equation (1.2.3.2-5)]. Phase scintillations, however, are not so limited and can be used to detect irregularities over a large range of scale sizes. Also they do not saturate but cover a wide dynamic range.

The temporal and spatial fluctuations of phase and amplitude are related to the power spectrum and autocorrelation function of electron density variations, the power spectrum and autocorrelation function being Fourier transforms of each other (Beckmann, 1967). Early analyses assumed a Gaussian form for the power spectrum (Briggs, and Parkin, 1963), but Rufenach (1972) assumed a power low form. The relation between irregularity size $l_X$ and the velocity of the moving pattern of irregularities. Assuming the pattern to be moving in the direction with velocity $v_X$, $l_X = v_X$, $T = v_X/f$ and $f = v_X/l_X$. The frequency f is that of the temporal variation in signal phase corresponding to a periodicity in electron density of $l_X$, and T is the period of the temporal variation. The vector velocity of the moving pattern of irregularities can be determined by the use of three spaced antennas when the direction of the velocity is originally unknown (Coles, 1978).

The model involving diffraction in an ionospheric screen or layer has been widely employed to analyze scintillation, but it has been asserted that it may not be suitable if the irregularities are not confined to a sufficiently thin layer and if amplitude variations already occur at the lower boundary of the layer. First order perturbation solutions of the scalar wave equation, based on the Rytov approximation or the method of smooth perturbations presented by Tatarski (1967, 1971) are said to provide a means of treating the general case (Jokipii, 1973; Woo and Ishimaru, 1973,1974; Crane, 1977; Ishimaru, 1978). The diffracting screen or layer model has been defended as being convenient and accurate for treating ionospheric scintillation (Bramley, 1977) and has been used by Rino (1979a, b) in his analyses of scintillation. Some proponents of the Rytov approximation say that the diffracting screen model gives good results in some cases but not in others, whereas the Rytov approximation is applicable generally. Some proponents of the diffracting screen model say that it gives good results, that it involves concepts equivalent to the use of a lumped constant equivalent circuit for treating transmission problems, and that the Rytov approximation does not always correctly predict observed scintillation characteristics.

### 1.2.3.2.3 Effect of Source Size, Interplanetary Scintillations

Stars twinkle in visible light but, because of their larger angular size, planets do not. The same effect of size occurs for radio waves. The reduction in scintillation when the source has an angular width greater than a certain value is due to the fact that the diffraction pattern on the ground is the convolution of the point source pattern and the brightness distribution of the source. For weak scattering, the angular width of the source $\Delta\theta$ must be less than the angular

width of the irregularities as seen from the ground if scintillation is to develop. The relation used by Lawrence, Little, and Chivers (1964) is that

$$\Delta\theta < L / 2\pi d \qquad (1.2.3.2\text{-}18)$$

for scintillation to occur, where L is the scale size of the irregularities and d is the distance to the irregularities. For strong scattering, they take

$$\Delta\theta < L / 2\pi d\phi \qquad (1.2.3.2\text{-}19)$$

for scintillation to be evident, where $\phi$ is the magnitude of the average phase change in radians and is greater than 1 radian. The effect of source size was recognized by Briggs (1961). Typically, radio sources must be smaller than about 6 to 10 minutes of arc if ionospheric scintillation is to develop.

In recording signals from radio sources of very small size along paths passing close to the Sun, Hewish, Scott, and Wills (1964) observed scintillations having short periods, typically around 1 s, which is small compared with the periods, typically around 30 s, that had been associated with ionospheric scintillations up to that time. For such short period scintillations to be recorded, the sources must have angular widths of about 0.5 second or arc or less. (The angular extent of sources can be determined by interferometry techniques.) On the basis of the relations embodied in equations (1.2.3.2-18) and (1.2.3.2-19) and taking into account that the signal paths passed through the solar wind close to the Sun, it was concluded that the scintillations were of interplanetary origin. An account of the early observations of interplanetary scintillation (IPS) has been provided by Cohen (1969). The use of IPS has become an important means for obtaining information about the solar wind (Woo, 1975, 1977).

Before IPS were recognized, it was noted that radio star signals that passed near the Sun experienced angular broadening (Hewish, 1955). What was actually observed was a decrease in signal amplitude. This decrease could not be explained on the basis of absorption or refraction but only on the basis of angular broadening due to scattering by electron density irregularities. Angular broadening has been vividly illustrated as such by two dimensional displays produced by a radio heliograph operating at 80 MHz beamwidth at the zenith of 3.9 min, produces a 2 deg square area picture of the sky every second.

When Pioneer 6, having a stable monochromatic signal was occulted by the Sun, another effect, spectral broadening, was observed (Goldstein, 1969). To record spectral broadening, the sidebands of the spacecraft signal are eliminated by filtering and only the pure carrier is recorded. Spectral broadening causes the carrier that originally has an exceedingly narrow width in frequency to be broadened in frequency. The phenomena may be caused by the Doppler shift of elements of radiation that are scattered from electron density irregularities or by amplitude scintillation or by a combination of both mechanisms.

### 1.2.3.2.4 Observed Characteristics of Scintillation

Scintillation is most severe in the equatorial region within +20 deg of the magnetic equator and at high latitudes, where two regions of peak scintillation activity have been reported. One corresponds to the auroral oval, and one is over the polar cap above 80 deg of geomagnetic latitude.. In the equatorial zone, scintillation is higher in the region of the equatorial anomaly from about 15 deg to 20 deg north and south of the equatorial and high latitude regions are the middle latitudes where activity is less intense. In all sectors pronounced nighttime maxima occur. The general pattern of occurrence is shown in Exhibit 1.2.3.2-1. A review of the global morphology of ionospheric scintillation has been provided by Aarons (1982). Some data concerning scintillation levels are shown in Exhibit 1.2.3.2-4 for the low frequencies of 137 and 254 MHz for which scintillation tends to be intense. The table includes $K_p$ values, which are measures of magnetic activity, and shows that scintillation increases with $K_p$ at sub auroral and auroral latitudes. At Ascension Island in the equatorial anomaly, 27 dB at Huancayo and Natal near the magnetic equator during the sunspot peak in 1979 and 1980 (Aarons et al., 1981). Further information about scintillation in the equatorial anomaly has been provided by Mullen et al. (1985).

(a) ≥10 dB peak to peak, equatorial latitudes

| Location | Frequency | Day | Night |
|---|---|---|---|
| | | (400-1600LT) | (1600-400LT) |
| Huancayo, Peru | 137 MHz | 3 | 14 |
| | 254 MHz | 2 | 7 |
| | | (600-1800LT) | (1800-600LT) |
| Accra, Ghana | 137 MHz | 0.4 | 14 |

(b) ≥12 dB peak to peak at 137 MHz, subauroral and auroral latitudes
(c)

| Location | $K_p$ | Day | Night |
|---|---|---|---|
| | | (500-1700LT) | (1700-500LT) |
| Sagamore Hill, MA | 0 to 3+ | 0 | 1.4 |
| | > 3+ | 0.1 | 2 |
| Goose Bay, Labrador | 0 to 3+ | 0.1 | 1.8 |
| | > 3+ | 1.6 | 6.8 |
| Narssarssuaq,Greenl. | 0 to 3+ | 2.9 | 18 |
| | | 19 | 45 |

(d) ≥10 dB peak to peak at 245 MHz, auroral latitudes

| Location | $K_p$ | Day | Night |
|---|---|---|---|
| | | (600-1800LT) | (1800-600LT) |
| Goose Bay, Labrador | 0 to 3+ | 0.1 | 0.1 |
| | > 3+ | 0.3 | 1.2 |
| Narssarssuaq,Greenl. | 0 to 3+ | 0.1 | 0.9 |
| | | 2.6 | 8.4 |

LT: Local Time

Exhibit 1.2.3.2-4
Percentage of Occurrence of Scintillation
*[Source: CCIR (1982, 1986b)]*

Significant scintillation has been recorded in even the 4 and 6 GHz bands at equatorial latitudes. In one case involving transmission on a 6 GHz uplink and a 4 GHz downlink, fading reached 8 dB peak to peak (Aarons, 1982). An examples of this unexpected scintillation fading at microwave frequencies at equatorial latitudes is illustrated for 6 GHz links in Exhibit 1.2.3.2-5 by Taur (1973), who presented further examples of the same type. Equatorial scintillation is often characterized by a sudden onset, and its occurrence varies considerably with location within the equatorial region. Basu et al. (1980) obtained data at 1.54 GHz at Huancayo, Peru for a 20 month period in 1976-1977 using the MARISAT satellite. Scintillation generally occurs after sunset and before midnight, with maximum intensities in roughly Feb.-March and Sept.-Oct. (see Exhibit 1.2.3.2-6). Aarons et al. (1988a) obtained data at 1.54 GHz during the peak of the sunspot cycle in 1979 and 1980 from Huancayo; Natal, Brazil; peak to peak fading greater than 27 dB was recorded at Ascension Island, and 7-9 dB were recorded at Huancayo and Natal. The latter two locations are close to the magnetic equator in what in known as the electrojet region. Ascension Island is at approximately 17 deg S dep latitude and is in the equatorial anomaly, namely the region from about 15 to 20 deg north and south of the magnetic equator itself (Rishbeth and Garriot, 1969). Additional information about scintillation in the equatorial anomaly has been presented by Mullen et al. (1985). Scintillation greater than 30 dB at 1.5 GHz and 7 dB at 4 GHz was observed. Fan and Liu (1983) describe studies of GHz equatorial scintillations in the Asian region. Peak to peak fluctuations up to 14 dB were recorded. Aarons (1985) and Franke and lie (1985) have modeled equatorial scintillation, with particular attention given to observations at Huancayo and Ascension Island, respectively.

Mid-latitude scintillation shows a well-established maximum near midnight, corresponding to the occurrence of spread F. Scintillation at middle latitudes is generally not intense, but some cases of severe scintillation have been recorded in Japan. During a magnetic storm on March 27, 1979, peak to peak scintillation of 18, 10, 15 and 3.5 dB were recorded at 136 MHz and 1.7, 4, and 12 GHz, respectively, on different paths in and around Japan (Minakoshi et al. 1981). Another report from Japan of severe scintillation, in this case of 1.5 GHz signals, has been provided by Karasawa et al. (1985). Signals from a MARISAT satellite over the Indian Ocean at an elevation angle of 17.3 deg were utilized. Fluctuations lasting for a long period and sometimes exceeding 30 dB peak to peak in the equinoctial month were observed and shorter spike like scintillations were also evident.

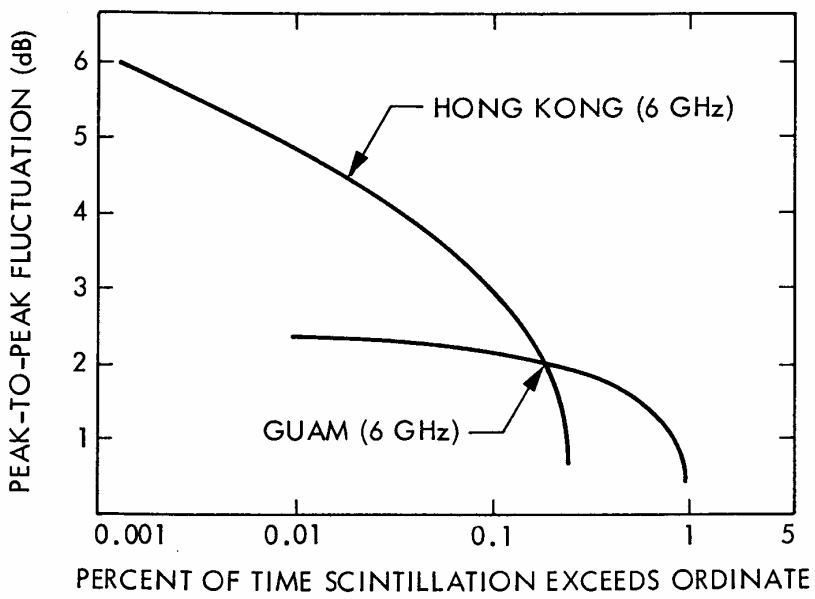


Exhibit 1.2.3.2-5
Scintillation, Guam and Hong Kong (Taur, 1973)
*[Source: Flock (1987), Figure 2.16]*

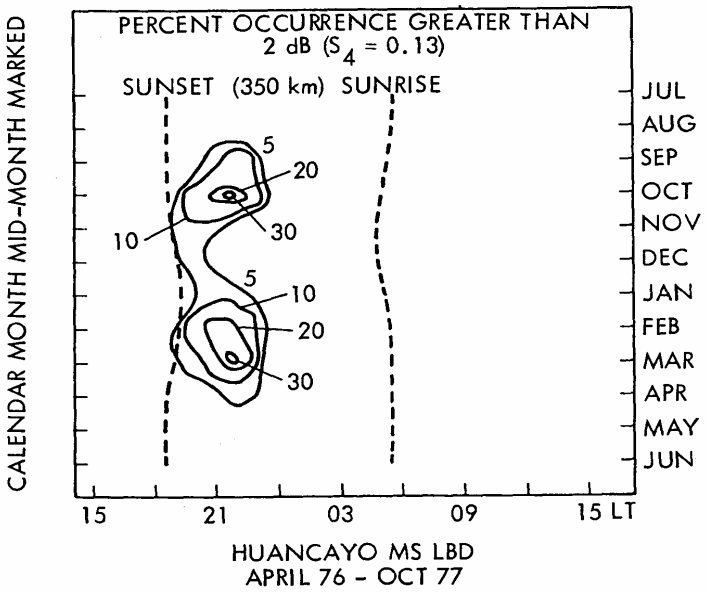


Exhibit 1.2.3.2-6
Monthly percentage of scintillation ≥ 2 dB, Huancayo, MARISAT, 1.54 GHz, (Basu et al., 1980)
*[Source: Flock (19897), Figure 2.17]*

Scintillation increases at high latitudes, the increase beginning near the region of the ionospheric trough. In the auroral oval, both discrete and diffuse aurora, as shown by Defense Meteorological Satellite images, have been correlated with scintillation ar 136-137 MHz (Martin and Aarons, 1977). Frihagen (1971), using 40 MHz transmissions, has reported two regions of peak scintillation activity at high latitudes, one corresponding to the auroral oval and one above 80 deg geomagnetic latitude over the polar cap. Aarons et al. (1981b) have prepared plots showing percentages of occurrence of scintillation greater than 10 dB in the polar cap at Thule, Greenland at a frequency of 250 MHz. Buchau et al. (1985) relates 250 MHz scintillation to ionospheric structures in the polar cap. S. Basu et al. (1985) report the first long term measurements of phase scintillations at high latitude at 250 MHz. The median and 90th percentile values of rms phase deviation at 250 MHz for an 82 second detrend interval are 2 and 6 rad, respectively, at both auroral and polar cap locations.

Measurements by Fremouw et al. (1978) employing 10 frequencies between 137 and 2981 MHz transmitted from a satellite in a high inclination orbit and recorded at equatorial and auroral latitudes (Ancon, Peru; Kwajalein Island; and Fairbanks, ALaska) showed an $f^{-1.5}$ variation of the intensity of amplitude scintillations with frequency for $S_4$ less than 0.4 and an $f^{-1}$ variation of phase scintillation with frequency. The HiLat mission, utilizing satellite P83-1 with a 10 frequency radio beacon, had the objective of obtaining quantitative information on the spatial and temporal spectra of high latitude amplitude and phase scintillation. The satellite was launched on June 27, 1983 from Vandenberg AurForce base. Early results of this mission have been presented by Fremouw et al. (1985).

Amplitude scintillations result in reduction of signal to noise ratio for a fraction of the time. Phase scintillations may or may not be important depending on the type of system. For digital systems, phase scintillations may be unimportant if the bit rate is much greater than the scintillation rate. Phase scintillations tend to be important for radio navigation systems such as GPS and for synthetic aperture radars. For positioning systems phase scintillation results in range jitter and consequent loss of precision in range (Rino, Gonzalez, and Hessing, 1981; Yeh and Liu, 1979) as increments of phase $\Delta\phi$ and corresponding changes in apparent range $\Delta R_\phi$ are related by $\Delta\phi=(2\pi/\lambda_o)\Delta R_\phi$ [equation (1.2.2.4-17)]. Loss of signal coherence is another possible effect from scintillation (Rino, Gonzalez, and Hessing, 1981). Loss of coherence across a band as narrow as 11.5 MHz at UHF was observed by Fremouw et al. (1978).

Amplitude scintillations can be described by use of power spectra, autocorrelation functions, cumulative probability distributions, fade duration distributions, and plots showing message reliability (Whitney and Basu, 1977). Power spectra have been presented by a number of authors including Rufenach (1972), Crane (1976), and Whitney and Basu (1977). Examples of power spectra are shown in Exhibit 1.2.3.2-7. Cumulative probability distributions show the percentage of time that signal amplitude exceeds specified dB values. The Nakagami-m distribution shows good agreement with observed distributions (Whitney and Basu, 1977; Fremouw et al., 1978; and Panter, 1972). For the m of this distribution equal to unity (not to be confused with the scintillation index m), the distribution is a Rayleigh distribution.

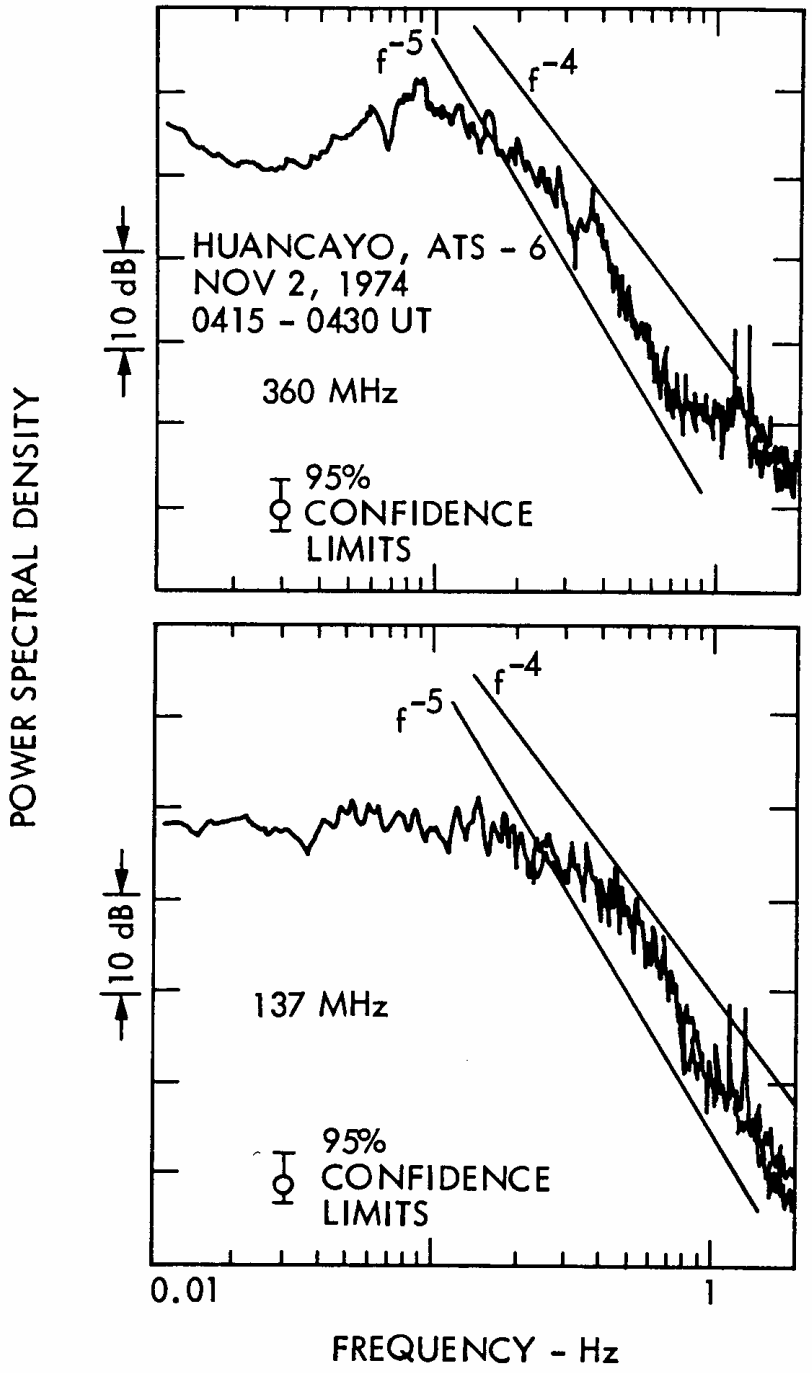


Exhibit 1.2.3.2-7
Typical power spectra for intense scintillations; $S_4 = 0.78$ at 360 MHz, $S_4 = 0.94$ at 137 MHz (Whitney and Basu, 1977)
*[Source: Flock (1987), Figure 2.18]*

The power spectra, cumulative probability distributions, etc. contain detailed information about scintillation characteristics, but frequently one is primarily interested in certain parameters such as mean value, standard deviation, scintillation index, and coherence time. The index $S_4$ is the ratio of standard deviation to mean value. Coherence time $\tau_C$ can be obtained from plots of the autocorrelation function and of the time for this function to decrease from unity to some specified value such as 0.5 or 1/e. Whitney and Basu (1977) used 0.5 in their analysis of scintillation data. For predicting bit error rate, the form of the probability distribution function is needed.

Considerable data have been accumulated on ionospheric scintillation, and the values quoted here give a rough idea of what margins may be needed to protect against ionospheric scintillation. Exhibit 1.2.3.2-8 gives values of fade depths at mid-latitudes (CCIR, 1986a). The data have commonly been presented as peak to peak values, and in the case of the 8 dB figure mentioned for 6 GHz - 4GHz links not much more than half of the 8 dB range appeared to involve a signal decrease. The needed margin may thus well be less than the peak to peak value. The increase in signal level, however, may in some cases present a problem of overload in itself. The data in the table illustrates that the fading period of scintillation varies over a large range and can be as long as several minutes. The fading period of GHz scintillation varies from 2 to 15 seconds.

| Percent of Time | Frequency (MHz) | | | |
|---|---|---|---|---|
| Exceeded | 100 | 200 | 500 | 1000 |
| 1.0 | 15.9 | 1.5 | 0.2 | 0.1 |
| 0.5 | 9.3 | 2.3 | 2.3 | 0.1 |
| 0.2 | 16.6 | 4.2 | 0.7 | 0.2 |
| 0.1 | 25.0 | 6.2 | 1.0 | 0.3 |

Exhibit 1.2.3.2-8
Distribution of Mid-Latitude Fade Depths in dB due to Ionospheric Scintillation
*[Source: CCIR (1982)]*

### 1.2.3.2.5 Prediction of Scintillation

Although ionospheric scintillation has been the subject of a great deal of theoretical and experimental study over the years and much is understood about the effect, the modeling and prediction methods available are still not at a mature state. A large amount of uncertainty is inherent in scintillation model predictions. The predicted margin requirements continue to evolve as more data, and higher quality data, becomes available. For example, in 1977, 22 dB margin was recommended to ensure 95% availability at 250 MHz (Spilker, 1977), while current

data would suggest less than 7 dB is necessary. The primary difficulty in modeling ionospheric effects arises from the large number of parameter dependencies and the consequent requirement for large amounts of data in order to characterize each dependence.

In the absence of sufficient direct measurements, propagation models typically rely on statistical characterization of the mechanism that produces the propagation impairment. For example, rain attenuation may be theoretically related to rain rate statistics on the surface of the earth, an easily measured quantity for which decades of data exist over wide areas. However, theoretical models for ionospheric scintillation have not been successful (Allnut, 1989, pg. 85). Moreover, there exists no local atmospheric correlate which may be as easily measured as rain rate. The sun spot number (SSN) correlates well with scintillation statistics over periods of a month or longer (Allnut, 1989, pg. 81), but many other local dependencies must be considered separately (geomagnetic location, time of day, etc.).

Because of the predictable long-term cyclic variation in annual statistics, the length of the expected life of the satellite system becomes a factor. If the system operates for less than 11 years, the relevant portion of the sun-spot cycle must be used. To the extent that SSN's can be predicted, annual link availability can be mapped from expected SSN using the ITU recommendation for this mapping. This eliminates one of the major sources of variability in availability and error in margin allocation.

An empirical method to estimate the effects of ionospheric scintillation developed by the ITU-R is provided in Section 2 of this handbook (Sec 2.1.5).

### 1.2.4 Transionospheric Propagation Predictions

For some satellite systems advance estimates of ionospheric parameters in the planning stage are sufficient, but for other systems continuously updated long term (e.g. monthly) or short term (e.g. daily) predictions may be needed. Furthermore, real time or near real time values of ionospheric parameters may be required in some cases.

The problem of ionospheric predictions was considered in a conference devoted to solar terrestrial predictions (Donnelly, 1978). Included in the proceeding of the conference is a report treating transionospheric propagation predictions (Klobuchar and Working Group, 1978). It is stated in the working group report that monthly values of TEC can probably be predicted within +20 percent for regions where a time history of TEC exists. However, even if monthly mean values could be predicted perfectly accurately, short-term variations from the difficulty arises from the ionospheric effects of geomagnetic storms. Theoretical capabilities were not considered to be capable of predicting storm related TEC behavior, and prediction procedures based on morphological data are the only alternative. The report discusses the problem and possible remedies.

Faraday rotation data from linearly polarized 137 MHz beacons of the geostationary satellites ATS-1, SIRIO, and Kiku-2 have been used by the Jet Propulsion Laboratory to measure TEC

and determine ionospheric corrections to range and Doppler data used for Voyager spacecraft navigation (Royden et al., 1980). By taking the difference between TEC values determined by Faraday rotation and TEC values from dual frequency transmission from Voyager (2295 MHz in the S band and 8415 MHz in the X band), the electron content of the path beyond the ionosphere is also determined. The electron content beyond the ionosphere includes that of the plasmasphere and the solar plasma. In passing by the moon Io of Jupiter, electrons in its atmosphere contributed to the total electron content along the path and made possible a comparison of experimental results and theoretical models of the electron density surrounding Io.

In addition to the periodical literature, URSI (International Scientific Radio Union), the ITU (International Telecommunications Union), and the series of Ionospheric Effects Symposia are good sources of information about the ionosphere and its effects, U.S. Commission G, Ionospheric Radio and Propagation of URSI, usually participates in two URSI meetings per year in the United States, and URSI holds international General Assemblies every three years. Propagation in Ionized Media, PI Series Volume, ITU-R Recommendations and the ITU working groups that contribute to it treat Propagation in Ionized Media [now part of ITU-R Study Group 3, Propagation].

## 1.3 TROPOSPHERIC EFFECTS

Radiowave transmissions on Earth-space links are subject to major atmospheric degradations in the troposphere, extending from the surface of the earth to about 20 km in altitude. The troposphere, and the gaseous constituents (oxygen, water vapor) and hydrometeors (rain, snow, cloud particles, etc.) it contains, can impair satellite communication links in one or more of the following ways;

- o a reduction in signal amplitude (**attenuation**),
- o **depolarization** of the radiowave,
- o an increase in thermal noise (**radio noise**) in the system,

and, for certain special conditions, particularly for low elevation angle systems,

- o amplitude and phase **scintillation**,
- o a change in **angle-of-arrival** of the signal,

and, for wideband transmissions,

- o amplitude and phase **dispersion**.

Each of these effects is introduced and briefly discussed below. The appropriate sub-sections where further information can be found in Section 1 of the Handbook are listed with the description.

**Attenuation.** Attenuation is the term used to describe a reduction in signal amplitude caused by constituents of the Earth's atmosphere, or conditions in the atmosphere, which are present in the transmission path. Attenuation is caused by the gaseous components of the atmosphere (always present), and by hydrometers (clouds, rain, fog, and snow) which can be present for certain periods of time. Hydrometers are the products formed by the condensation of atmospheric water vapor. Hydrometer attenuation experienced by a radiowave involves both absorption and scattering processes.

*Gaseous Attenuation* is the reduction in signal amplitude caused by the gaseous constituents of the Earth's atmosphere which are present in the transmission path. Gaseous attenuation is an absorption process, and the primary constituents of importance at space communications frequencies are oxygen and water vapor. Gaseous attenuation increases with increasing frequency, and is dependent on temperature, pressure, and humidity. ***(Section 1.3.1)***

*Rain attenuation* can produce major impairments in space communications, particularly in the frequency bands above 10 GHz. Because of its severity and unpredictability, rain attenuation rightly receives the most attention in the satellite system design process for frequencies above 10 GHz. ***(Section 1.3.3)***

*Cloud and fog attenuation* is much less severe than rain attenuation, however it must be considered in link calculations because it is normally present for a much larger percentage of the time than rain. ***(Section 1.3.2)***

*Dry snow and ice particle attenuation* is usually so low that it is unobservable on space communications links operating below 50 GHz.

In all of the factors affecting satellite communications in the troposphere, attenuation is increased significantly with low elevation angles, where the total path through the troposphere is longer, and the effects can by more severe. Virtually all prediction models for tropospherеic effects require elevation angle as a critical input parameter

**Depolarization.** Depolarization refers to a change in the polarization characteristics of a radiowave caused by a) hydrometers, primarily rain or ice particles, and b) multipath propagation. A depolarized radiowave will have its polarization state altered such that power is transferred from the desired polarization state to an undesired orthogonal polarized state, resulting in interference or crosstalk between the two orthogonal polarized channels. Rain and ice depolarization can be a problem in the frequency bands above about 12 GHz, particularly for `frequency reuse' communications links that employ dual independent orthogonal polarized channels in the same frequency band to increase channel capacity. Multipath depolarization is generally limited to very low elevation angle space communications, and will be dependent on the polarization characteristics of the receiving antenna. ***(Sections 1.3.3, 1.3.4)***

The effect of rain depolarization interference is fundamentally different from the amplitude reduction or noise increase propagation effects in that increasing the link power does not reduce the interference. Rain can cause scattering of electromagnetic energy out of the line-of-sight, resulting in increased leakage of uplink power into the receive beam of an adjacent satellite, or between terrestrial line-of-site systems and low-angle Earth station antennas. A power increase will raise the level of the desired and the interfering signals simultaneously.

**Scintillation.** Earth stations operating at low elevation angles are subject to scintillation caused by tropospheric turbulence. This consists of fast random fluctuations in the amplitude and phase of the signal. The effects of scintillations on the channel depend on the receiver antenna characteristics, type of modulation used and the receiver performance. The power spectrum of the fluctuation falls off quickly with increasing frequency, so the effects should be expected to be primarily brief signal drop-outs or losses of synchronization, rather than any actual modulation of the information-carrying waveforms. ***(Section 1.3.5)***

**Angle of Arrival.** Angle of Arrival describes a change in the direction of propagation of a radiowave caused by refractive index changes in the transmission path. Angle of arrival variations are a refraction process, and results in an apparent shift in the location of satellite position. (Section 1.3.6)

**Dispersion.** A change in the frequency and phase components across the bandwidth of a radiowave, caused by a dispersive medium is described as *dispersion* or *frequency dispersion*. A dispersive medium is one whose constitutive components (permittivity, permeability, and conductivity) depend on frequency (temporal dispersion) or wave direction (spatial dispersion).[1] The *coherence bandwidth* is defined as the upper limit on the information bandwidth or channel capacity that can be supported by a radiowave, caused by the dispersive properties of the atmosphere. Another degradation affiliated with dispersion is termed *antenna gain degredation*. Antenna gain degradation is an apparent reduction in the gain of a receiving antenna caused by amplitude and phase dispersion across the aperture. This effect can be produced by intense rain, however, it is usually only observable with very large aperture antennas at frequencies above about 30 GHz and for very long path lengths through the rain, i.e. low elevation angles. ***(Section 1.3.7)***

**Wet Surface Effects**. Recent measurements with the NASA Advanced Technology Satellite (ACTS) have highlighted another significant degradation for satellite communications links, related to rain attenuation. The presence of water on the surfaces of the antenna (reflector, feed cover) can add additional attenuation, above that caused by rain in the path itself. This effect is heavily dependent on antenna surface characteristics and on the material used. ***(Section 1.3.8)*** Preliminary prediction models are available to evaluate the quantitative effects of the problem. ***(Section 2.2.7)***

**Radio Noise.** Radio noise describes the presence of undesired signals or power in the frequency band of a communications link, caused by natural or man-made sources. Radio noise can degrade the noise characteristics of receiver systems and affect antenna design or system performance. The primary natural noise sources for frequencies above about 1 GHz are atmospheric gases (oxygen and water vapor), rain, clouds, and surface emissions. Man-made sources include other space or terrestrial communications links, electrical equipment, and radar systems. Extraterrestrial cosmic noise must only be considered for frequencies below about 1 GHz. The classical laws of physics and black body radiation specify that anything that absorbs electromagnetic energy radiates it as well. The energy radiated by tropospheric absorbing media (oxygen, water vapor, rain drops, cloud particles, etc.) is incoherent and broadband. It is received by the receive antenna along with the desired signal, and appears at the receiver output as thermal noise - indistinguishable from the thermal noise generated in the receiver front end. The effect of the received noise energy is accounted for by adding "radio noise" (also referred to as sky noise or atmospheric noise) to the receiver system noise temperature. The radio noise temperature is directly related to the attenuation that the absorbing medium produces. ***(Section 1.4)***

[1] Note: The term dispersion is also used to denote the differential delay experienced across the bandwidth of a radiowave propagating through a medium of free electrons, such as the ionosphere or a plasma.

All of the tropospheric degradations described above produced on a satellite will be dependent on a number of system parameters and path conditions. Propagation impairments caused by the troposphere are generally dependent on the following system parameters:

***Operating Frequency***

With the exception of signal attenuation by gaseous absorption lines, the severity of tropospheric impairments *increases* with frequency.

***Antenna Elevation Angle and Polarization***

The length of the part of the propagation path passing through the troposphere varies inversely with elevation angle. Accordingly, propagation losses, noise, and depolarization also increase with decreasing elevation angle. Rain attenuation is slightly polarization-sensitive. Depolarization is also polarization-sensitive, with linear horizontal and circular polarization being the most susceptible.

***Earth Station Altitude***

Because less of the troposphere is included in paths from higher altitude sites, impairments are less.

***Receiver Noise Temperature***

The level of the receive system noise determines the relative contribution of radio noise temperature to system noise temperature, and thus the effect of radio noise on the downlink signal-to-noise ratio.

***Local Meteorology***

Local weather conditions determine the quantitative levels of rain, clouds, scintillation (dependent on temperature and humidity), and virtually all of the effects described above. An understanding of the statistics of weather parameters is essential to successfully evaluating satellite communications propagation effects. Section 1.5 provides a summary of databases for critical meteorological parameters.

The following sections describe each of the major tropospheric propagation factors in further detail.

### 1.3.1 Atmospheric Gases

A radiowave propagating through the Earth's atmosphere will experience a reduction in signal level due to the gaseous components present in the transmission path. Signal degradation can be minor or severe, depending on frequency, temperature, pressure, and water vapor concentration. Atmospheric gases also affect radio communications by adding atmospheric noise (i.e. radio noise) to the link.

The principal interaction mechanism involving the gaseous constituents and a radiowave is molecular absorption, which results in a reduction in signal amplitude (attenuation) of the radiowave. The absorption of the radiowave results from a quantum level change in the rotational energy of the molecule, and occurs at a specific resonant frequency or narrow band of frequencies. The resonant frequency of interaction depends on the energy levels of the initial and final rotational energy states of the molecule.

There are many gaseous constituents in the Earth's atmosphere that can interact with a radiowave link. The principal components of the dry atmosphere, and their approximate percentage by volume, are;

oxygen (21%),
nitrogen (78%),
argon (0.9%), and
carbon dioxide (0.1%),

All components are well mixed to a height of about 80 km (Battan, 1979). Water vapor is the principal variable component of the atmosphere, and at sea level and 100% relative humidity, it constitutes about 1.7 % by volume of the US Standard Atmosphere (ITU-R Rec. P.840-2, 1997).

Only *oxygen* and *water vapor* have observable resonance frequencies in the bands of interest, up to about 100 GHz, for space communications. Oxygen has a series of very close absorption lines near 60 GHz and an isolated absorption line at 118.74 GHz. Water vapor has lines at 22.3 GHz, 183.3 GHz, and 323.8 GHz. Oxygen absorption involves magnetic dipole changes, while water vapor absorption consists of electric dipole transitions between rotational states.

Exhibit 1.3.1-1, illustrates the frequency dependence of gaseous attenuation for frequencies up to 1000 GHz (ITU-R P.676-3, 1997). Two curves are shown, Curve A for moderate humid conditions, and Curve B for a dry atmosphere. The attenuation is given in decibels per kilometer of path length, (dB/Km), usually referred to as *specific attenuation.* Gaseous absorption is dependent on atmospheric conditions, most notably, air temperature and water vapor content. Barometric pressure has a minor influence on attenuation. The curves were determined for a barometric pressure of 101.3 kpa or 1013 mb which is the pressure of one standard atmosphere and a temperature of 15° C or 59° F. Curve A is for 7.5 $g/m^3$ absolute humidity which corresponds to 58.7% relative humidity at 59° F. The exhibit illustrates distinct peaks in the curves at different frequencies for water vapor and oxygen. For frequencies less than 30 GHz,

water vapor causes a large attenuation in the vicinity of 22.3 GHz. Oxygen demonstrates its largest attenuation around 60 GHz, in the band up to 350 GHz. There are other peaks in gaseous absorption up to 1000 GHz. The structure of the specific attenuation curves does not change with varying weather conditions, but the levels do.

Exhibit 1.3.1-2 shows the effect of path length on gaseous attenuation. The exhibit shows the total gaseous attenuation observed on a satellite path located in Washington DC with elevation angles from 5 to 30 degrees. The values for the U.S. standard atmosphere, with an absolute humidity of 7.5 $g/m^3$ were assumed. (The curves were calculated from the Leibe Model, described in Section 2.2.1.1). The stark effect of the oxygen absorption lines at around 60 GHz is seen. The water vapor absorption line at 22.3 GHz is observed. As the elevation angle is decreased, the path length through the troposphere increases, and the resultant total attenuation increases. For example, at 30 GHz, the path attenuation increases from about 1 dB to nearly 4 dB as the elevation angle decreases from 30 to 5 degrees.

Procedures for calculation of the gaseous attenuation from atmospheric gases are presented in Section 2.2.1 of this handbook.

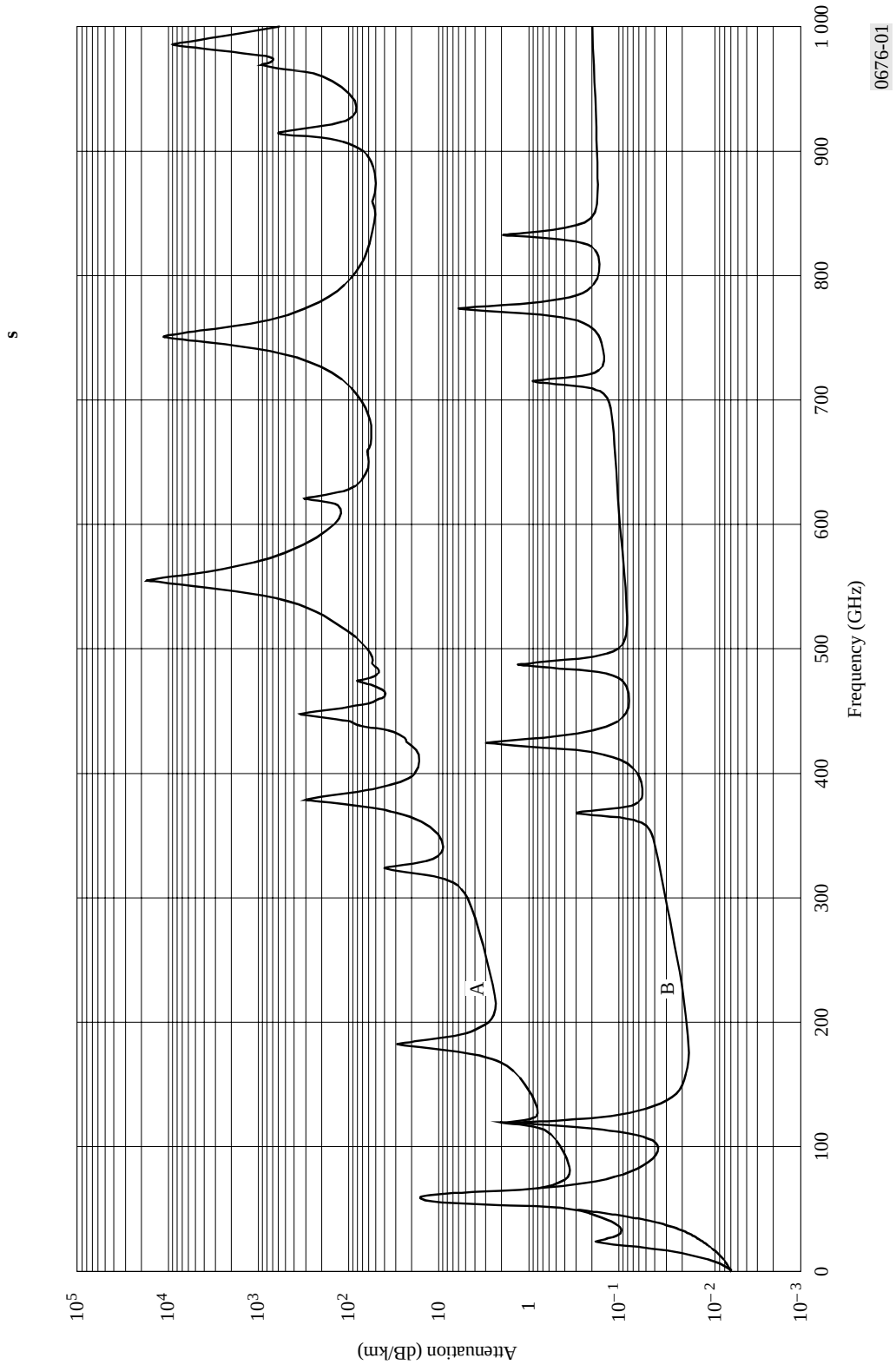


Exhibit 1.3.1-1. Specific attenuation due to atmospheric gases
*[Source: ITU-R P.676-3 (1997)]*

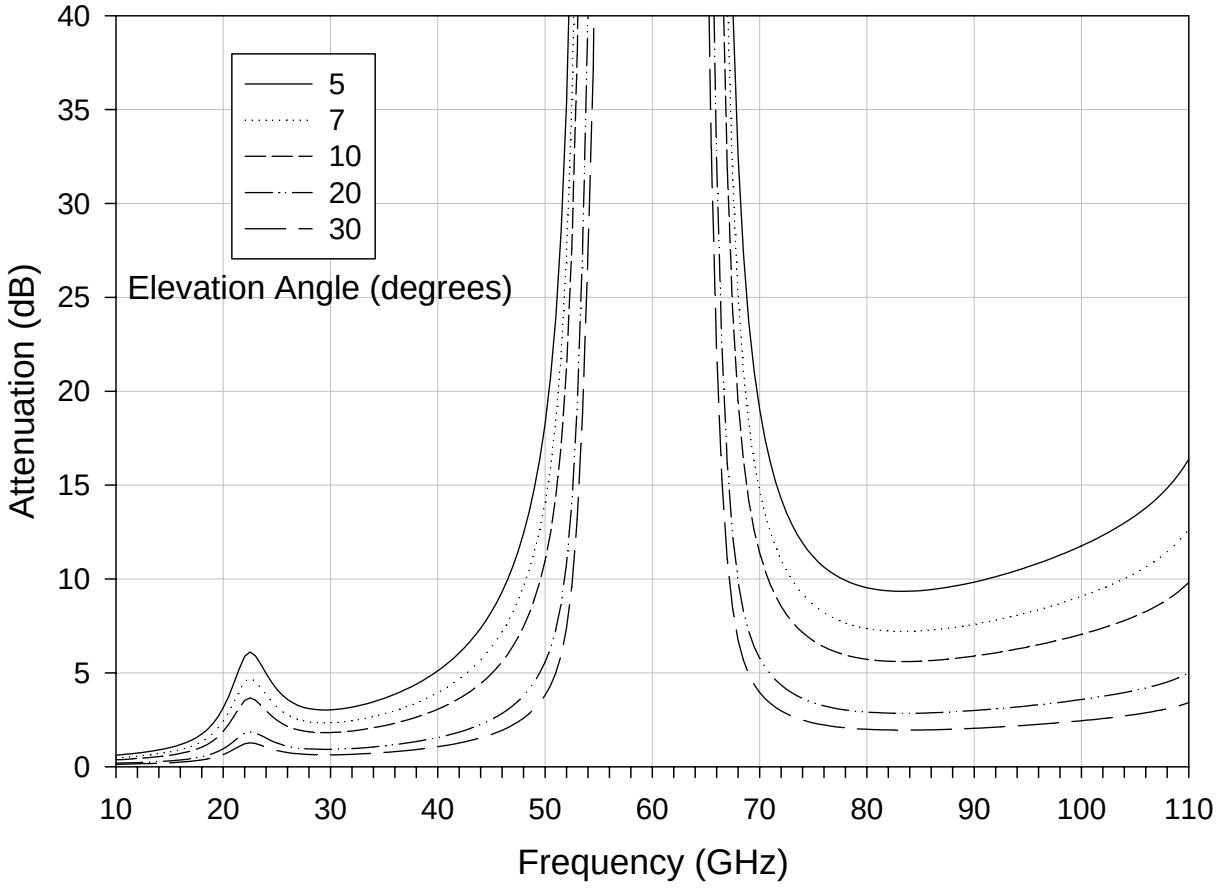


Exhibit 1.3.1-2
Total path gaseous attenuation versus frequency for elevation angles from 5 to 30 degrees.
Location: Washington DC.

### 1.3.2 Clouds, Fog

Although rain is the most significant hydrometer affecting radiowave propagation, the influence of clouds and fog can also be present on an earth-space path. Clouds and fog generally consist of water droplets of less than 0.1 mm in diameter, while raindrops typically range from 0.1 mm to 10 mm in diameter. Clouds are water droplets, not water vapor, however the relative humidity is usually near 100 % within the cloud. High-level clouds, such as cirrus, are composed of ice crystals which do not contribute substantially to radiowave attenuation but can cause depolarization effects (see Section 1.3.4).

Attenuation due to fog is typically not significant for frequencies less than about 100 GHz. The liquid water density in fog is typically about 0.05 g/m$^3$ for medium fog (visibility of the order of 300 m) and 0.5 g/m$^3$ for thick fog (visibility of the order of 50 m).

The average liquid water content of clouds varies widely, ranging from 0.05 to over 2 g/m$^3$. Peak values exceeding 5 g/m$^3$ have been observed in large cumulus clouds associated with thunderstorms, however peak values for fair weather cumulus are generally less than 1 g/m$^3$. Exhibit 1.3.2-1 summarizes the concentration, liquid water content, and droplet diameter for a range of typical cloud types.

| **Cloud Type** | **Concentration** ***(no/cm$^3$)*** | **Liquid Water** ***(g/ m$^3$)*** | **Average Radius** ***(microns)*** |
|---|---|---|---|
| Fair-weather cumulus | 300 | 0.15 | 4.9 |
| Stratocumulus | 350 | 0.16 | 4.8 |
| Stratus (over land) | 464 | 0.27 | 5.2 |
| Altostratus | 450 | 0.46 | 6.2 |
| Stratus (over water) | 260 | 0.49 | 7.6 |
| Cumulus congestus | 2-7 | 0.67 | 9.2 |
| Cumulonimbus | 72 | 0.98 | 14.8 |
| Nimbostratus | 330 | 0.99 | 9.0 |

Exhibit 1.3.2-1
Observed Characteristics of Typical Cloud Types
*[Source: Slobin (1982)]*

#### 1.3.2.1 Specific Attenuation for Cloud Attenuation

The specific attenuation within a cloud or fog can be written as:

$$\gamma_c = \kappa_c M \qquad \text{dB/km} \tag{1.3.2.1-1}$$

where:

$\gamma_C$ is the specific attenuation of the cloud, in dB/km,

$\kappa_c$ is the specific attenuation coefficient, in (dB/km)/(g/m$^3$), and

M is the liquid water density in g/m$^3$.

The small size of cloud and fog droplets allows the Rayleigh approximation to be employed in the calculation of specific attenuation. This approximation is valid for radiowave frequencies up to about 100 GHz. A mathematical model based on Rayleigh scattering, which uses a double-Debye model for the dielectric permittivity $\varepsilon(f)$ of water, can be used to calculate the value of $\kappa_c$ for frequencies up to 1000 GHz:

$$\kappa_c = \frac{0.819 f}{\varepsilon''(1+\eta^2)} \qquad (\text{dB/km})/(\text{g/m}^3) \tag{1.3.2.1-2}$$

where f is the frequency in GHz, and:

$$\eta = \frac{2+\varepsilon'}{\varepsilon''} \tag{1.3.2.1-3}$$

The complex dielectric permittivity of water is given by:

$$\varepsilon''(f) = \frac{f(\varepsilon_0 - \varepsilon_1)}{f_p\left[1+\left(\frac{f}{f_p}\right)^2\right]} + \frac{f(\varepsilon_1 - \varepsilon_2)}{f_s\left[1+\left(\frac{f}{f_s}\right)^2\right]} \tag{1.3.2.1-4}$$

$$\varepsilon'(f) = \frac{(\varepsilon_0 - \varepsilon_1)}{\left[1+\left(\frac{f}{f_p}\right)^2\right]} + \frac{(\varepsilon_1 - \varepsilon_2)}{\left[1+\left(\frac{f}{f_s}\right)^2\right]} + \varepsilon_2 \tag{1.3.2.1-5}$$

where:

$$\varepsilon_0 = 77.6 + 103.3\left(\frac{300}{T} - 1\right)$$
$$\varepsilon_1 = 5.48 \tag{1.3.2.1-6}$$
$$\varepsilon_2 = 3.51$$

with T the temperature, in K.

The principal and secondary relaxation frequencies are:

$$f_p = 20.09 - 142\left(\frac{300}{T} - 1\right) + 294\left(\frac{300}{T} - 1\right)^2 \quad \text{GHz} \qquad (1.3.2.1\text{-}7)$$

$$f_s = 590 - 1500\left(\frac{300}{T} - 1\right) \quad \text{GHz} \qquad (1.3.2.1\text{-}8)$$

Exhibit 1.3.2-2 shows the values of the specific attenuation $K_C$ at frequencies from 5 to 200 GHz and temperatures between –8° C and 20° C.

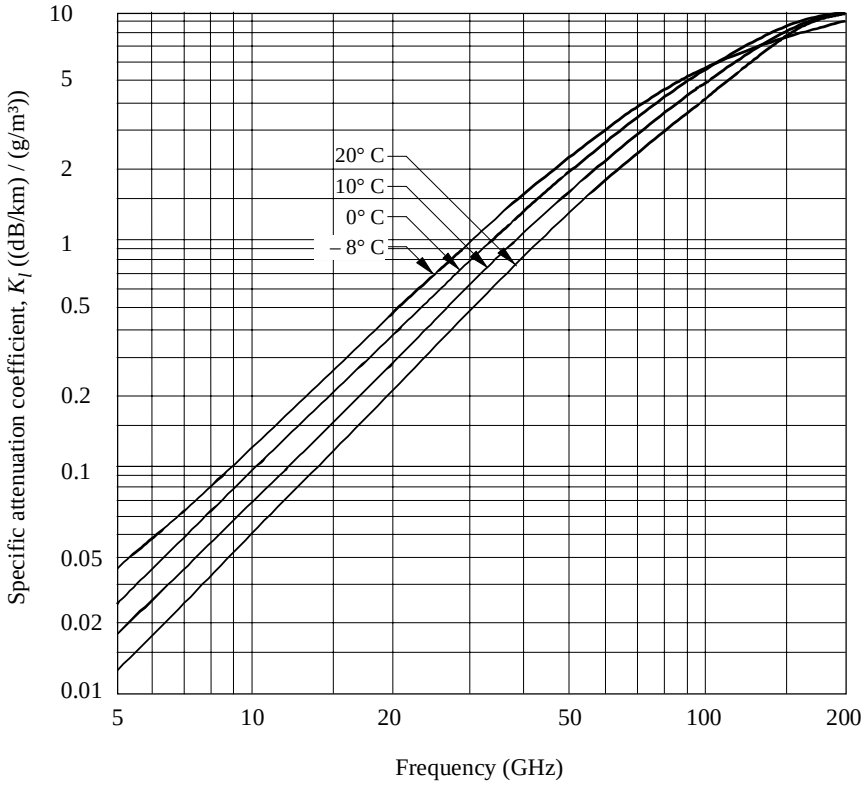


Exhibit 1.3.2-2
Specific Attenuation for Clouds as a function of Frequency and Temperature
*[Source ITU-R Rec. P.840-2 (1997)]*

### 1.3.2.2 Total Cloud Attenuation

The total attenuation due to clouds, $A_T$, can be

$$A_T = \frac{L\,\kappa_c}{\sin\theta} \qquad \text{dB} \qquad (1.3.2.1\text{-}9)$$

determined from the the statistics of
where

$\theta$ is the elevation angle,

$\kappa_c$ is the specific attenuation coefficient, in (dB/km)/(g/m$^3$), and

L is the total columnar content of liquid water, in kg/m$^2$ or, equivalently, in mm of precipitable water.

Statistics of the total columnar content of liquid water may be obtained from radiometric measurements or from radiosonde launches. In the absence of local measurements, the total columnar content of cloud liquid water (normalized to 0°C) values are available in ITU-R Rec. P.840-2 (1997).

Exhibit 1.3.2-3 shows the total cloud attenuation as a function of frequency, for elevation angles from 5 to 30 degrees. The calculations were based on stratus clouds with a cloud depth of 0.67 km, cloud bottom of 0.33 km, and a liquid water content of 0.29 g/m$^3$. The cloud attenuation is seen to increase with frequency and with decreasing elevation angle.

Procedures for the calculation of cloud attenuation are presented in Section 2.2.2 of this handbook

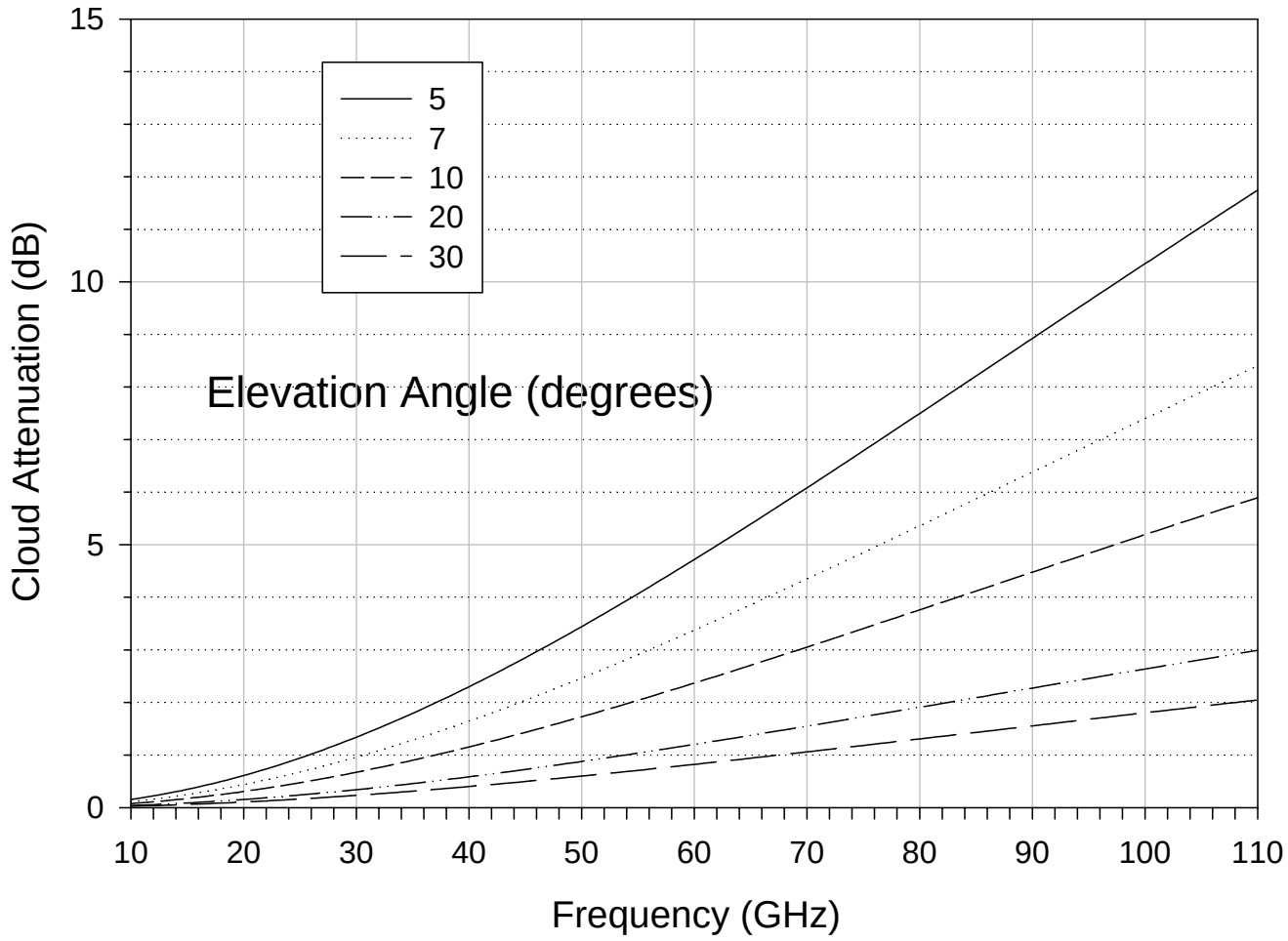


Exhibit 1.3.2-3
Total cloud attenuation as a function of frequency, for elevation angles from 5 to 30 degrees

.

.

### 1.3.3 Rain Attenuation and Depolarization

Rain on the transmission path is the major tropospheric effect of concern for earth-space communications, particularly for systems operating in the frequency bands above 10 GHz. Raindrops absorb and scatter radiowave energy, resulting in *rain attenuation* (a reduction in the transmitted signal amplitude), which can degrade the reliability and performance of the communications link. The non-spherical structure of raindrops also can change the polarization characteristics of the transmitted signal, resulting in *rain depolarization* (a transfer of energy from one polarization state to another). Rain effects are dependent on wavelength (i.e. frequency), rain rate, drop size distribution, drop shape (oblateness) and, to a lesser extent, ambient temperature and pressure.

The attenuating and depolarizing effects of the troposphere, and the statistical nature of these effects, are affected by macroscopic and microscopic characteristics of rain systems. The macroscopic characteristics include size, distribution and movements of rain cells, the height of melting layers and the presence of ice crystals. The microscopic characteristics include the size distribution, density and oblateness of both raindrops and ice crystals. The combined effect of the characteristics on both scales leads to the cumulative distribution of attenuation and depolarization versus time, the duration of fades and depolarization periods, and the specific attenuation/depolarization versus frequency.

#### 1.3.3.1 Spatial Structure of Rain

The relative impact of rain conditions on the transmitted signal depends on the spatial structure of rain. Three types of rain structure are important in the evaluation of rain effects on earth space communications; stratiform rain, convective rain, and cyclonic storm conditions.

**Stratiform Rain** In midlatitude regions, stratiform rainfall is the type of rain which typically shows stratified horizontal extents of hundreds of kilometers, duration times exceeding one hour and rain rates less than about 25 mm/h (1 inch/h). Stratiform rain usually occurs during the spring and fall months and, because of the cooler temperatures, results in vertical heights of 4 to 6 km. For communications applications, stratiform rain represents a rain rate which occurs for a sufficiently long period that a link margin may be required to exceed the attenuation associated with a one-inch per hour (25 mm/h) rain rate.

**Convective Rain** Convective rains arise from vertical atmospheric motions resulting in vertical transport and mixing. The convective flow occurs in a cell whose horizontal extent is usually several kilometers. The cell extends to heights greater than the average freezing layer at a given location because of convective upwelling. The cell may be isolated or embedded in a thunderstorm region associated with a passing weather front. Because of the motion of the front and the sliding motion of the cell along the front, the high rain rate duration is usually only

several minutes in extent. These rains are the most common source of high rain rates in the U.S. and temporate regions of the world.

**Cyclonic Storms** Tropical cyclonic storms (hurricanes) often pass over the eastern seaboard of North America during the August-October time period. These circular storms are typically 50 to 200 km in diameter, move at 10-20 kilometers per hour, extend to melting layer heights up to 8 km and have high (greater than 25 mm/h) rain rates.

Stratiform and cyclonic rain types cover large geographic locations and the spatial distribution of total rainfall from one of these storms is expected to be uniform. Likewise the rain rate averaged over several hours is expected to be rather similar for ground sites located up to tens of kilometers apart. Convective storms, however, are localized and tend to give rise to spatially non-uniform distributions of rainfall and rain rate for a given storm.

### 1.3.3.2 Classical Description For Rain Attenuation

The classical development for the determination of rain attenuation on a transmitted radiowave is based on three assumptions describing the nature of radiowave propagation and precipitation (Ippolito, 1986);

1. The intensity of the wave *decays exponentially* as it propagates through the volume of rain.

2. The raindrops are assumed to be *spherical* water drops, which both scatter and absorb energy from the incident radiowave.

3. The contributions of each drop are *additive* and are *independent* of the other drops. This implies a "single scattering" of energy, however, the empirical results of the classical development do allow for some "multiple scattering" effects.

The attenuation of a radiowave propagating through a volume of rain of extent L in the direction of propagation can be expressed as

$$A = \int_0^L \alpha \, dx \qquad (1.3.3.2\text{-}1)$$

where $\alpha$ is the specific attenuation of the rain volume, expressed in dB/km, and the integration is taken along the extent of the propagation path, from x = 0 to x = L.

Consider a plane wave with a transmitted power of $p_t$ watts incident on a volume of uniformly distributed spherical water drops, all of radius r, extending over a length L in the direction of

wave propagation, as shown in Exhibit 1.3.3.2-1. Under the assumption that the intensity of the wave decays exponentially as it propagates through the volume of rain, the received power, $p_r$, will be

$$p_r = p_t\, e^{-k\,L} \qquad (1.3.3.2\text{-}2)$$

where k is the attenuation coefficient for the rain volume, expressed in units of reciprocal length.

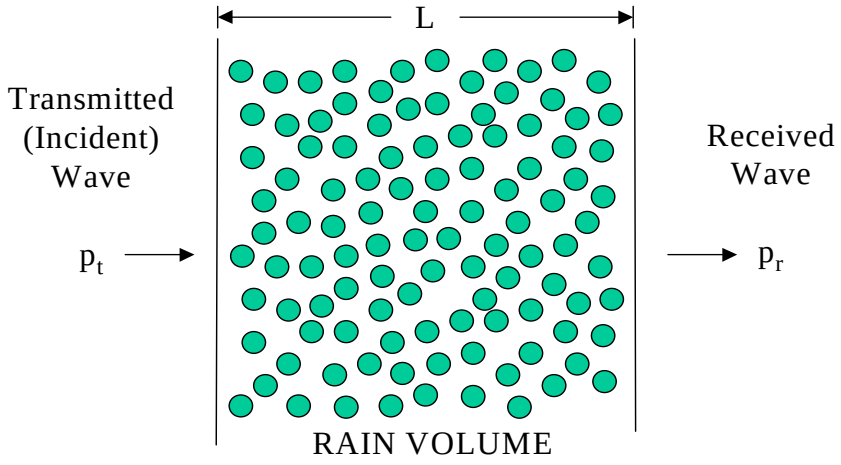


Exhibit 1.3.3.2-1
Plane Wave Incident on a Volume of Spherical Uniformly Distributed Water Drops

The attenuation of the wave, usually expressed as a positive decibel (dB) value, is given by

$$A(\mathrm{dB}) = 10\log_{10}\left(\frac{p_t}{p_r}\right) \qquad (1.3.3.2\text{-}3)$$

Converting the logarithm to the base e and employing Equation (1.3.3.2-2)

$$A(\mathrm{dB}) = 4.343\,k\,L \qquad (1.3.3.2\text{-}4)$$

The attenuation coefficient k is expressed as

$$k = \rho\, Q_t \qquad (1.3.3.2\text{-}5)$$

where $\rho$ is the *drop density*, i.e. the number of drops per unit volume, and,
$Q_t$ is the *attenuation cross-section* of the drop, expressed in units of area.

The cross-section describes the physical profile that an object projects to a radiowave. It is defined as the ratio of the total power extracted from the wave [watts] to the total incident power density [watts/(meter)$^2$], hence the units of area, (meter)$^2$.

For raindrops, $Q_t$ is the sum of a scattering cross-section, $Q_s$, and an absorption cross-section, $Q_a$. The attenuation cross section is a function of the drop radius, r, wavelength of the radiowave, $\lambda$, and complex refractive index of the water drop, m. That is

$$Q_t = Q_s + Q_a = Q_t(r, \lambda, m) \tag{1.3.3.2-6}$$

The drops in a 'real' rain are not all of uniform radius, and the attenuation coefficient must be determined by integrating over all of the drop sizes, i.e.

$$k = \int Q_t(r, \lambda, m)\, \eta(r)\, dr \tag{1.3.3.2-7}$$

where $\eta(r)$ is the drop size distribution. $\eta(r)dr$ can be interpreted as the number of drops per unit volume with radii between r and r + dr.

The specific attenuation, $\alpha$, in dB/km, is found from Equations 1.3.3.2-4 and 1.3.3.2-7, with L = 1 km,

$$\alpha\left(\frac{dB}{km}\right) = 4.343 \int Q_t(r, \lambda, m)\, \eta(r)\, dr \tag{1.3.3.2-8}$$

The above result demonstrates the dependence of rain attenuation on drop size, drop size distribution, rain rate, and attenuation cross-section. The first three parameters are characteristics of the rain structure only. It is through the attenuation cross-section that the frequency and temperature dependence of rain attenuation is determined. All of the parameters exhibit time and spatial variability's which are not deterministic or directly predictable, hence most analyses of rain attenuation must rely on statistical analyses to quantitatively evaluate the impact of rain on communications systems.

The solution of Equation (1.3.3.2-8) requires $Q_t$ and $\eta(r)$ as a function of the drop size, r.

$Q_t$ can be found by employing the classical scattering theory of Mie for a plane wave radiating an absorbing sphere (Mie, 1908).

Several investigators have studied the distributions of raindrop size as a function of rain rate and type of storm activity, and the drop size distributions were found to be well represented by an exponential of the form

$$\eta(r) = N_0\, e^{-\Lambda r} = N_0\, e^{-\left[cR^{-d}\right]r} \qquad (1.3.3.2\text{-}9)$$

where R is the rain rate, in mm/h, and r is the drop radius, in mm. $N_0$, $\Lambda$, c, and d are empirical constants determined from measured distributions (Ippolito, 1986).

The total rain attenuation for the path is then obtained by integrating the specific attenuation over the total path L, i.e.

$$a(dB) = 4.343 \int_0^L \left[ N_0 \int Q_t(r, \lambda, m)\, e^{-\Lambda r} dr \right] dl \qquad (1.3.3.2\text{-}10)$$

where the integration over l is taken over the extent of the rain volume in the direction of propagation. Both $Q_t$ and the drop size distribution will vary along the path and these variabilities must be included in the integration process. A determination of the variations along the propagation path is very difficult to obtain, particularly for slant paths to an orbiting satellite. These variations must be approximated or treated statistically for the development of useful rain attenuation prediction models.

### 1.3.3.3 Attenuation and Rain Rate

When measurements of rain attenuation on a terrestrial path were compared with the rain rate measured on the path, it was observed that the specific attenuation (dB/km) could be well approximated by

$$\alpha\left(\frac{dB}{km}\right) \cong a\, R^b \qquad (1.3.3.3\text{-}1)$$

where R is the rain rate, in mm/h, and a and b are frequency and temperature dependent constants. The constants a and b represent the complex behavior of the complete representation of the specific attenuation as given by Equation (1.3.3.2-8). This relatively simple expression for attenuation and rain rate was observed directly from measurements by early investigators such as Ryde & Ryde (1945), and Gunn & East (1954), however, analytical studies, most notably that of Olsen, Rogers, & Hodge (1978), have demonstrated an analytical basis for the $aR^b$ expression. Appendix C of Ippolito (1986) provides a full development of the analytical basis for the $aR^b$ representation described above.

The use of the $aR^b$ expression is included in virtually all current published models for the prediction of path attenuation from rain rate.

An example of the application of one of the models, the Crane Global Model, is shown in Exhibit1.3.3.2-2. The exhibit presents the rain attenuation expected for 99% of an average year, for operating frequencies from 10 to 110 GHz. The plots are for a ground terminal located in Washington, DC, and are shown for elevation angles to the satellite from 5 to 30 degrees.

Several general characteristics of rain attenuation are seen on the Exhibit. Rain attenuation increases with increasing frequency, and with decreasing elevation angle. Rain Attenuation levels can be very high, particularly for frequencies above 30 GHz. These plots are for a 99% annual link availability, which corresponds to a link outage (un-availability) of 1% or about 88 hours oer year.

Several models and procedures for the prediction of rain attenuation on satellite paths, including the Global Model, are presented in Section 2.2.4 of this handbook.

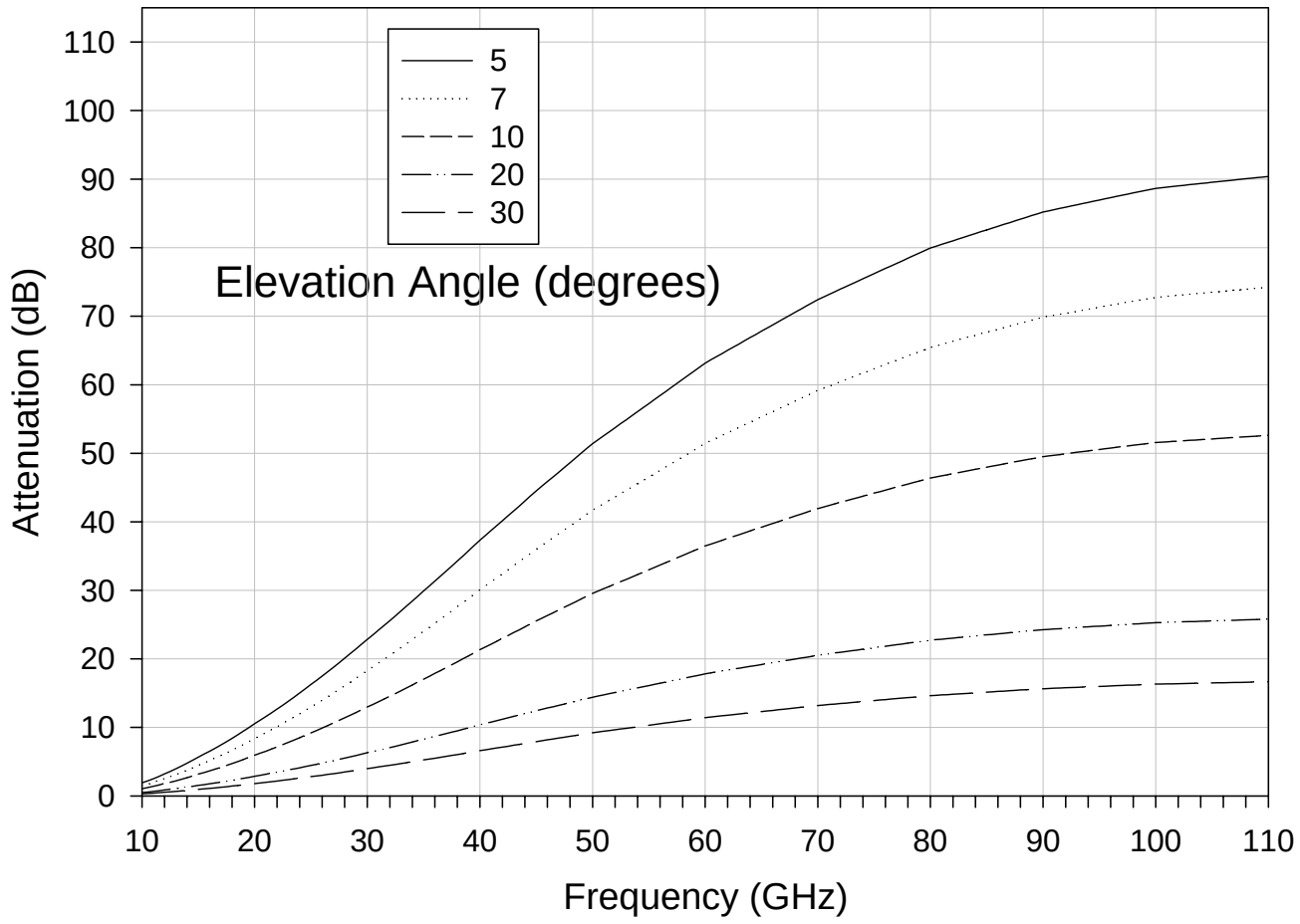


Exhibit1.3.3.2-2
Total path rain attenuation as a function of frequency and elevation angle
Location: Washington, DC
Availability: 99%
Prediction Model: Crane Global Model (see Section 2.2.4.2)

### 1.3.3.4 Rain Depolarization

Rain induced depolarization is produced from a differential attenuation and phase shift caused by non-spherical raindrops. As the size of rain drops increase, their shape tends to change from spherical (the preferred shape because of surface tension forces) to oblate spheroids with an increasingly pronounced flat or concave base produced from aerodynamic forces acting upward on the drops. Furthermore, raindrops may also be inclined to the horizontal (canted) because of vertical wind gradients. Therefore the depolarization characteristics of a linearly polarized radiowave will depend significantly on the transmitted polarization angle.

An understanding of the depolarizing characteristics of the earth's atmosphere is particularly important in the design of frequency reuse communications systems employing dual independent orthogonal polarized channels in the same frequency band to increase channel capacity. Frequency reuse techniques, which employ either linear or circular polarized transmissions, can be impaired by the propagation path through a transferal of energy from one polarization state to the other orthogonal state, resulting in interference between the two channels.

Exhibit 1.3.3.4-1 shows a representation of the depolarization effect in terms of the E-field (electric field) vectors in a linearly polarized transmission link. The vectors $E_1$ and $E_2$ are the transmitted vertical and horizontal direction waves polarized 90 degrees apart (orthogonal) to provide two independent signals at transmission. The transmitted waves will be depolarized by the medium into several components, as shown by Exhibit 1.3.3.4-1.

The *cross-polarization discrimination*, XPD, is defined for the linearly polarized waves as

$$XPD_1 = 20 \log \frac{|E_{11}|}{|E_{12}|} \qquad (1.3.3.4\text{-}1a)$$

for the linear vertical (1) direction, and

$$XPD_2 = 20 \log \frac{|E_{22}|}{|E_{21}|} \qquad (1.3.3.4\text{-}1b)$$

for the linear horizontal (2) direction,

where $E_{11}$ ($E_{22}$) is the received electric field in the co-polarized (desired) direction and $E_{12}$ ($E_{21}$) is the electric field converted to the orthogonal cross-polarized (undesired) direction.

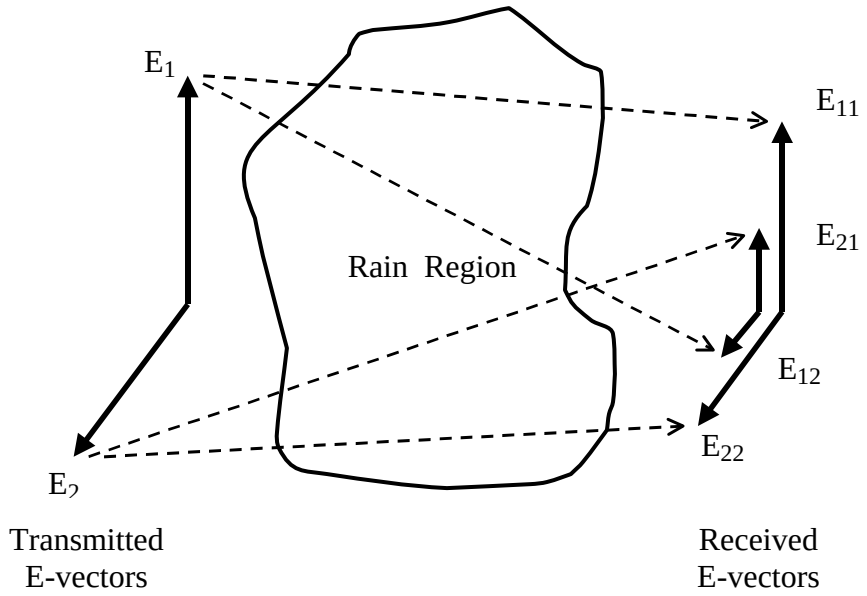


Exhibit 1.3.3.4-1
Depolarization components of linearly polarized waves

A closely related parameter is the *isolation*, I, which compares the co-polarized received power with the cross-polarized power received in the same polarization state, i.e.

$$I_1 = 20\log\frac{|E_{11}|}{|E_{21}|} \qquad (1.3.3.4\text{-}2a)$$

for the vertical direction, and

$$I_2 = 20\log\frac{|E_{22}|}{|E_{12}|} \qquad (1.3.3.4\text{-}2b)$$

for the horizontal direction.

Isolation takes into account the performance of the receiver antenna, feed and other components, as well as the propagating medium. When the receiver system polarization performance is close to ideal, then XPD and I are nearly identical, and only the propagating medium contributes depolarizing effects to system performance.

The XPD and I for circular polarized transmitted waves can also be defined. The XPD for circular polarized can be shown to be nearly equivalent to the XPD for linear or horizontal polarized wave oriented at $45^0$ from the horizontal (Ippolito, 1986).

The determination of the depolarization characteristics of rain requires knowledge of the canting angle of the raindrops, defined as the angle between the major axis of the drop and the local horizontal, shown as θ in Exhibit 1.3.3.4-2.

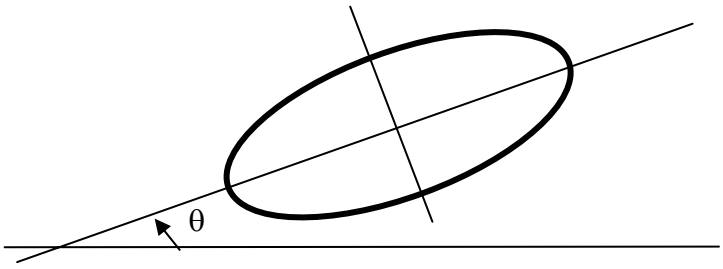


Exhibit 1.3.3.4-2
Canting Angle for Oblate Spheroid Rain Drop

The canting angle for each raindrop in a typical rain will be different and will be constantly changing as it falls to the ground, since the aerodynamic forces will cause the drop to 'wobble' and change orientation. Hence, for the modeling of rain depolarization a *canting angle distribution* is usually required and the XPD is defined in terms of the mean value of the canting angle. Measurements on earth-space paths using satellite beacons have shown that the average canting angle tends to be very close to 0 degrees (horizontal) for the majority of non-spherical raindrops (Arnold, et. al., 1980). Under this condition, the XPD for circular polarization is identical to the XPD for linear horizontal or vertical polarization oriented at 45 degrees from the horizontal.

When measurements of depolarization observed on a radiowave path were compared with rain attenuation measurements concurrently observed on the same path, it was noted that the relationship between the measured statistics of XPD and co-polarized attenuation, A, could be well approximated by the relationship

$$XPD = U - V \log A \qquad \text{(dB)} \qquad (1.3.3.4\text{-}3)$$

where U and V are empirically determined coefficients which depend on frequency, polarization angle, elevation angle, canting angle, and other link parameters. This discovery is similar to the $aR^b$ relationship observed between rain attenuation and rain rate discussed in Section 1.3.3.3.

A theoretical basis for the relationship between rain depolarization and attenuation given above was developed by Nowland et al (1977), from small argument approximations applied to the scattering theory of Oguchi for an oblate spheroid raindrop.

For most rain depolarization prediction models, semi-empirical relations can be used for the U and V coefficients. An example of the application of a rain depolarization prediction model is shown in Exhibit 1.3.3.4-3. The exhibit shows cross polarization discrimination, XPD, as a function of frequency and elevation angle. The curves are for a ground terminal in Washington, DC, and the link availability was set at 99%. The Chu Model (Section 2.2.5.1.1) was used for the calculations.

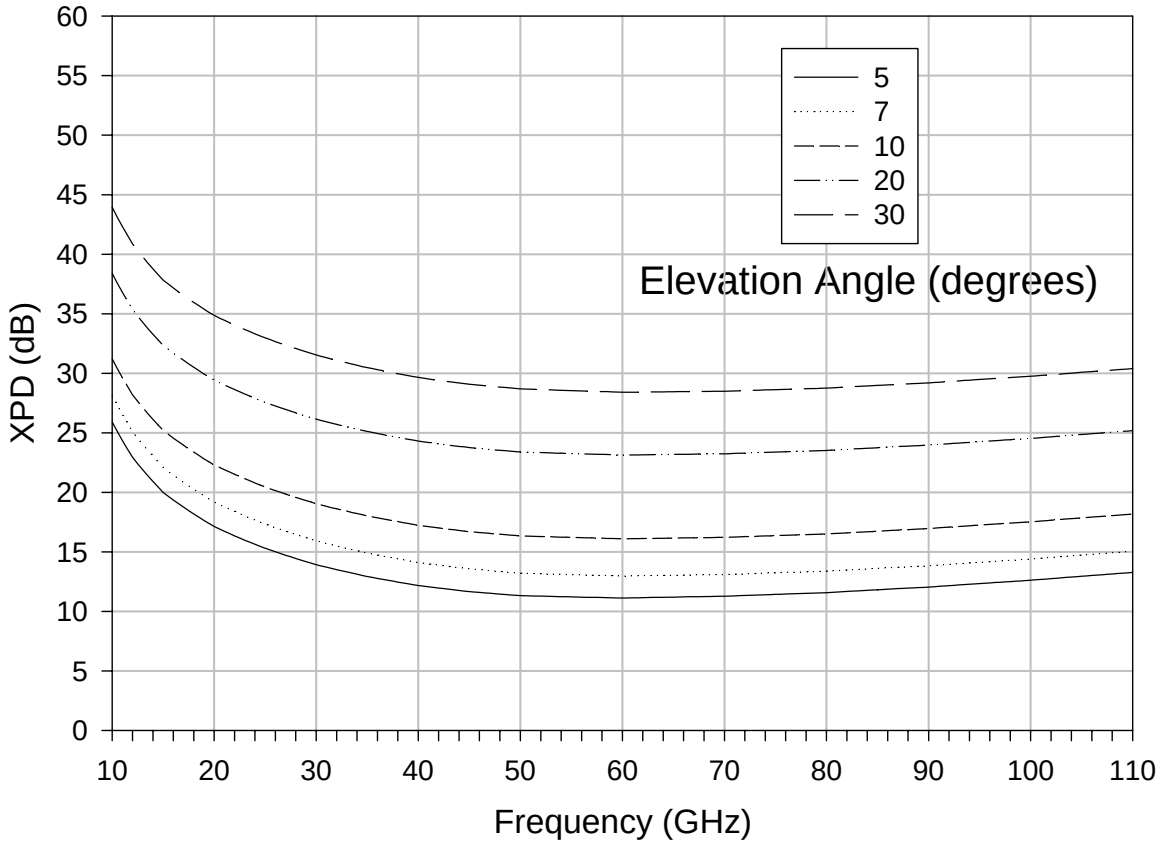


Exhibit 1.3.3.4-3
Rain Depolarization XPD as a function of frequency and elevation angle
Location: Washington, DC
Availability: 99%
Prediction Model: Chu Semi-Empirical Model (see Section 2.2.5.1.1)

Several models and procedures for the prediction of rain depolarization are provided in Section 2.2.5 of this handbook.

### 1.3.4 Ice Depolarization

A second source of depolarization on an Earth-space path, in addition to rain, is the presence of ice crystals in clouds at high altitudes. Ice crystal depolarization is caused primarily by differential phase shifts rather than differential attenuation, which is the major mechanism for raindrop depolarization. Ice crystal depolarization can occur with little or no co-polarized attenuation. The amplitude and phase of the cross-polarized component can exhibit abrupt changes with large excursions.

Ice crystals form around dust particles in shapes influenced by the ambient temperature. In cirrus clouds they may exist for an indefinite time, but in cumulonimbus clouds they follow a cycle of growth by sublimation, falling and melting in the lower reaches of the cloud. Radio, radar and optical observations confirm that cloud ice crystals possess some degree of preferred orientation related to the orientation of the electrostatic field. The crystals range in size from 0.1 to 1 mm and concentrations range from $10^3$ to $10^6$ crystals/$m^3$. The variation in concentration and occurrence of events may be due to the variation of "seed" nuclei in various air masses. For example, continental air masses contain more dust nuclei than maritime air masses and so occurrences of ice-crystal depolarization occur more frequently at inland ground stations.

Temperature and aerodynamic forces influence the shape of ice crystals. The two preferred shapes for ice crystals are *needles* and *plates*. At temperatures of $-25^0$C the crystals are mainly needles, while for temperatures of $-25^0$C to $-9^0$C they are mainly plates. The crystals are very light and tend to fall very slowly. (Allnutt, 1989).

An “anomalous” form of depolarization was observed in early depolarization measurements in the United States using the linearly polarized 20 GHz ATS-6 beacon, but it was not recognized as ice depolarization until the ATS-6 measurements in Europe a year later, and the CTS and COMSTAR measurements in the United States which followed (Bostian & Allnutt, 1979). Ice depolarization effects have been observed at frequencies from 4 GHz to 30 GHz and higher (Ippolito, 1986).

Exhibit 1.3.4-1 shows an example of an ice depolarization event observed by Vogel (1980) at Austin, Texas with the 11.7 GHz CTS beacon. The cross-polarized signal level begins to increase at 2300 h, reaching a peak change of about 14 dB, while the co-polarized attenuation remains less than 1 dB.

Exhibit 1.3.4-2 provides another example of ice depolarization, observed by Shutie, et al, (1977) at Slough, England with the 30 GHz ATS-6 beacon. The first event, beginning at about 2338 h, occurred during intense lightning, and the next two events occurred during rain, as indicated by the notes on the plot. The XPD degraded by over 20 dB during the intense lightning, with copolarized attenuation remaining less than 5 dB, and with little time correlation between the

two. The XPD variations during the rain periods, on the other hand, are well correlated with the co-polarized attenuation variations.

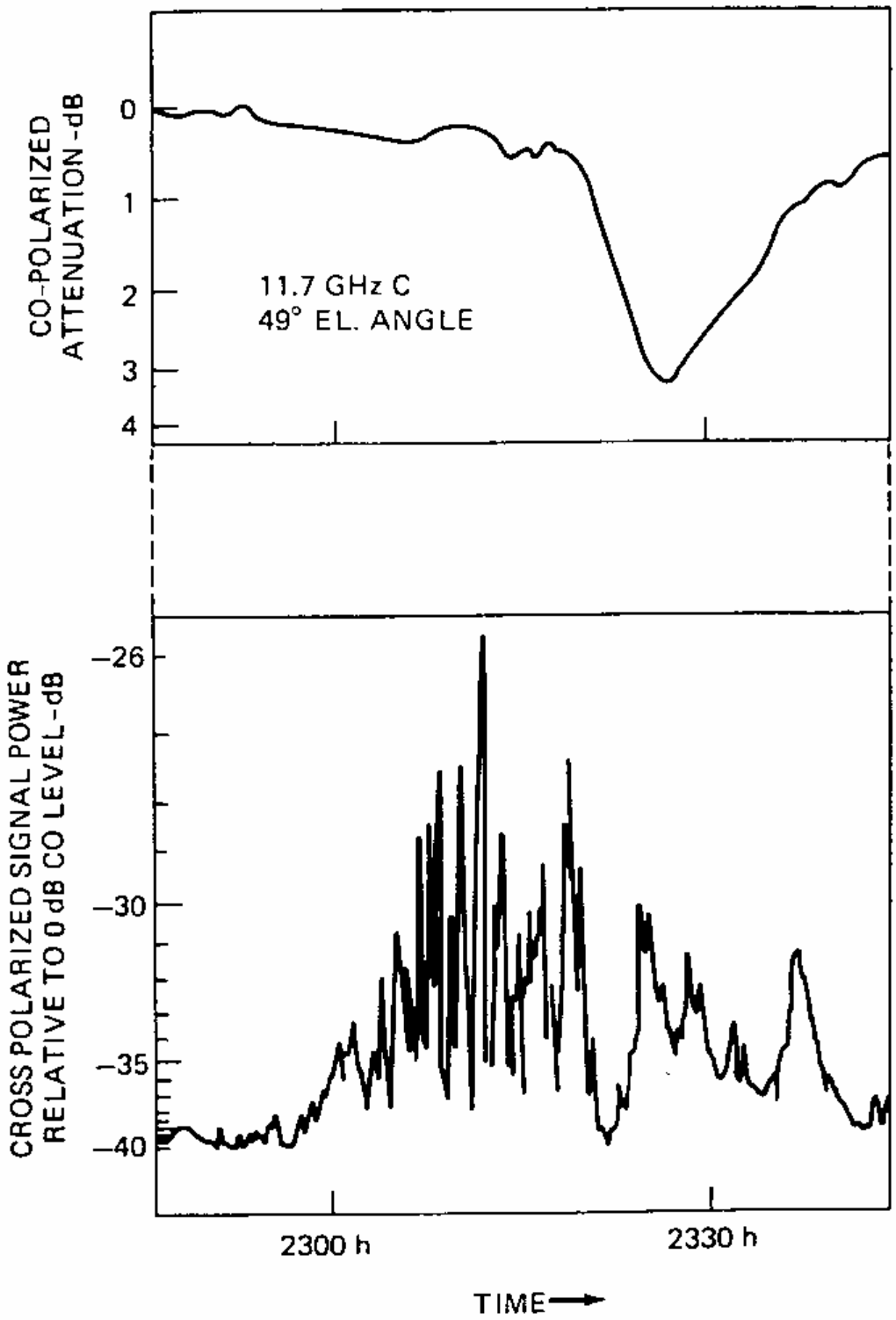


Exhibit 1.3.4-1
Ice Depolarization event at Austin, Texas, June 26, 1976.
Frequency: 11.7 GHz, Elevation Angle: $49^0$
*[Source: Ippolito, 1986]*

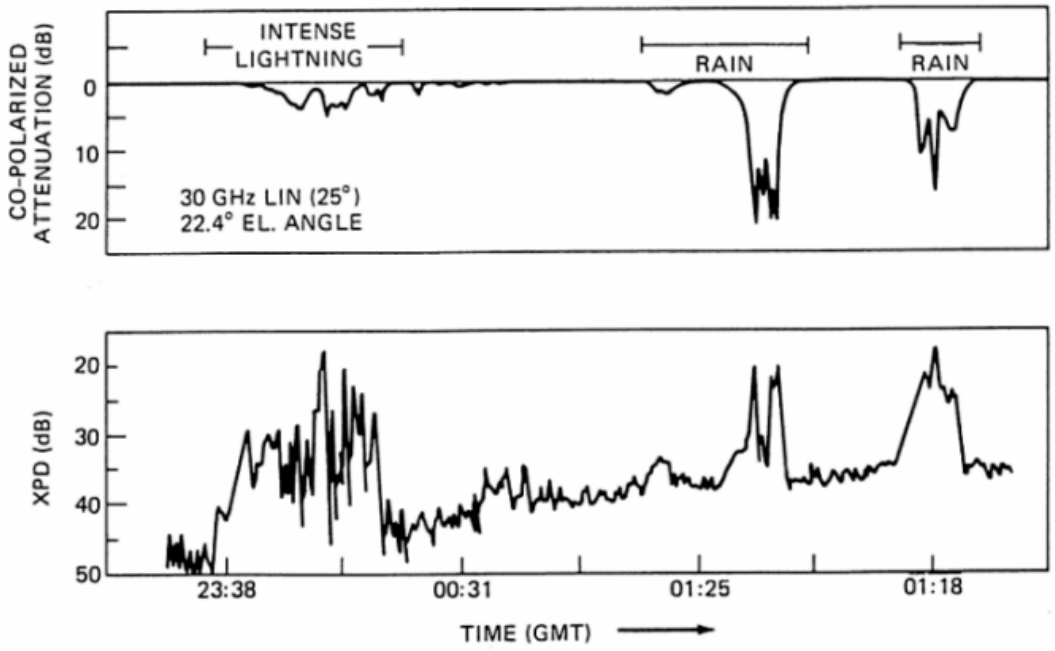


Exhibit 1.3.4-2
Ice Depolarization observed at Slough, England, July 14-16, 1976.
Frequency: 30 GHz, Elevation Angle: $22.4^0$
*[Source: Ippolito, 1986]*

These examples are typical of ice depolarization events observed on satellite paths. Ice depolarization often (but not always!) occurs several minutes before the appearance of a severe rain attenuation event. Ice depolarization characteristics have been observed in the presence of clouds, light precipitation, and in clear sky, as well as during the occurrence of lightning discharges.

The contribution of ice depolarization to the total depolarization on a radiowave link is difficult to determine from direct measurement, but can be inferred from observation of the copolarized attenuation during depolarization events. The depolarization which occurs when the copolarized attenuation is low, (i.e., less than 1 to 1.5 dB), can be assumed to be caused by ice particles alone, while the depolarization which occurs when copolarized attenuation is higher can be attributed to both rain and ice particles (Ippolito, 1986).

Two methods for the prediction of ice depolarization on a satellite path are provided in Section 2.2.6 of this handbook.

### 1.3.5 Tropospheric Scintillation

Scintillation describes the condition of rapid fluctuations of the signal parameters of a radiowave caused by time dependent irregularities in the transmission path. Signal parameters affected include amplitude, phase, angle of arrival, and polarization. Scintillation effects can be produced in both the ionosphere and in the troposphere. Electron density irregularities occurring in the ionosphere can affect frequencies up to about 6 GHz, while refractive index irregularities occurring in the troposphere cause scintillation effects in the frequency bands above about 3 GHz.

The mechanisms and characteristics of ionospheric and tropospheric scintillation differ, and they are discussed separately in this handbook. Ionospheric scintillation is discussed in Section 1.2.3.2.
This section focuses on tropospheric scintillation.

Tropospheric scintillation is produced by refractive index fluctuations in the first few kilometers of altitude and is caused by high humidity gradients and temperature inversion layers. The effects are seasonally dependent, vary day-to-day, and vary with the local climate. Tropospheric scintillation has been observed on line of site links up through 10 GHz and on earth space paths at frequencies to above 30 GHz.

To a first approximation, the refractive index structure in the troposphere can be considered horizontally stratified, and variations appear as thin layers that change with altitude. Slant paths at low elevation angles, that is, highly oblique to the layer structure, thus tend to be effected most significantly by scintillation conditions.

The general properties of the refractive index of the troposphere are well known. The atmospheric radio ***refractive index***, or index of refraction, n, at radiowave frequencies, is a function of temperature, pressure, and water vapor content. For convenience, since n is very close to 1, the refractive index properties are usually defined in terms of N units, or radio ***refractivity***, as

$$N = (n-1)\,x10^{6} = \frac{77.6}{T}\left(p + 4810\frac{e}{T}\right) \qquad (1.3.5\text{-}1)$$

where:

p is the atmospheric pressure in millibars (mb),
e is the water vapor pressure in mb, and
T is the temperature, in degrees Kelvin.

The first term in Eq. 1.3.5-1 is often referred to as the “dry term”

$$N_{dry} = 77.6 \frac{P}{T} \qquad (1.3.5\text{-}2)$$

and the second term as the "wet term"

$$N_{wet} = 3.732 \text{ x } 10^5 \frac{e}{T^2} \qquad (1.3.5\text{-}3)$$

This expression is accurate to within 0.5% for frequencies up to 100 GHz.

The long term mean dependence of refractivity is found to be well represented by an exponential of the form,

$$N = 315\, e^{-\frac{h}{7.36}} \qquad (1.3.5\text{-}4)$$

where h is the altitude, in km. This approximation is valid for altitudes up to abour15 km (ITU-R Rec. P.453-6, 1997).

Small scale variations of refractivity, such as those caused by temperature inversions or turbulence, will produce scintillation effects on a satellite signal. Quantitative estimates of the level of amplitude scintillation produced by a turbulent layer in the troposphere are determined by assuming small fluctuations on a thin turbulent layer and applying turbulence theory considerations of Tatarski (1971). Amplitude scintillation is expressed as the log of the received power, i.e.

$$x(dB) = \log r \qquad (1.3.5\text{-}5)$$

The variance of the log of the received power, $\sigma^2_x$, is then found as

$$\sigma_x^2 = 42.25 \left( \frac{2\pi}{\lambda} \right)^{7/6} \int_0^L C_m^2(x)\, x^{5/6}\, dx \qquad (1.3.5\text{-}5)$$

where

$C^2_m$ is a refractive index structure constant,
$\lambda$ is the wavelength,
x is the distance along the path, and
L is the total path length.

A precise knowledge of the amplitude scintillation depends on $C^2_m$ , which is not easily available.

Equation (1.3.5-5) shows that the r.m.s. amplitude fluctuation, $\sigma_x$ , varies as $f^{7/12}$. Measurements at 10 GHz which show a range of from 0.1 to 1 dB, for example, would scale at 100 GHz to a range of about 0.38 to 3.8 dB.

### 1.3.5.1 Scintillation Measurements

The most predominant form of scintillation observed on earth-space communications links involves the amplitude of the transmitted signal. Scintillation increases as the elevation angle decreases, since the path interaction region increases. Scintillation effects increase dramatically as the elevation angle drops below about 10 degreees.

Several authors have reported scintillation effects at frequencies from 2 to above 30 GHz [Ippolito (1986), Salonen et al (1996), Otung (1996), Peeters et al (1997), Vogel et al (####)] The measurements showed broad agreement for scintillation at high elevation angles (20 to 30 degrees). In temperate climates the scintillation is on the order of 1 dB peak-to-peak in clear sky in the summer, 0.2 to 0.3 dB in winter, and 2 to 6 dB in cloud conditions. Scintillation fluctuations varied over a large range, however, with fluctuations from 0.5 Hz to over 10 Hz. A much slower fluctuation component, with a period of 1 to 3 minutes, was often observed along with the more rapid scintillation discussed above. At low elevation angles, (below 10 degrees), scintillation effects increased drastically. Deep fluctuations of 20 dB or more were observed, with durations of a few seconds in extent.

Exhibit 1.3.5.1-1 shows an example of low elevation amplitude scintillation measurements at 2 and 30 GHz made with the ATS-6 at Columbus, Ohio, reported by Devasirvathm and Hodge (1977). The elevation angles were 4.95 degrees (a), and 0.38 degrees (b). Measurements of this type were made in clear weather conditions up to an elevation angle of 44 degrees, and the data are summarized in Exhibit 1.3.5.1-2, where the mean amplitude variance is plotted as a function of elevation angle. The curves on the figure represent the minimum r.m.s. error fits to the assumed cosecant power law relation

$$\sigma_x^2 \approx A(\csc\theta)^B \qquad (1.3.5.1\text{-}1)$$

where $\theta$ is the elevation angle. The resulting B coefficients, as shown on the figure, compare well within their range of error with the expected theoretical value of 1.833 for a Kolmogorov type turbulent atmosphere.

Similar measurements were taken at 19 GHz with the COMSTAR satellites at Holmdel, N.J. (Titus & Arnold, 1982). Both horizontal and vertical polarized signals were monitored, at elevation angles from 1 to 10 degrees. Amplitude scintillation at the two polarization senses were found to be highly correlated, leading the authors to conclude that amplitude scintillation is independent of polarization sense.

Methods for the prediction of tropospheric scintillation on satellite paths are provided in Section 2.2.8.1 of this handbook. A prediction method for scintillation caused by clouds is provided in Section 2.2.8.2.

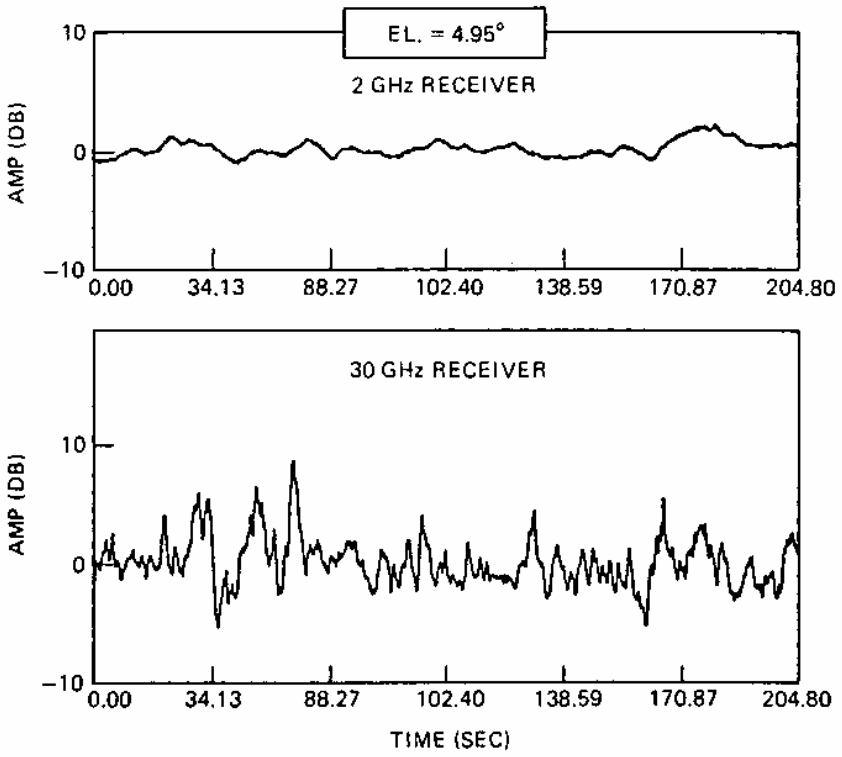


(a)

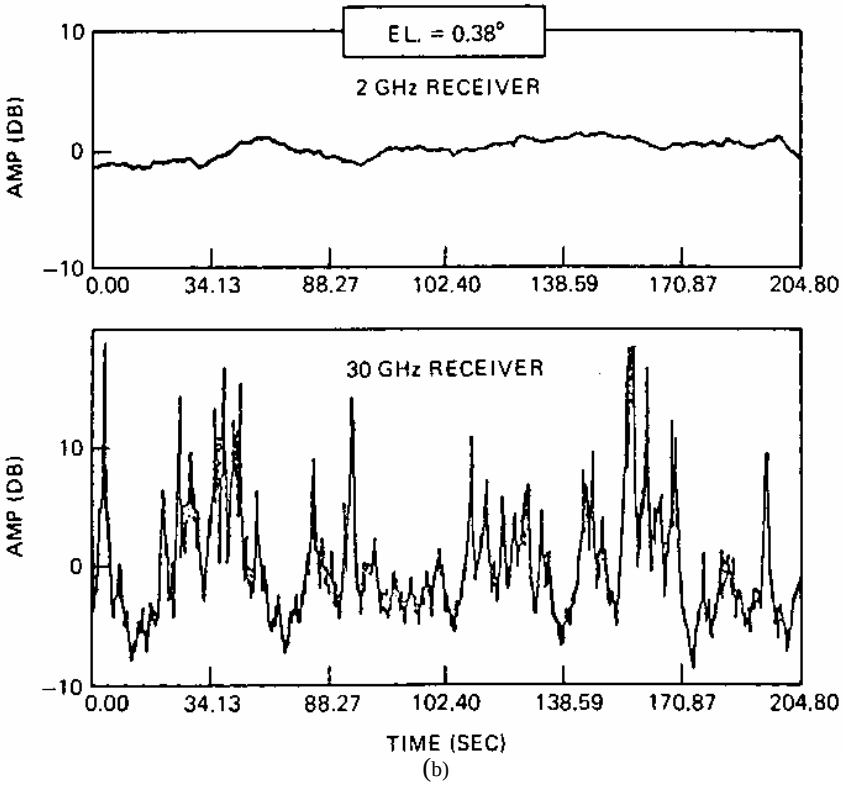


(b)

Exhibit 1.3.5.1-1
Amplitude Scintillation on a Satellite Link for Low Elevation Angles
*[Source: Ippolito (1986)]*

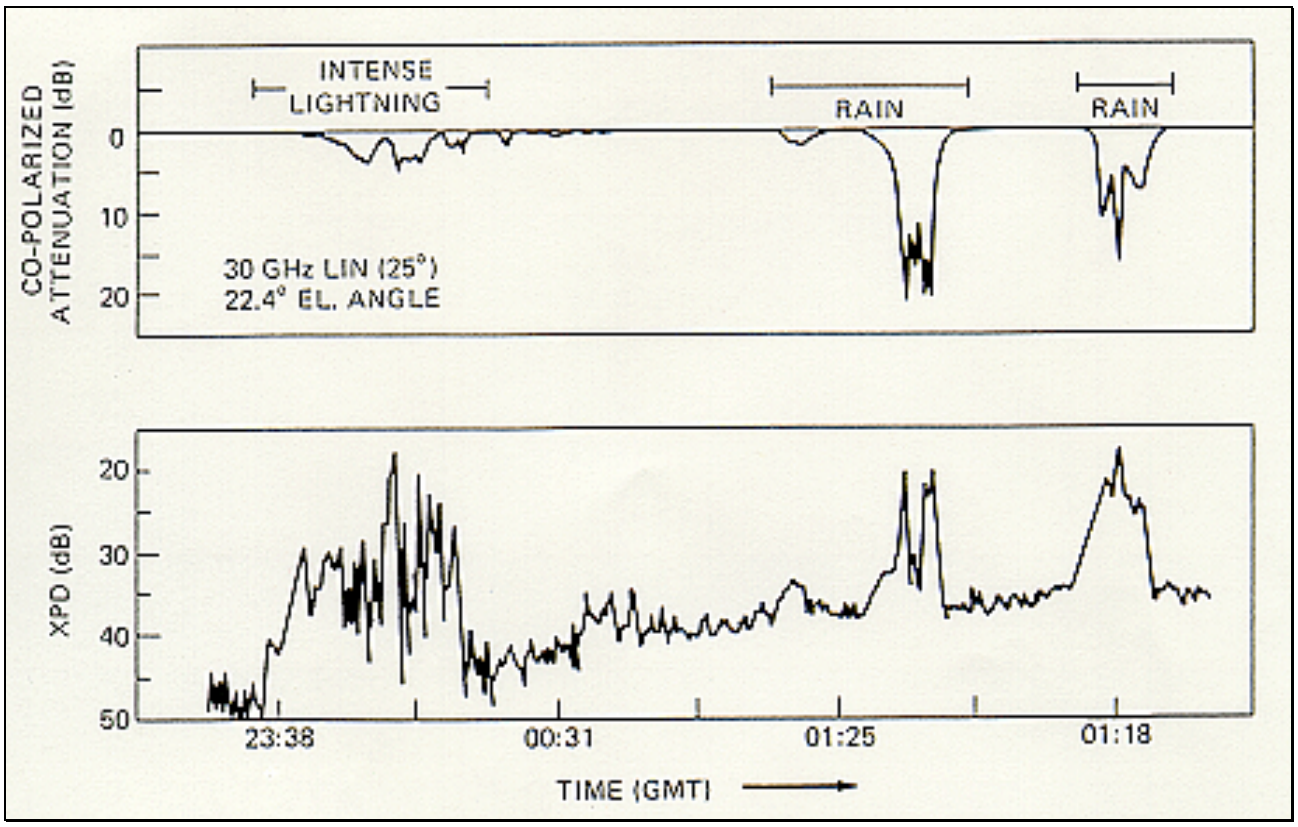


Exhibit 1.3.5.1-2
Mean Amplitude Variance for Clear Weather Conditions, at 2 and 30 GHz,
as a function of elevation angle
*[Source: Ippolito (1986)]*

## 1.4 RADIO NOISE

Satellite system designers must be concerned with noise sources which are both man-made and naturally occurring. Observed noise causes an increase in the receiver antenna temperature leading to an increase in the overall system noise. Radio or sky noise is produced by any natural absorbing medium that interacts with the radiowave; thus, radio noise is emitted by both terrestrial and extraterrestrial matter. Noise sources include gaseous atmosphere (oxygen and water vapor), hydrometers (rain and clouds), extraterrestrial objects (sun, moon, planets, etc.), and man-made electronic devices.

Accurate noise prediction is critical especially for systems such as the NASA deep space tracking network that implements very low noise communication receivers. Figure 1.4.1 illustrates the minimum expected radio noise levels for satellite communication systems. The horizontal axis is frequency from 10 MHz to 100 GHz while the vertical axis is noise figure in dB. Noise figure is defined as

$$F_a(dB) = 10\log\left(\frac{t_a}{t_o}\right) \tag{1.4-1}$$

where $t_a$ is the antenna noise temperature and $t_o$ is the ambient reference temperature of 290°K. Antenna noise is conveniently treated in terms of noise temperature, since the two parameters are linearly related. In circuit theory the noise power, $p_n$, which is transferred to a matched load is

$$p_n = kTB \text{ watts} \tag{1.4-2}$$

where k is Boltzmann's constant, T is noise temperature in degrees (Kelvin), and B is the bandwidth (Hertz). Meanwhile, thermal radiation from gaseous atmosphere is given by the Rayleigh-Jeans longwave approximation to Plank's equation

$$p_n' = \frac{2kT}{\lambda^2} = 22.2kTf^2 \tag{1.4-3}$$

where f is frequency (GHz). Note the ambiguity in the frequency dependence of the two relationships. However, since noise temperature, in its circuit theory usage, will be implemented, this difference is not of prime concern. Figure 1.4.1 illustrates the relationship between noise figure and the transmitting frequency. Below 30 MHz, galactic noise and atmospheric noise dominate the calculation unless the link is around a populated area with man-made noise sources. Above 30 MHz, galactic noise is insignificant. Around 1 GHz, noise from the sun, atmospheric constituents, and rain begin to have a dominant effect in noise calculation.

Terrestrial sources include gaseous atmospheric constituents (oxygen and water vapor), hydrometers (rain and clouds) and man-made electronic devices. Extraterrestrial sources include the sun, the moon, planets, quasars, pulsars, etc.

### 1.4.1 Uplink Noise Sources

For the uplink, the earth-viewing satellite antenna observes the earth's surface emission and atmospheric constituents. Since the satellite antenna typically includes a portion of the earth's surface within its half-power beamwidth, the earth's surface emission noise is more significant than the atmospheric constituents for the uplink.

The earth viewing (uplink) antenna of an orbiting satellite typically includes only a portion of the earth's surface within its half-power beamwidth. The observed noise is a complex function of atmospheric and surface temperature, elevation angle, frequency, and antenna gain. A major factor in the observed noise temperature is the fraction of land (high brightness temperature) to sea (low brightness temperature) in the main antenna beam.

### 1.4.2 Downlink Noise Sources

For the downlink, a receiving antenna (for the earth station) absorbs energy from both the antenna main beam and the side lobes; thus, the noise sources are not necessarily in direct line of sight. The downlink noise sources includes gaseous atmospheric constituents, hydrometers, ground surface emissions, and the cosmic background.

An earth station observing a satellite at a high elevation angle may be considered to be receiving sky noise from the antenna boresight direction. As the elevation angle of the satellite decreases, thermal noise emission from the Earth's surface will be increasingly observed in the antenna's side lobes. This section reviews the sky noise component and its contribution to satellite communications system performance.

Antenna noise is conveniently treated in terms of noise temperature, since the two parameters are linearly related. In circuit theory the noise power, $p_n$, which is transferred to a matched load is

$$p_n = kTB \text{ watts} \qquad (1.4.2\text{-}1)$$

where k is Boltzmann's constant, T is noise temperature in (degrees) Kelvin, and B is the bandwidth in Hertz. Thermal radiation from gaseous atmosphere is given by the Rayleigh-Jeans Longwave approximation to Plank's equation

$$p_n' = \frac{2kT}{\lambda^2} = 22.2kTf^2 \qquad (1.4.2\text{-}2)$$

where f is the frequency in GHz. Note the ambiguity in the frequency dependence of the two relationships. However, we will be considering noise temperature in its circuit theory usage so the difference is not of prime concern.

## 1.5 PROPAGATION DATA BASES

### 1.5.1 Meteorological Parameters

This section discusses the many sources for obtaining meteorological data. Meteorological data typically available to the public may be considered in two forms. The first form represents point measurements, usually collected at the surface. Point data from the surface is the most readily available data both in terms of length of time for data collection and number of collection sites. This data is useful to designers of terrestrial RF systems who are concerned with atmospheric effects. However, most terrestrial systems operate at or below 2 GHz, where the impacts of weather on system performance are minimal. Satellite system designers are often more affected by the atmosphere due to the response of the typically higher operating frequencies.

Designers of satellite systems may approximate atmospheric conditions along a slant path from surface values. An excellent reference currently in wide usage comes from ITU-R Recommendation P.835-1 (Rec. P.835). Rec. P.835 provides formulae for scaling temperature, water vapor density, and barometric pressure with respect to altitude above the ground. In addition, many slant path attenuation models assume surface parameters as inputs. Empirical terms for scaling along a slant path are then embedded within the model.

The second form of data available to system designers considers conditions along a vertical path. This data is more useful to designers of earth-space links. Path data may provide a total content of some atmospheric constituent such as water vapor or hydrosols (the liquid water in clouds), or the data may provide a vertical profile called a sounding.

Sounding data is, by far, the most useful. Unfortunately, it suffers the limitations of being:

- Less readily available;
- Collected less frequently;
- In need of copious amounts of storage space;
- Implemented into attenuation models through much more complex algorithms.

However, when available, atmospheric profile data is worth the effort to implement because the accuracy of the attenuation results is vastly improved.

Presently, many individual organizations are collecting weather statistics. However, there are few common standards in recording and archiving procedures between the organizations. Archival formats that do exist are usually derived to benefit meteorologists, not satellite propagologists. As a result, when generating long-term distributions, data sets may require certain conversions and/or adjustments in order to tell the propagation analyst what s/he really wishes to know. In other cases, assumptions must be applied to the data in order to work with it in a useable form. Examples of this are presented in Exhibit 1.5-1.

| Data of Interest to Meteorologist | Units | Data of Interest to Systems Engineer | Units |
|---|---|---|---|
| Rain Accumulation | Inches | Point Rain Rate (*a.k.a.:* Intensity) | mm/hr |
| Relative Humidity | % | Water Vapor Density (*a.k.a.:* Absolute Humidity) | $g/m^3$ |
| Cloud Cover | % | Cloud Liquid Water Content | $kg/m^2$ |
| High and Low Temperature | °C or °F | Average Temperature | °C or K |

**Exhibit 1.5-1. Data Formats Desired For Different Applications**

### 1.5.2 Point Data

Point data, usually taken at the surface, is the data most frequently available. It is typically collected from ground stations monitoring temperature, relative humidity, barometeric pressure, wind speed and direction, and rain accumulation. Depending on the intended purpose of the site, records of weather observations may be taken as often as every 5 minutes or as infrequently as once a day. Often, these datasets will be merged to create monthly, seasonal, or annual averages. Because rain rate is typically modeled as being uniform in a vertical direction, rain rate measurements are usually recorded at a point on the surface only.

#### 1.5.2.1 NOAA

One of the largest collections of publicly accessible weather data, including point data, is at the National Climatic Data Center (NCDC) located in Asheville, NC. NCDC operates as an office under the National Oceanic and Atmospheric Administration (NOAA). Much of the federally funded environmental, climatic, and atmospheric research performed in the U.S. is, in fact, sponsored by NOAA or one of its offices.

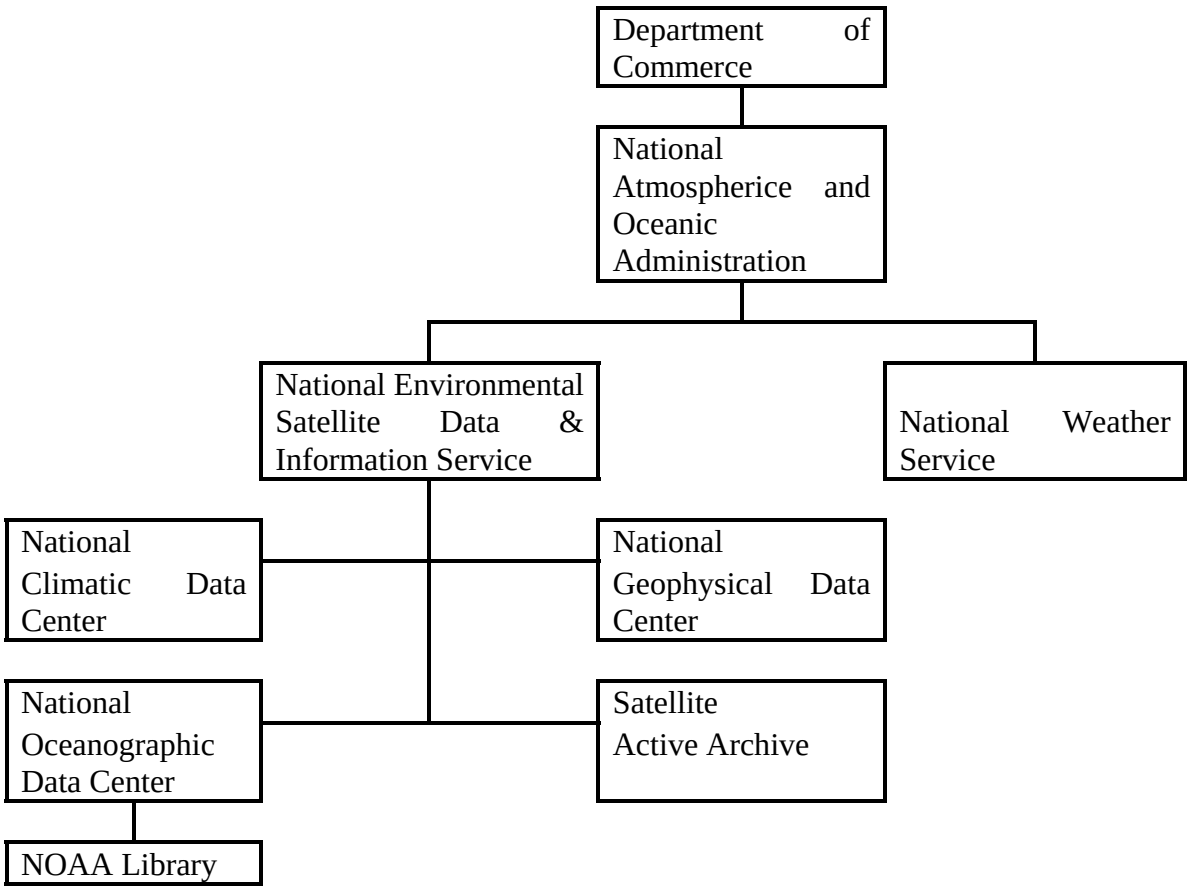


Exhibit 1.5-2 Organization of Relevant NOAA Offices

NCDC's more useful surface observation datasets tend to be exclusive to the U.S. with some data for nearby North American locations mixed in. Among the more useful data sets are:

- **First Order Summary of Day Data** - This data set provides daily measures of high, low, and mean temperature; degree days; precipitation accumulation; snow fall and accumulation; water equivalent of snow and ice on the ground; max wind speed and direction; sunshine; cloud cover; and indicators of fog, thunderstorms, ice pellets, hail, rain, snow, glaze, blowing snow, or dust. This data is provided for a large selection of locations across the U.S. Some of this data is provided for free online however, it is usually just a few months of recently collected statistics. Older data that has been archived can be ordered for a fee. The data is available on hardcopy or magnetic media.

- **Precipitation Accumulation Data** - Precipitation accumulation data are available for ground station observations taken intervals of one hour, 15 minutes, or 5 minutes. The more frequent the observation times, the fewer the number of participating stations. Some models

do exist for converting rain accumulation statistics to rain rate statistics. However, they usually require collection times of 1 minute or less and become notoriously inaccurate as rain rates increase.

These and many other useful datasets are available by contacting NCDC at:

| | |
|---|---|
| National Climatic Data Center | Tel: (704)271-4800 |
| Federal Building | Fax: (704)271-4876 |
| 37 Battery Park Ave | e-mail: orders@ncdc.noaa.gov |
| Asheville, NC 28801 | Web: www.ncdc.noaa.gov |

Their web site at provides a good index of available data, its origins, and any fees required for delivery.

#### 1.5.2.2 ITU-R

The International Telecommunications Union (ITU) is a subcouncil of the United Nations (UN) which focuses on international telecommunications issues. The Radiocommunications sector of the ITU (ITU-R) Study Group 3 (SG3 - formerly known as Study Groups 5&6) creates recommendations that specifically address atmospheric propagation modeling. The ITU-R provides the following SG3 databases and recommendations.

- The database of Study Group 5 (DBSG5) is a software record of all the results of propagation studies submitted to the ITU-R. These records are global and contain measured annual rain rate statistics. Often the statistics are reproduced in a very limited fashion however, the records always provide references to find out more on the origin of the data.

- ITU-R Rec. P.837 provides a global set of maps defining point rain rate characteristics. Rec. P.837 begins by identifying 15 unique rain climatologies. Each climatology is called a rain region and has its own point rain rate distribution. The maps show what locations each region best represents. The ITU-R also distributes software that accepts latitude and longitude as inputs and returns the rain region associated with that location. While these maps are among the most widely used, it must be remembered that the point rain rate distribution associated with a particular region is an expected distribution. There will be some variability within each region.

- A proposed dataset for global surface water vapor density and cloud liquid water is also planned for release by the ITU-R in the near future. This data represents multi-year statistics across the globe with a 1.5° latitude longitude resolution. It was derived from data collected by the European Center for Medium range Weather Forecasts (ECMWF).

- ITU-R Rec.P.1058 contains a call for and a description of a desired global terrain database. This database, when created, will provide ground elevation, building heights, and population data. At this time, the database is not yet in existence.
  Software products as well as other ITU-R publications including recommendations are available through:

| | |
|---|---|
| ITU Sales and Marketing Service | Tel: +41 22 730 6141 |
| Place des Nations | Fax: +41 22 730 5194 |
| CH-1211 Geneva 20 | e-mail: sales@itu.ch |
| Switzerland | Web: www.itu.ch |

#### 1.5.2.3 Other

A global model for point rain rate can be found embedded in the following rain attenuation model that will be discussed later.

- The Crane Global rain attenuation model provides maps covering the entire world. These maps define twelve rain related climatologies or rain regions. Each region has its own expected distribution of point rain rate. Every point on the planet is associated with one of the twelve regions. Again with these maps, some variability will exist between locations within the same region. Dr. Crane is still updating the maps, as new data becomes available. For the most recent maps see:

  Electromagnetic Wave Propagation Through Rain
  Robert K. Crane
  John Wiley & Sons, Inc. ©1996
  ISBN:

### 1.5.3 Path Data

Path data provides a look at the total content of various atmospheric constituents along a propagation path. This provides far more information than point data alone. Most often, path data is generated for water vapor and hydrosols (cloud liquid water) because these parameters vary with height and are present along more of the propagation path. For satellite applications, water vapor and cloud liquid water become an increasing concern at frequencies above 10 GHz. Particular attenuation should be paid to water vapor and hydrosols when operating at Ka band or higher. Path data comes in two basic forms: 1) Total column data and 2) Profile data.

#### 1.5.3.1 Total Column Data

Total column data is a measure of the total content of a particular atmospheric constituent integrated from the surface to some arbitrary cutoff height. The total column data does not necessarily provide information as two the distribution of the constituent along the vertical path. This is an improvement over point measurements such as surface observations.

Models that predict path conditions based on point observations predict what will typically happen rather during normal circumstances than what "could" happen during extreme circumstances. For this reason, total column data tends to provide a far more accurate picture of the possible extremes values of atmospheric properties that are most often in question.

#### 1.5.3.1.1 NASA

Databases of water vapor density and hydrosols are available from NASA through their collection of Distributed Active Archive Centers (DAAC). A total of nine DAACs are currently operating under NASA. Each maintains archives of different data. Catalogs of datasets are available online. All DAAC data is FREE!

A DAAC which is particularly useful to systems engineers is located at the Global Hydrology and Climate Center located at the Marshall Space Flight Center (MSFC) in Huntsville, AL. Multiple datasets from the Special Sensor Microwave/Imager (SSM/I) provide excellent long-term antenna temperature measurements. These, in turn, can be used to determine path values of water vapor and hydrosols. Datasets representing daily, pentad (five-day), and monthly averages are available. In many cases the MSFC DAAC provides processed data with surface and path statistics already generated.

For more information about these and other datasets, the MSFC DAAC can be contacted via:

| | |
|---|---|
| MSFC DAAC User Services | Tel: (205)922-5932 |
| Global Hydrology and Climate Center | Fax: (205)922-5859 |
| 977 Explorer Blvd | e-mail: msfc@eos.nasa.gov |
| Huntsville, AL 35806 | Web: wwwdaac.msfc.nasa.gov |

A second dataset of interest to satellite systems engineers comes from the NASA Water Vapor Project (NVAP). NVAP is a merged dataset using three different sources. It provides daily, pentad, and monthly global statistics of water vapor at various levels in the atmosphere. The dataset used to be located at the MSFC DAAC but has recently been transitioned to the DAAC located at Lewis Research Center. Information on NVAP can be retrieved by contacting the Lewis DAAC on the web at http://eosdis.larc.nasa.gov.
Because many of the additional datasets being archived at various DAACs are moving it may be best to contact the general DAAC users homepage. This homepage provides descriptions and links to all nine NASA DAACs - http://spso.gsfc.nasa.gov/eos_homepage/daacs.html.

Instantaneous path averaged rain rates may also be collected for specific areas from the DAAC at MSFC. The MSFC DAAC holds a number of rain rate datasets. Two that are of primary interest are: 1) NOAA-NASA Special Sensor Microwave/Imager (SSM/I) Pathfinder Level 2 Precipitation Rate Product and 2) U.S. Composite Reflectivity (2 km x 2km) From National Weather Service Radars.

The SSM/I is a passive microwave sensor aboard the Defense Meteorological Satellite Program (DMSP) satellite F8. The precipitation rate dataset is based on 16 months of measurements using the SSM/I. This dataset is has a number of advantages because it provides global coverage using a single measuring device. The drawbacks are that it does not provide the preferred "long-term" statistics and the resolution on the ground at 25 $km^2$ is approximately an order of magnitude wider than most convective rain events.

The composite reflectivity data combines radar-based weather measurements taken across the continental United States (CONUS) every fifteen minutes. From reflectivity values (dBz), rain rates may be calculated directly using a single equation. At 2 $km^2$, this data is a much higher resolution than the SSM/I however, it still does not provide the point rain rate values required by most rain attenuation models.

#### 1.5.3.2 Profile Data

When available, profile data is the most useful and informative data with respect to the providing a two-dimensional view of the distribution of atmospheric constituents along a path. Profile data can be found from time to time via radar reflectivity measurements but is most often collected with a radiosonde. A radiosonde is an instrument carried aloft by a balloon. It transmits temperature, pressure, humidity, and wind speed and direction back to a ground station as it passes vertically through the atmosphere. Models exist which also may be utilized to indirectly calculate hydrosol content from radiosonde data.

Radiosondes measurements have been performed for many years. They are currently released at 00:00 and 12:00 GMT daily around the world. Caution should be used when comparing radiosonde data from various locations around the world as significant differences in instrumentation have been reported [Segal, 1996 - private communication].

An excellent radiosonde dataset is provided by NCDC and is called, "Radiosonde Data of North America 1946-1993." This dataset provides 47 consecutive years of measurements taken around North America. The package comes as a four CD-ROM set and has a rudimentary search tool to extract desired data.

### 1.5.4 Miscellaneous Sources of Atmospheric Data

A good dataset can be hard to find. When in doubt keep digging. It is often just a matter of more elbow grease. If the above sources do not have the data required for a particular applications there are other good sources of miscellaneous climatological data.

### 1.5.4.1 WMO

The World Meteorological Organization (WMO) is the subcouncil of the UN which focuses on international climatological research. It collects data through its 176 member states and six member territories. Its most active weather-monitoring program is called the World Weather Watch. Using four near-polar orbiting satellites, five geosynchronous earth-orbiting satellites, 10,000 land observation sites, 7,000 ship based observation points, and 300 moored or drifting weather monitoring buoys, the WMO collects 15 million characters and 2,000 weather charts a day. This data is processed by 3 world, 35 regional, and 183 national meteorological centers.

| | |
|---|---|
| WMO | Tel: +41 22 730-8111 |
| 41, avenue Gueseppe-Motta | Fax: +41 22 734-2326 |
| 1211 Geneva 2 | e-mail: ipa@www.wmo.ch |
| Switzerland | Web: www.wmo.ch |

### 1.5.4.2 CDIAC

The Carbon Dioxide Information Analysis Center (CDIAC) at the Oak Ridge National Laboratory in Oak Ridge, TN provides information to international researchers. The information focuses on $CO_2$ and levels of other trace gases which may be used as measures of global climate change. The have a particularly interesting dataset called, "Climatological Data for Clouds Over the Globe From Surface Observations."

| | |
|---|---|
| CDIAC | Tel: (615)574-0390 |
| Oak Ridge National Laboratory | Fax: (615)574-2232 |
| P.O. Box 2008 | e-mail: cdp@stc10.ctd.ornl.gov |
| Oak Ridge, TN 37831-6335 | Web: |

### 1.5.4.3 UCAR

The University Corporation for Atmospheric Research (UCAR) collects and archives large amounts of atmospheric path data. Many of these datasets are global and are the products of ongoing research from the member universities. In addition, UCAR manages the National Center for Atmospheric Research (NCAR). NCAR now serves over 60 UCAR member institutions, plus affiliates both within and beyond U.S. borders. Along with its original and still primary sponsor, the National Science Foundation, NCAR is supported by a number of U.S. agencies and programs.

UCAR
P.O. Box 3000
Boulder, CO 80307-3000

Tel: (303)497-8600
Fax: (303)497-8610
e-mail: butterwo@ucar.edu
Web: www.ucar.edu

NCAR
1850 Table Mesa Dr.
Boulder, CO 80303

Tel: (303)497-1000
Fax: (303)497-8610
e-mail: n/a
Web: www.ncar.ucar.edu

## 1.6 REFERENCES – SECTION 1


Aarons, J. (1982), "Global Morphology of Ionospheric Scintillations." Proc. of the IEEE, Vol. 70, No. 4, April 1982, pg. 360-378.

Aarons, J. (1985), "Construction of a model of equatorial scintillation intensity," Radio Science, vol.20, No. 3, pp 397-402, May-June 1985.

Aarons, J. et al. (1981a), "Microwave equatorial scintillation intensity during solar maximum," Radio Science, Vol. 10, pp.939-945, Sept.-Oct 1981.

Aarons, J., et al. (1981b), "UHF Scintillation Activity Over Polar Latitudes." Geophys. Research Lett., Vol. 8, No. 3, Mar 1981, pg. 277-280.

Aarons, J., J.P. Whitney, and R.S. Allen (1971), "Global morphology of ionospheric scintillates," IEEE Proccedings, vol. 59, pp. 159-127, Feb. 1971.

Akasofu, S.I. (1968), *Polar and Magnetospheric Subsystems*. New York: Springer-Verlag.

Allnut, J. E. (1989), *Satellite-to-ground radiowave propagation*, Peter Peregrinus Ltd, London.

Arnold, H. W.,Cox, D. C., Hoffman, H. H., and Leck, R. P. (1980), "Characteristics of Rain and Ice Depolarization for a 19- and 28- GHz Propagation Path from a Comstar Satellite," IEEE Trans. on Antennas and Propagation, Vol. AP-28, No. 1, pp. 22-28.

Balsley, B.B. (1969), "Some characteristics of non-two-stream irregularities in the equatorial electrojet," J. Geophys. Res., vol. 74, pp. 2333-2347, May 1, 1969.

Banerjee, P.K., R. S. Dabas, and B. M. Reddy (1992), "C and L band transionospheric scintillation experiment: Some results for applications to satellite radio systems." Radio Science, Vol. 27, No. 6, Nov.-Dec. 1992, pg. 955-969.

Baron, M.J. (1974), "Electron densities within aurorae and other auroral E-region characteristics," Radio Science, vol.9, pp. 314-348, Feb. 1974.

Barton, C.E (1996)., Revision of International Geomagnetic Reference Field Released, EOS Transactions 77, #16, Apr 16, 1996.

Basu, S. et al. (1980), "Long-term 1.5 GHz amplitude scintillation measurements at the magnetic equator," Geophysical Research Letters, vol.7, pp. 259-262, April 1980.

Basu, S. et al. (1985), Morphology of phase and intensity scintillation in the auroral oval and polar cap," Radio Science, vol. 20, No. 3, pp. 347-356, May-June 1985.

Basu, S., et al (1988), "Ionospheric constraints on VHF/UHF communications links during solar maximum and minimum periods." Radio Science, Vol. 23, No. 3, May-June 1988, pg. 363-378.

Battan, L.J. (1979), *Fundamentals of Meteorology*, Prentice Hall, New York.

Beckmann, P. (1967), *Probability in Communication Engineering*. New York: Harcout, Brace, and World.

Blesing, R.G. and P.A. Deneison (1972), "Coronal broadening of the Crab Nebula 1969-1971: observations," Proc. Astron. Soc. Australia, vol.2., pp. 84-86, March 1972.

Booker, H.G. (1975), "The role of the magnetosphere in satellite and radiostar scintillation," J. Atoms. Terr.Phys., vol. 37, pp. 1089-1098, Aug. 1975.

Booker, H.G. (1979), "The role of acoustic gravity waves in the generation of spread-F and ionospheic scintillation," J. Atmos. Terr. Phys., vol. 41, pp. 501-515, May 1979.

Bostian, C.W, and J. Allnutt (1979), "Ice Crystal Depolarization on Satellite-Eareth Microwave Radio Paths," IEE, Vol. 126, No. 10, pp. 951-960.

Bowhill, S.A. (1961), "Statistics of a radio wave diffracted by a random ionosphere," J. of Research of NBS, vol. 65D, pp. 275-292, May-June 1961.

Bramley, E.N. (1977), "The accuracy of computing ionospheric radio wave scintillation by the thin phase screen approximation," J. Atmos. Terr. Phys., vol.39, pp. 367-373.

Briggs, B.H. (1961), "The correlation of radio star scintillations with geomagnetic disturbances," Geophysical J., vol.5, pp. 306-317, Oct. 1961.

Briggs, B.H. and I.A. Parkin (1963), "On the variation of radio star and satellite scintillations with zenith angle," Atmos. Terr. Phys., vol.25, pp. 339-365, June 1963.

Buchau, J. et al. (1985), "Ionospheric structures in the polar cap: their origin and relation to 250 MHz scintillation," Radio Science, Vol. 20, No. 3, pp. 325-338, May-June 1985.

Budden, K.G. (1961), *Radio Waves in the Ionosphere*, Cambridge: Cambridge U. Press.

Budden, K.G. (1985), *The Propagation of Radio Waves*, Cambridge: Cambridge U. Press.

Callahan, P.S. (1975), "Columnar content measurements of the solar- wind turbulence near the sun," Astrophys. J., vol. 199, pp.227-236, July 1, 1975.

CCIR, Report 565-3 (1986a), "Propagation Data for broadcasting from satellites," in Volume V, *Propagation in Non-ionized Media, Recommendations and Reports of the CCIR, 1986*. Dubrovnik: Int. Telecomm. Union.

CCIR, Report 263-6 (1986b), "Ionospheric effects upon earth-space propagation," in Volume VI, *Propagation in Ionized Media, Recommendations and Reports of the CCIR, 1986*. Dubrovnik: Int. Telecomm. Union.

CCIR, Report 725-1 (1986c), "Ionospheric Properties," in Volume VI, *Propagation in Ionized Media, Recommendations and Reports of the CCIR, 1986*. Dubrovnik: Int. Telecomm. Union.

Cohen, M.H. (1969), "High-resolution observations of radio sources," Annual Rev. of Astron. and Astrophys., vol. 7, pp.619-664.

Coles, W.A.(1978), "Interplanetary scintillations," Space Science Review., vol. 21, pp. 411-425.

Corry, R.J., L.C. Humphrey, M. C. Jeruchim, J. H. Moore, W. C. Peterson, and R. J. Wolfe (1990), "Attenuation statistics of UHF signals due to vegetation, ionospheric, and polarization-mismatch effects", Final Report, Aug. 1990.

Costa, J.J. (1980), "UHF communications to mobile users via satellite," Hughes Aircraft Company, Sept. 1982.

Craft, H.D. and L.H. Weaterlund (1972), "Scintillations at 4 to 6 GHz caused by the ionosphere," *10th Aerospace Science Meeting*, AIAA Paper No. 72-179.

Crain, C.M., H.G. Booker, and J.A. Ferguson, "Use of refractive scattering to explain SHF scintillations (1979)," Radio Science, vol. 14, pp. 125-134, Jan.-Feb.

Crane, R.K. (1977), "Ionospheric scintillation," Proc. EEE, Vol. 65, No. 2, pp.180-199, Feb. 1977.

Crane, R.K. (1976), "Spectra of ionospheric scintillations," J. Geophys. Res., vol.81, pp. 2041-2050, May 1.

CRC (1972), *Handbook of Chemistry and Physics*, Weast, R.C. ed, 52nd Edition, p. F189. Cleveland, OH: Chemical Rubber Co.

Cronyn, W.M.(1970), "The analysis of radio scattering and space probe observations of small-scale structure in the interplanetary medium," Astrophys. J., vol. 161, pp. 755- 763, Aug.

Davies, K., G.K. Hartmann, and R. Leitinger (1977), "A comparison of Several methods for estimating columnar electron content of the plasmasphere," J. Atmos. Terr. Phys., vol. 39, pp. 571-580, May.

Davies, K. (1965), *Ionospheric Radio Propagation*. Washington, DC: Supt. of Documents, U.S. Government Printing Office.

Davies, K. (1969), *Ionospheric Radio Waves*.Waltham, MA: Blaisdell Pub. Co.

Davies, K., (1980), "Recent progress in satellite radio beacon studies with particular emphasis on the ATS-6 radio beacon experiment," Space Sci. Rev., vol. 25, pp. 357-430, April 1980.

Davies, K. (1989), *Ionospheric Radio*, Peter Peregrinus Ltd., on behalf of The Institution of Electrical Engineers.

Devasirvathm, D.J.M. & D.B. Hodge (1977), "Amplitude Scintillation of Earth-Space Propagation Paths at 2 and 30 GHz," Ohio State University, Tech. Report 4299-4, March 1977.

Donnelly, R.F. (ed.) (1978), *Solar Terrestrial Predictions Propagations*, Volumes 1-4. Boulder, CO: Environ. Res. Labs., NOAA.

Evans, J.V. (1969), "Theory and practice of ionospheric study by Thomson scatter radar," Proc. IEEE, vol. 57, pp. 496-530, April.

Fang, D.J. and C.H. Liu (1984), "Statistical characterization of equatorial scintillation in the Asian region." Radio Science, Vol. 19, No. 1, Jan-Feb, pg. 345-358.

Fang, D.J. and C.H. Liu (1983), "A morphological study of gigahertz scintillation in the Asian region," Radio Science, vol. 18, no.2, pp. 241-252, Mar-Apr.

Farley, D.T. (1963), "A plasma instability resulting in field aligned irregularities in the ionosphere," J. Geophys. Res, vol. 68, pp. 6083-6097, Nov. 15.

Feldstein, Y.I. (1986), "A quarter of a century with the auroual oval," EOS, vol. 67, Oct. 7, 1986.

Flock, W.L. (1987), *Propagation Effects on Satellite Systems at Frequencies Below 10 GHz, A Handbook for Satellite Systems Design*, NASA Reference Publication 1108(02), Washington, D.C.

Flock, W.L. (1979), *Electromagnetics and the Environment: Remote Sensing and Telecommunications*. Englewood Cliffs, NJ: Prentice Hall.

Franke, S.J., and C.H. Liu (1985), "Modeling of Equatorial multifrequency scintillation," Radio Science, vol. 20, pp. 403-415. May-June.

Fremouw, E.J., et al. (1978), "Early results from the DNA wideband satellite experiment - ecomplex signal scintillation," Radio Science, vol.13, pp.167-187, Jan.-Feb.

Fremouw, E.J., et al. (1985), "The HiLat satellite mission," Radio Science, vol.20, pp. 416-424, May-June 1985.

Frihagen, J. (1971), "Occurrence of high latitude ionospheric irregularities giving rise to satellite scintillation," J. Atmos. Terr. Phys., vol. 33, pp. 21-30.

Goldstein, G.S. and J.A. Klobuchar (1974), "Seasonal and diurnal variations in the total electron content of the ionosphere at invariant latitude 54 degrees," AFCRL-TR-74-0294. Bedford, MA: Air force Camb. Res. Labs., 28 June.

Gunn, K.L.S., and T.W.R. East (1954), "The microwave properties of precipitation particles," Quarterly J. Royal Meteor. Soc., Vol. 80, pp. 522-545.

Hanson, W.B. (1965), "Structures of the ionosphere," in Johnson, F.S. (ed.), *Satellite Environment Handbook*, Stanford U. Press.

Hay, J.S., S.J. Parsons, and J.W. Phillips (1946), "Fluctuations in cosmic radiation at radio frequencies," Radio Science, vol. 158, p. 234, Aug. 17.

Heron, M.L. (1980),"Transequatorial propagation through equatorial plasma bubbles - discrete events," Radio Science, vol. 15, pp. 829-835, July-Aug.

Hewish, A. (1952), "The diffraction of galactic radio waves as a method of investigating the irregular structure of the ionosphere," Proc. Royal Soc. of London, Series A, vol. 214, pp. 494-514, 9 Oct.

Hewish, A. (1955), "The irregular structure of the outer regions of the solar corona," Proc. Royal Soc. of London, Series A, vol. 228, pp. 238-251, 22 Feb.

Hewish, A., P.F. Scott, and D. Wills (1964), "Interplanetary scintillation of small diameter radio sources," Nature, vol. 203, pp. 1214-1217.

Hines, C.O. et al. (1974), *The Upper Atmosphere in Motion*, Geophysical Monograph 18. Washington, DC: A. Geophys. Union.

Houpis, H. L.F. and L.J. Nickisch (1991), "An ionospheric propagation prediction method for low latitudes and mid latitudes." Radio Science, Vol. 26, No. 4, Jul-Aug 1991, pg. 1049-1057.

Hunsucker, R.D. (1974), "Simulaneous riometer and incoherent scatter radar observations of the auroral D region," Radio Science, vol. 9, pp. 335-340, Feb. 1974.

Ippolito, L. J., Jr. (1986*), Radiowave Propagation in Satellite Communications*. Van Nostrand Reinhold Company, New York

Ippolito, L.J. Jr. (1989), *Propagation Effects Handbook for Satellite Systems Design - A Summary of Propagation Impairments on 10 to 100 GHz Satellite Links With Techniques for System Design*, NASA Reference Publication 1082(04), Washington, D.C.

Ishimaru, A., Wave (1978), *Propagation and Scattering in Random Media*, vol.2. New York: Academic Press.

ITU-R (1994), *Ionospheric effects influencing radio systems involving spacecraft" and Annex 1: "Ionospheric effects upon Earth-space propagation*. International Telecommunications Union, Geneva.

ITU-R, Rec. P.453-6 (1997): The Radio Refractive Index: its Formula and Refractivity Data, International Telecommunications Union, Geneva.

ITU-R, Rec. P.531-4 (1997): Ionospheric Propagation Data and Prediction Methods Required for the Design of Satellite Services and Systems, International Telecommunications Union, Geneva.

ITU-R Rec. P.676-3 (1997): Attenuation By Atmospheric Gases, International Tele-communications Union, Geneva.

ITU-R, Rec. P. 679-1 (1994), International Tele-communications Union, Geneva.

ITU-R, Rec. P.835-2 (1997); Reference Standard Atmospheres, for Gaseous Attenuation, International Telecommunications Union, Geneva.

ITU-R, Rec. P.840-2 (1997); Attenuation Due to Clouds and Fog, International Tele-communications Union, Geneva.

Johnson, A. and J. Taagholt (1985), "Ionospheric effects on $C^3I$ satellite communications systems in Greenland." Radio Science, Vol. 20, No. 3, May-Jun 1985, pg. 339-346.

Jokipii, J.R. (1973), "Turbulence and scintillations in the interplanetary plasma," Ann. Rev. of Astron. and Astrophys., vol. 11, pp. 1-28.

Karasawa, Y., K. Yasukawa, and M. Yamada (1985), "Ionospheric scintillation measurements at 1.5 GHz in mid-latitude region, " Radio Science, vol.20, no. 3, 643-651, May-June.

Kelso, J.M. (1964), *Radio Ray Propagation in the Ionosphere*. New York: McGraw-Hill.

Klobuchar, J.A. (1978), "Ionospheric effects on satellite navigation and air traffic control systems," in *Recent Advances in Radio and Optical Progation for Modern Communication, Navigation, and Detection Systems, AGARD Proceedings - LS - 93,* ISBN 92-835-1280-4. NTIS: Springfield, VA 22161, April.

Klobuchar, J.A., (leader) and Working Group (1978), "B. Trans-ionospheric propagation predictions," in R.F. Donnelly (ed.), vol. 2: *Working Group Reports and Reviews of Solar-Terrestrial Predictions Proceedings*, pp. 217-245, Boulder, CO: Environ. Res. Labs., NOAA.

Langel, R.A., D.R. Barraclough, D.J. Kerridge, V.P. Golovkov, T.J. Sabaka, and R.H. Estes (1988), Definitive IGRF Models for 1945, 1950, 1955, and 1960, J. Geomagn. Geoelectr. 40, 645.

Lawrence, R.S., C.G. Little, and H.J.A. Chivers (1964), "A survey of ionospheric effects upon earth space propagation," Proc. IEEE, vol. 52, pp. 4-47.

Leadabrand, R.L. et al. (1972), "Chatanitka, Alaska auroual zone incoherent scatter facility," Radio Science, vol.7, pp.747-756. July.

Lee, M.C., et. al. (1982), "Depolarization of VHF geostationary satellite signals near the equatorial anomaly crests," Radio Science, vol. 17, pp. 399-409, Mar-Apr.

Little, C.G. and A.C.B. Lovell (1950), "Origin of the fluctuations in the intensity of radio waves from galactic sources: Jodrell Bank Obserations," Nature, vol.165, pp.423-424, March 18, 1950.

Malin, S.R.C. and D.R. Barraclough (1981), "An algorithm for synthesizing the geostationary field," Computers and Geoscience, vol. 7, No. 4, pp 401-405.

Martin, E. and J. Aarons (1977), "F layer scintillation and the aurora," J. Geophys. Res., vol. 82, pp. 2717-2722, July 1, 1977.

Mie, G. (1908), Ann. Physik, Vol. 25, p.377.

Millman, G.H. and G.M. Reinsmith (1974), An analysis of the incoherent scatter Faraday rotation technique for ionospheric propagation error correction," General Electric Tech. Inf. Series R 74EMH2, Syracuse, NY, Feb.

Millman, G.H. (1980), Ionospheric electron Content Effects on Earth-Space Radio Propagation (R80EMH11). Syracuse, NY: General Electric, Dec.

Minakoshi, H. et al. (1981), "Severe ionospheric scintillation associated with magnetic storm on March 22, 1979," J. Radio Res. Labs (Japan), vol. 28, pp.1-9, Mar-Jul.

Minakoshi, H. et al. (1985), "Severe ionospheric scintillation observed at Ascension Island from 1980 through 1982," Radio Science, vol. 20, pp. 357-365, May-June.

Mullen, J. P., E. MacKenzie, Santimay Basu, and H. Whitney (1985), "UHF/GHz scintillation observed at Ascension Island from 1980 through 1982." Radio Science, Vol. 20, No. 3, May-June, pg. 357-365.

Nowland, W. L., Olsen, R. L., and Shkarofsky, I. P. (1977), "Theoretical Relationship Between Rain Depolarization and Attenuation," Electronics Letters, Vol. 13, No. 22, pp. 676-678, October 27, 1977.

Olsen, R.L., D.V. Rogers, and D.B. Hodge (1978), "The $aR^b$ relation in the calculation of rain attenuation," IEEE Trans. on Antennas and Propagation, Vol. AP-26, No. 2, pp. 318-329, March 1978.

Otung, I.E. (1996), "Prediction of Tropospheric Amplitude Scintillation on a Satellite Link," IEEE Trans. on Antennas and Propagation, Vol. 44, No. 1, pp. 1600-1607..

Panter, P.F. (1972), *Communication Systems Design*. New York: McGraw Hill.

Peddie, N.W. (1982), "International geomagnetic reference field: the third generation," J. of Geomag. and Geoelct., vol. 34, pp. 309-327.

Peeters, Geoffroy, F. Marzano, G. d'Auria, C. Riva, & D. Vanhoenacker-Janvier (1997), "Evaluation of Statistical Models for Clear-Air Scintillation Prediction Using Olympus Satellite Measurements," International Journal of Satellite Communications, Col. 15, pp. 73-88.

Ratcliffe, J.A. (1972), *An Introduction to the Ionosphere and Magnetosphere*. Cambridge University Press.

Rino, C.L. and E.J. Fremouw (1977), "The angle dependence of singly scattered wave-fields," J. Atmos. Terr. Phys, vol. 39, pp. 859-868, Aug.

Rino, C.L. (1979a), "A power law phase screen model for ionospheric scintillation, 1. Weak scatter," Radio Science, vol. 14, pp. 1135-1145, Nov.-Dec.

Rino, C.L. (1979b), "A power law phase screen model for ionospheric scintillation, 2. Strong scatter," Radio Science, vol. 14, pp. 1147-1155, Nov.-Dec.

Rino, C.L., V.H. Gonzales, and A.R. Hessing (1981), "Coherence band width loss in transionospheric radio propagation," Radio Science, vol. 16, pp. 245-255, March-April.

Rishbeth, H. and O. K. Garriott (1969), *Introduction to Ionospheric Physics*. New York: Academic Press.

Royden, H.N., D.W. Green, and G.R. Walson (1980), "Use of Faraday rotation data from beacon satellites to determine ionospheric corrections for interplanetary spacecraft navigation." *COSPAR/URSI Symposium on Scientific and Engineering Uses of Satellite Radio Beacons*, Warsaw. Poland, May 19-23.

Rufenach, C.L. (1982), "Power Law wave number spectrum deduced from ionospheric scintillation observations," J. Geophys. Res., vol. 77, pp. 4761-4772, Sept.1.

Ryde, J.W., and D. Ryde (1945), "Attenuation of centimetere and millimetre waves by rain, hail, fogs, and clouds," Rep. No. 8670, Research Laboratories of the General Electric Co., Wembley, England.

Salonen, E.T., J.K. Tervonen & W.V. Vogel (1996), "Scintillation Effects on Total Fade Distributions for Earth-Satellite Links," IEEE Trans. On Antennas and Propagation, Vol. 44, No. 1, pp. 23-27.

Shutie, P.F., J.E. Allnut, & E.C. Mackenzie (1977), "Depolarization Results at 30 GHz Using Transmissions from the ATS-6 Satellite," *URSI Commission F, Open Symposium on Propagation in Non-Ionized Media*, La Baule, France, April 28-May 6, 1977.

Slobin, S.D.(1982), "Microwave noise temperature and attenuation of clouds: statistics of these effects at various sites in the United States, Alaska, and Hawaii," *Radio Science*, Vol. 17, No. 6, pp. 1443-1454, Nov.-Dec. 1982.

Smith, E.K. and R.E. Edelson (1980), "Radio propagation through solar and other extraterrestrial ionized media," JPL Pub. 79-117. Pasadena, CA: Jet Propulsion Lab., Jan. 15, 1980.

Smith, E.K. (1974), A Study of Ionospheric Scintillation as it Affects Satellite Communication, Office of Telecomm., U.S. Dept. of Commerce, Tech. Memorandum 74-186, Nov.

Smith, F.G. (1950),"Origin of the fluctuations in the intensity of radio waves from galactic sources: Cambridge observations," Nature, vol. 165, pp. 422-423, March 18.

Tatarski, V.E. (1971), *The Effects of the Turbulent Atmosphere on Wave Propagation.* Springfield, VA: National Technical Information Service.

Tatarski, V.E. 1961), *Wave Propagation in a Turbulent Medium.* New York; McGraw-Hill.

Taur, R.R. (1973), "Ionospheric scintillation at 4 and 6 GHz," COMSAT Tech. Rec., vol. 3, pp. 145-163, Spring.

Titus, J.M., & H.W. Arnold (1982), "Low Elevation Angle Propagation Effects on COMSTAR Satellite Signals," Bell System Technical Journal, Vol. 61, No. 7, pp. 1567-1572, Sept.

Vogel, W. J.(1980), "CTS Attenuation and Cross Polarization Measurements at 11.7 GHz," Final Report, Report No. 22576-1, June 1980.

Vogel, W.J., G.W. Torrence, & J.E. Allnutt (____), Scintillation Fading on a Low Elevation Angle Satellite Path: Assessing the Austin Experiment at 11.2 GHz," ????

Whitney, H.E. and S. Basu (1977), "The effect of ionospheric scintillation on VHF/UHF satellite communication," Radio Science, vol. 12, no. 1, pp 123-133, Jan.-Feb.

Whitney, H.E., J. Aarons, and C. Malik (1969), "A proposed index for measuring ionospheric scintillation," Planet. Space Science, vol. 7, pp 1069-1073.

Woo, R. and A. Ishimaru (1974), "Effects of turbulence in a planetary atmosphere on radio occultation," IEEE Trans. Antennas Propagate., vol. AP-22, pp. 566-573, July 1974.

Woo, R. and A. Ishimaru (1973), "Remote sensing of the turbulence characteristics of a planetary atmosphere by radio occultation of a space probe," Radio Science, vol.8 pp. 103-108, Feb.

Woo, R. (1977), "Measurements of the solar wind using spacecraft radio scattering observations," in Study of Travelling Interplanetary Phenomena, Shea, M.A. and D.F. Smart (eds.), pp. 81-100. Dordrecht, Holland: D. Reidel Pub. Co.

Woo, R. (1975), "Multi-frequency techniques for studying interplanetary scintillation," Astrophysics. J., vol. 201, pp. 238-248, Oct.1.

Woodman, R.F. and C. La Hoz (1976), "Radar observations of F-region equatorial irregularities," J. Geophys. Res., vol. 81, pp. 5447-5466, Nov.1.

Yeh, K.C. and G.W. Swenson (1964), "F-region irregularities studies by scintillation of signals from satellites," Radio Science (Sec.D., J. of Research, National Bureau of Standards), vol. 68D, pp. 881-894, Aug.

Yeh, K.C., and C. Liu (1979), "Ionospheric effects on radio communication and ranging pulses," IEEE Trans. Antennas Propagation, Vol. AP-27, pp. 747-751, Nov.